EUR 4070 e

European Atomic Energy Community - EURATOM
FIAT SpA, Sezione Energia Nucleare - Torino
Società ANSALDO SpA - Genova

FORCED CONVECTION BURNOUT AND HYDRODYNAMIC INSTABILITY EXPERIMENTS FOR WATER AT HIGH PRESSURE

Part V : Analysis of heating and burnout experiments in a double channel test section, with transversely varying heat generation

by

G.P. POZZI, G. PREVITI and P. SALA
(FIAT)

1968

Contract No. 008-61-12 PNII

LEGAL NOTICE

This report is on sale at the addresses listed on cover page 4

at the price of FF 16.50	FB 165.—	DM 13.20	Lit. 2 060	Fl. 11.95

When ordering, please quote the EUR number and the title, which are indicated on the cover of each report.

Printed by Guyot, s.a.
Brussels, September 1968

EUR 4070 e

FORCED CONVECTION BURNOUT AND HYDRODYNAMIC INSTABILITY EXPERIMENTS FOR WATER AT HIGH PRESSURE

Part V : Analysis of heating and burnout experiments in a double channel test section, with transversely varying heat generation,
by G.P. POZZI, G. PREVITI and P. SALA (FIAT)

European Atomic Energy Community - EURATOM
FIAT SpA ,Sezione Energia Nucleare - Torino
Società ANSALDO SpA - Genova
Contract No. 008-61-12 PNII
Brussels, September 1968 - 114 Pages - 16 Figures - FB 165

The analysis of some heating and burnout tests performed in a double channel test section has been performed. The calculation method used in this analysis was a digital program that solves the mass, energy and momentum equations of a mono- (or two) phase fluid in a tridimensional domain.

First some heating tests with no bulk boiling have been analyzed : the calculation outlet temperature distribution in the various subchannels has been

EUR 4070 e

FORCED CONVECTION BURNOUT AND HYDRODYNAMIC INSTABILITY EXPERIMENTS FOR WATER AT HIGH PRESSURE

Part V : Analysis of heating and burnout experiments in a double channel test section, with transversely varying heat generation,
by G.P. POZZI, G. PREVITI and P. SALA (FIAT)

European Atomic Energy Community - EURATOM
FIAT SpA ,Sezione Energia Nucleare - Torino
Società ANSALDO SpA - Genova
Contract No. 008-61-12 PNII
Brussels, September 1968 - 114 Pages - 16 Figures - FB 165

The analysis of some heating and burnout tests performed in a double channel test section has been performed. The calculation method used in this analysis was a digital program that solves the mass, energy and momentum equations of a mono- (or two) phase fluid in a tridimensional domain.

First some heating tests with no bulk boiling have been analyzed : the calculation outlet temperature distribution in the various subchannels has been

compared with the experimental outlet temperature distribution.

Next a systematic analysis of the burnout tests has been performed, with different heating on the burnout rod, on the adiacent rod and on the shell.

compared with the experimental outlet temperature distribution.

Next a systematic analysis of the burnout tests has been performed, with different heating on the burnout rod, on the adiacent rod and on the shell.

EUR 4070 e

European Atomic Energy Community - EURATOM
FIAT SpA, Sezione Energia Nucleare - Torino
Società ANSALDO SpA - Genova

FORCED CONVECTION BURNOUT AND HYDRODYNAMIC INSTABILITY EXPERIMENTS FOR WATER AT HIGH PRESSURE

Part V : Analysis of heating and burnout experiments in a double channel test section, with transversely varying heat generation

by

G.P. POZZI, G. PREVITI and P. SALA
(FIAT)

1968

Contract No. 008-61-12 PNII

SUMMARY

The analysis of some heating and burnout tests performed in a double channel test section has been performed. The calculation method used in this analysis was a digital program that solves the mass, energy and momentum equations of a mono- (or two) phase fluid in a tridimensional domain.

First some heating tests with no bulk boiling have been analyzed : the calculation outlet temperature distribution in the various subchannels has been compared with the experimental outlet temperature distribution.

Next a systematic analysis of the burnout tests has been performed, with different heating on the burnout rod, on the adiacent rod and on the shell.

KEYWORDS

BURNOUT
HEATING
TESTING
RODS
PROGRAMMING
DIGITAL SYSTEMS
MASS
ENERGY
MOMENTUM
DIFFERENTIAL EQUATIONS
TEMPERATURE
THERMAL DIFFUSION
FLUID FLOW
TWO-PHASE FLOW
VELOCITY

I N D E X

LIST OF FIGURES

SUMMARY

The analysis of some heating and burnout tests performed within the frame of an EURATOM - FIAT - ANSALDO Contract for nuclear propulsion studies with a double channel test section has been made: in these tests it was possible to uniformely heat the burnout rod, the adjacent rod and the shell independently (see Reference 1).

The calculation method used in this analysis was a digital program that solves the mass, energy and momentum equations of a mono- (or two-) phase fluid in a tridimensional domain.

First some heating tests with no bulk boiling and no burnout have been analyzed: the calculated outlet temperature distribution in the various subchannels has been compared with the experimental outlet temperature distribution. Varying parametrically the value of the thermal diffusion coefficient, the best value of this parameter (to be used in burnout calculation) has been determined as the value giving the best agreement between theoretical and experimental temperature distribution.

Next a systematic analysis of the burnout tests has been performed. The tests have been divided in four groups:

- Group A : only burnout rod heated;
- Group B : different heating on burnout rod and on adjacent rod;
- Group C : different heating on burnout rod and on shell;
- Group D : different heating on burnout rod, on adjacent rod, and on shell.

Two different subdivisions of the cross sectional flow area have been considered for the analysis: a schematization with 8 subchannels and a schematization with 10 subchannels. In both cases satisfactory agreement between experimental and theoretical results has been found inserting in the W-3 Westinghouse burnout correlation the local qualities and mass velocities found with the tridimensional digital program.

The experimentally found effect of the adjacent rod and of the shell on the burnout flux of the burnout rod has been checked theoretically.

(*) Manuscript received on July 24, 1968.

§ 1. PURPOSE OF THE ANALYSIS

In this report the theoretical analysis of a certain number of heating and burnout experiments, (performed at SORIN-Heat Transfer Laboratory in the frame of a Contract (*) between EURATOM-FIAT-ANSALDO) is presented: the experiments have been carried out using a double channel test section with radially non-uniform heat generation.

The results of these experiments have been reported in Reference 1 ; in the present paper reference is made to these experiments by quoting the number of the specific experiment and its execution day, month, year (for example, TEST 40 (26-7-67).

It is useful to remember that the test section consisted (see fig. 1a) of two stainless steel cylindrical tubes (rod A, called burnout rod, and rod B, called adiacent rod), and of two hydraulic channels in communication through the surface S. The two channels were enclosed in a shell with alternate curved cylindrical surface G and rectilinear strips L.
The geometrical dimensions of the test section has been indicated in fig. 1a.
During the experiment it was possible to electrically heat the burnout rod, the adiacent rod, and the shell independently.

The shell was heated in order to better simulate the thermal hydraulic conditions of the coolant in a rod bundle, in which every rod is surrounded by four rods generally heated (see fig. 1b).

It was not possible to avoid the presence of plane walls L in the shell: these walls introduce in the channels an additional hydraulic resistance and an additional heat flux (if the shell is heated), that are not present in the flow channels of a fuel bundle (see fig. 1b) and produce alterations in the temperature and velocity local profiles(**). The heat flux was axially uniform both on the rods and on the shell.

It is worth while to remember that the instrumentation useful for the theoretical analysis of the tests was the following:

a) indicator of the electrical power furnished to rods and shell;

b) one inlet flow meter;

c) one average coolant pressure indicator;

d) one thermocouple for inlet temperature measurement;

e) five thermocouples for the exit temperature distribution (the five thermocouples were located at the exit in the point indicated by T_1, T_2, T_3, T_4, T_5 in figure 1a;

f) a burnout detector.

(*) - Contract No.008-61-12 PNII.

(**) - However, due to different thickness, the flat walls generate only the 13,74% of the shell overall power.

For a detailed description of the experimental apparatus and the analysis of measurement precision see Reference 9 .

The purpose of the present analysis has been the following one: to calculate with a suitable method the local values of the thermal hydraulic variables (enthalpy and mass velocity) in the hydraulic channels and next to evaluate the burnout flux through a suitable burnout correlation. If the comparison between calculated and measured burnout fluxes is good in a wide range of pressure, flow and inlet temperature, it will be correct to use the same calculation method in the design of a fuel bundle core with rod diameter and pitch of the same or similar values as in the present test section.

In the majority of the present burnout tests, the burnout rod, the adiacent rod and the shell were differently heated: in fact the main purpose of the experimental research was to analyze how the burnout flux of a rod is influenced by the heat flux of the adiacent rods.

It is evident a priori that the temperature and mass velocity distribution cannot be considered as uniform in a plane (x,y) normal to the test section vertical axis; some heat crosses continuously the surface S (see fig. 1a) between the left channel enclosing the burnout rod and the right channel enclosing the adiacent rod, owing to both turbolent diffusion and net mass transfer. The hypothesis of considering the two channels as closed that is without lateral mass and heat exchange, is clearly incorrect (see Appendix 3) ; the velocity and enthalpy field is tridimensional.

It was then necessary to use an open channel calculation method, outlined in its essential features in Appendix 1. Here is sufficient to say that this method consists in solving the mass, energy and momentum equations for a mono-(or two-)phase fluid in a tridimensional domain: following the difference finite method, this domain is subdivided in a suitable number of cells (or control volumes) and in each cell the average value of enthalpy, pressure and velocity (with its three components x, y, z) are calculated.

A point that has been considered with care is the most suitable subdivision of the test section flow area in cells. The subdivision in 2 or 4 subchannels has been discarded a priori due to poor approximation (the cross flow redistribution and turbolent mixing analysis require a more detailed schematization). Two schematizations have been adopted: the schematization A with 8 subchannels and the schematization B with 10 subchannels, sketched in figure 2. These two schematizations gave results comparable with regard to the distribution of enthalpy and mass velocity in the test section; the differences can be explained on the basis of the equations and correlations explained presented in Appendix 1. In Appendix 3 some comments are reported on these differences and on their implications on burnout evaluation.

The schematization B was introduced in order to avoid the problem relative to the choice of the equivalent diameter to be used in the burnout

correlation. This point will be discussed in Section 4. Here it is sufficient to say that the analysis of the results obtained with the 10-subchannels schematization indicates the way of obtaining correct burnout results from the 8 subchannels schematization.

§ 2. EVALUATION OF SUBCHANNEL TEMPERATURE DISTRIBUTION AND DETERMINATION OF THE THERMAL DIFFUSION COEFFICIENT

In order to evaluate in detail the burnout flux distribution in the various sybchannels, it is necessary to know the value of the turbolent flow rate W see Appendix 1 that crosses the boundary surface between two adjacent cells due to turbolence. This quantity, or better the value of the thermal diffusion coefficient γ that is given as input to the THINC program, is a function of the geometry of the test section (mainly of rod diameter and pitch).

Some heating tests have been utilized in order to obtain the proper value of the thermal diffusion coefficient to be next used in the burnout calculations: in these heating tests the effective heat flux is well below the value of the corresponding burnout flux and the outlet enthalpy below the saturation enthalpy.

For every experimental test, the value of the thermal diffusion coefficient γ has been changed parametrically in order to establish that value of γ in correspondence to which the calculated subchannel outlet temperature distribution best fitted the experimental outlet thermocouple profile.

In Table I of Appendix 4 the results of RUN 1 bis (9-11-66) analysis are reported; both the 8-subchannels and the 10-subchannels schematization has been used.

Table II of Appendix 4 showes the similar results of RUN 2 (10-11-66). In figg. 3, 4, 5, 6 the theoretical subchannel outlet enthalpy rise distribution of these heating runs is compared with the experimental enthalpy rises, as deduced from thermocouple readings.

Some remarks can be done. The 10-subchannels schematization is more sensitive that the 8-subchannels schematization to a change in thermal diffusion coefficient γ ; this is clearly due to the fact that in the first case is largely greater the lateral area between the various subchannels through which the turbolent heat exchange happens.

The comparison between theoretical and experimental subchannel enthalpy rise must be accepted in a semiquantitative manner. Namely with THINC program the average values of outlet enthalpy in every subchannel is calculated, while experimentally the values of outlet temperature in the

points T_1, T_2, T_3, T_4, T_5 (see fig. 1a) are measured: there is no reason that these temperatures be equal to the outlet average temperatures in certain subchannels of the 8-subchannels (or the 10-subchannels) schematization, as calculated by THINC.

In the present analysis, no attempt has been done in order to evaluate theoretically the transverse (x,y) temperature and velocity distribution in the various subchannels of the test section; this problem has been solved in the literature in the case of simple geometries (flow between parallele plates, flow inside round tubes). More complex geometries (like that relative to the present test section) requires the numerical solution of the partial differential equations of turbolent flow.

However from figures 3 and 5 one can observe the large error produced by assuming zero turbolent diffusion ($\chi = 0.$). In subchannels with no heated surfaces, there is no enthalpy rise: namely the heat dont enter the subchannel neither because turbolent diffusion, nor because effective mass lateral transfer, as can be seen from the value of the subchannel outlet mass velocities G_{out} in Table I and II. Also not realistic appears a value of χ close to $2. \div 3. \times 10^{-2}$, for the outlet enthalpy distribution results too depressed in the subchannels surrounding the heated rod and too high in the other subchannels.

The most probable value of χ is around

$$1. \div 1.5 \times 10^{-2}$$

This value agrees quite well with the value of thermal diffusion coefficient obtained in FIAT always in the frame of the present contract (see Reference 6). The method may be so summarized: at the inlet of a fuel element at temperature T_1, a stream of water at temperature T_2 was injected in a particular channel C; this stream mixes with the water of adjacent channels. The axial variations of water temperature in the channel C are measured and, through the analytical solution (see Reference 7) of a diffusion equation giving the theoretical variation of axial temperature, the value of the eddy thermal diffusivity (*) and hence the Peclet number Pe (*) can be obtained.

(*) - The Peclet number Pe is a dimensionless quantity used in thermal mixing calculation; defined as $Pe = \epsilon / V_{axial} \cdot De$, is related to the thermal diffusion coefficient χ by the relation

$$\chi = \frac{Pe}{a} \times De,$$

a being the lateral flow area per unit length (see also Appendix 1).

In the case a fuel element without grids and ferrules (bare bundle), a value of 0.4×10^{-2} (*) was found for the Peclet number independent with good approximation from the Reynolds number. From this the following value for figure 1 rod bundle geometry has been obtained

$$\gamma = 1.45 + 1.46 \times 10^{-2}$$

It is worthwhile to observe that in the hot water injection mixing tests, the turbolent heat diffusion across the surface S_{min} of figure 14b has been measured, i.e. the 8-subchannel schematization A was virtually considered.

In the present analysis both the 8-subchannel schematization A and the 10-subchannel schematization B has been considered. In all these three case a value of $\gamma = 1.5$ seems to be the more realistic.

(*) It was necessary to correct this value because of the small differences in rod diameter and pitch, between the figure 1 present geometry and the geometry used in Reference 6 mixing tests. This correction has been done in two different way:

a) by multiplying the Peclet number found in FIAT by the quantity

$$\frac{De^{(1)}}{De^{(0)}} \times \frac{S^{(1)}}{S^{(0)}}$$

where

$De^{(1)}$ (or $De^{(0)}$) is the equivalent diameter of figure 1 geometry (or Reference 6 geometry respectively)

$S^{(1)}$ (or $S^{(0)}$) are the analogous value of rod spacing;

this procedure has been suggested in Reference 8 .

b) utilizing an experimental plot (see Reference 6) giving the Peclet number as a function of the ratio PD ≡ pitch/diameter. This plot, obtained by collecting mixing tests with different geometries, may be approximated with a strait line having the following derivative

$$\partial (Pe)/_{\partial (PD)} = 1.36 \times 10^{-2}$$

The following values were obtained for the thermal diffusion coefficient

$$\gamma = 1.4624 \times 10^{-2} \quad \text{(method (a))}$$

$$\gamma = 1.4526 \times 10^{-2} \quad \text{(method (b))}$$

Remembering the significance of γ (see Appendix 1), one can conclude that the ratio $V_{trans.}/V_{axial}$ can be regarded as a constant independent from the orientation of the surface S across which the transverse turbolent velocity $V_{trans.}$ is considered (see figure 14b).

This is an experimental support to the fact that the turbolence can be considered as isotropic.

From what has been said above, it appears that an interval in which the thermal diffusion coefficient γ is comprised instead of the exact value of γ can be determined from the analysis of the outlet temperature profiles. It is natural to ask oneself if this partial indetermination of the value of γ can lead to a serious uncertainty in the calculation of the theoretical burnout flux.

The parametrical analysis of a certain number of experimental burnout test has shown that this fact does not happen. Figure 7 shows the result of this analysis relative to burnout run 45 (26-7-67), that belongs to burnout group A (burnout tests with heat flux only on the burnout rod; see the following section 3 and, for the description of the experimental conditions, Table III in Appendix 4): in this diagram the variation of departure nucleate boiling ratio DNBR with the thermal diffusion coefficient γ in the subchannel 3 of 10-subchannels schematization is shown. Also the variation of the enthalpy rise ΔH and of the ratio between outlet and inlet mass velocity on which burnout depends are reported. It can be seen that, aside the case $\gamma = 0$ (no thermal turbolent mixing), the DNBR does not change too much varying the thermal diffusion coefficient; namely the deviations of DNBR from 1 are smaller than the error in W-3 burnout correlation. (*)

Also the ratio G_{out}/G_{in} between outlet and inlet mass velocity (that in an index of the flow redistribution) is nearly constant varying the thermal diffusion coefficient (always aside the value $\gamma = 0$.).
The enthalpy rise ΔH instead is more sensible to a variation of γ, as was already observed in the analysis of the outlet temperature profiles.

(*) We have selected in burnout literature some experimental burnout tests performed in round tubes having values of hydraulic diameter and heated length close to the values relative to the present double channel test section heated length and infinite matrix equivalent diameter (for the definition and meaning of the latter see Section 4).
We have then numerically verified that the error done by W-3 burnout correlation in predicting the burnout flux of such tests (made with values of operating pressure, inlet subcooling and mass velocity close to the values examined in the present report) is very small (less than 10%).

Since this behaviour with χ was observed in the analysis of other burnout tests, it has been decided to perform the systematic analysis of the experimental burnout test with a value of χ equal to 1.4×10^{-2}.

§ 3. BURNOUT TEST ANALYSIS

Using the determined value of the thermal diffusion coefficient the thermal-hydraulic conditions and the burnout flux of a number of experimental burnout tests have been calculated.

For the comparison of experimental results and theoretical predictions, the $\{\Delta H_{SUB}; \phi_{B.O.}\}$ diagram was systematically used: on the abscissa the subcooling enthalpy difference $\Delta H_{SUB} = H_{SAT} - H_{in}$ has been plotted, on the ordinate the burnout flux (both experimental and calculated) (*) has been reported. Each diagram is relative to a fixed value of the average coolant pressure, inlet mass velocity and distribution of power between burnout rod, adjacent rod and shell.

It has been retained the subdivision adopted in [1] of the burnout tests in the following four groups:

- group A : burnout tests with heat flux only on the burnout rod;
- group B : burnout tests with different heating on the burnout rod and on the adjacent rod;
- group C : burnout tests with different heating on the burnout rod and on the shell;
- group D : burnout test with different heating on the burnout rod, on the adjacent rod and on the shell.

(*) - See Appendix 2 for the correct definition of calculated burnout flux.

The most important data for the analyzed cases are as follows:

1) Group A.

The burnout fluxes have been evaluated for three different values of the nominal (*) inlet mass velocity: 100; 300; 450 lbm/sec.ft^2.

In figg. 8a, 8b, 8c the results of this analysis have been reported; the three diagrams refer to the three values of the nominal inlet mass velocity quoted above. All the burnout tests have been analyzed both with the 8 and 10-subchannels schematization.

The experimental conditions and the detailed results of the burnout tests analyzed in order to draw the above diagrams have been reported in Table III of Appendix 4. When the analysis has been done using the 8-subchannels schematization, the infinite matrix equivalent diameter (defined in Section 4) has been introduced in the W-3 burnout correlation.

2) Group B.

The burnout fluxes have been evaluated for two different values of the nominal inlet mass velocity (100. and 450. lbm/sec.ft^2) and for two different values of the ratio $\phi_A/\phi_{B.O.}$ between the flux on the adjacent rod and the flux on the burnout rod; the values used were $\phi_A/\phi_{B.O.} = 0.6$ and $\phi_A/\phi_{B.O.} = 0.96$.

The results of the analysis have been summarized in figg. 9a, 9b and 9c. For the experimental conditions and the detailed results see Table IV of Appendix 4.

The above tests have been analyzed with the 10-subchannels schematization.

3) Group C.

In the experimental burnout tests belonging to this group, the inlet mass velocity was retained fixed to the nominal value of 300. lbm/sec.ft^2. Two different values of the ratio $\phi_S/\phi_{B.O.}$ between the heat flux on the curved cylindrical surface of the shell and the heat flux on the burnout rod, that is 0.45 and 0.83.

(*) - This is a reference value used in order to distinguish the different burnout tests. The effective value of the inlet mass velocity has been reported in the Tables collected in Appendix 4 that give the experimental conditions of each run.

The scattering of some experimental burnout flux around a straight line in the $\{ \Delta H_{SUB}, \phi_{B.O.} \}$ diagram may be due to the fact that all the tests reported in the diagram have not exactly the same inlet mass velocity.

The results of this analysis are shown in figg. 10a and 10b. For the experimental conditions and the detailed results see Table V of Appendix 4. The above tests have been analyzed with the 10-subchannels schematization.

4) Group D.

In the experimental burnout tests belonging to this group the inlet mass velocity was retained fixed to the nominal value of 300. lbm/sec.ft^2. Three different pairs of values relative to $\phi_A/\phi_{B.O.}$ have been analyzed

$\frac{\phi_A}{\phi_{B.O.}}$	$\frac{\phi_S}{\phi_{B.O.}}$
0.43	0.41
0.58	0.55
0.87	0.82

The results of this analysis are shown in figg. 11a, 11b and 11c. For the experimental conditions and the detailed results see Table VI of Appendix 4. The above tests have been analyzed with the 10-subchannels schematization.

§ 4. REMARKS AND CONCLUSIONS

From the above analysis some remarks can be made:

a) the thermal hydraulic analysis of heating and burnout tests in open channel configurations (like those examined in the present report) can be quite satisfactorly performed with an open channel thermal hydraulic calculation procedure; that is by solving the tridimensional equations expressing the conservation of mass, energy and momentum.

b) the burnout flux of a rod in an open channel configuration is also function of the heat flux of the adjacent rods. This is clearly shown in figure 11, which plots the variation of the ratio

$$R = \frac{\text{burnout flux with adjacent rod flux } \phi_A}{\text{burnout flux with zero adjacent rod flux}} \qquad (4\text{-}1)$$

with the ratio $\phi_A/\phi_{B.O.}$ between the adjacent rod heat flux and the burnout rod heat flux; burnout tests of group A and group B have been utilized in order to obtain this figure, the shell in all tests being unheated.

Figure 12 represents the similar plot relative to burnout tests in which the shell, instead of the adjacent rod, has been heated: in this case $\phi_S/\phi_{B.O.}$ represents the ratio between the heat flux on the curved cylindrical surface of the shell and the heat flux on the burnout rod. (*)

One can observe that the decrease of R with the heat flux ratio $\phi_A/\phi_{B.O.}$ (or $\phi_S/\phi_{B.O.}$) is greater when the shell is heated than when the adjacent rod is heated. This is due:

1) to the fact that the curved cylidrical surface G of the shell is more close to the burnout rod than the adjacent rod (this is more true if one considers that burnout starts always on burnout rod A in a spot close to thermocouple T_1 (see figure 1a; this has been detected experimentally (**) and confirmed

---

(*) - In the definition of the ratio R the same operating conditions (pressure, inlet mass flow and inlet temperature) for the burnout flux at numerator and denominator are supposed.
In drawing figures 11 and 12, the possible difference in subcooling enthalpy difference $\Delta H_{SUB.}$ between two burnout tests to be compared has been taken into account with the following relation

$$\phi_{B.O.}(\Delta H'_{SUB.}) = \phi_{B.O.}(\Delta H_{SUB.}) + \left(\frac{\partial \phi_{B.O.}}{\partial H_{SUB.}}\right) \times (\Delta H'_{SUB.} - \Delta H_{SUB.}); \qquad (4\text{-}2)$$

from the analysis of group A burnout tests (burnout tests with heat flux only on the burnout rod) a value of + 0.627 (Btu/sec.ft^2) / (Btu/lbm) has been derived for the partial derivative $\frac{\partial \phi_{B.O.}}{\partial H_{SUB.}}$. This correction has been done in all the points reported in figures 11 and 12 taking as reference ΔH_{SUB} the subcooling of the burnout test with zero adjacent rod flux.

(**)- In the present test section there is not an experimental detector of the point on the burnout rod where nucleate boiling starts; however an examination of some burnout rods after a number of burnout tests revealed a marked spot with different colour on the burnout rod surface.
This spot happens at the end of the burnout rod, is high 1" and large 2" approximatively and is placed on the rod surface on the opposite side with respect to the adjacent rod, close to the cylindrical curved surface G, where the water thickness is smaller.
This spot has been explained as the trace of a thermal excursion, hence of burnout (SORIN engineers' personal communication).

by theoretical analysis; it is clear that the burnout spot is more close to a curved cylindrical surface of the shell than to the adjacent rod and than more influenced by the former;

2) to the fact that with equal values of $\phi_A/\phi_{B.O.}$ and $\phi_S/\phi_{B.O.}$ the power given to the test section is greater when the shell is heated than when the adjacent rod is heated;

3) to the fact that the mass velocity in the flow area between the two rods (subchannel 4 of 8-subchannels schematization) is higher than the mass velocity in the flow area near the burnout rod but on the opposite side (subchannel 1 in 8-subchannels schematization) due to differences in hydraulic diameter (see Appendix 3); and hence burnout flux tends to be lower.

The ratio R has been also plotted as a function of the ratio $(0.5 \times P_S/P_{B.O.})$, P_S being the total power generated by the shell (only one half of the shell gives power to the water enclosing burnout rod and $P_{B.O.}$ the burnout power. In this case the decrease of R with $(0.5 \times P_S/P_{B.O.})$ is smaller than the decrease of R with $\phi_S/\phi_{B.O.}$, but always greater than the decrease of R with

$$\frac{P_A}{P_{B.O.}} \equiv \frac{\phi_A}{\phi_{B.O.}}$$ (P_A is the power of the adjacent rod):

this can be see in figure 13 where the two R variation (POWER RATIO and FLUX RATIO straight line) have been reported. This result confirms the assertion that the heating of the shell has more influence on burnout rod's burnout flux than the heating of the adjacent rod.

Some comments about the procedure here adopted for burnout evaluation in an open channel configuration. Both the 8-subchannels schematization and the 10-subchannels schematization gave theoretical burnout fluxes in reasonable agreement with the experimental burnout flux, although the distribution of thermal-hydraulic variables (enthalpy and mass velocity) obtained in the two case was not the same. However the numerical differences between the distribution of enthalpy and mass velocity obtained with the two schematization can be explained (see Appendix 3).

Also the agreement between theoretical calculations and experimental results in the analysis of the heating tests (see section 2) can be considered as satisfactory.

With the 10-subchannels schematization, no problem rises about the choice of the subchannel equivalent diameter to be used in the burnout correlation: using in all the subchannels the hydraulic diameter as equivalent diameter for the burnout calculation, the experimental burnout flux was checked with a maximum error of 5÷10%.

In fact the 10-subchannels schematization was tentatively introduced in order to avoid the DNB equivalent diameter problem.

Instead, trying to analyze with the 8-subchannels schematization the burnout tests of group A and group B in which the shell was not heated, neither using the hydraulic diameter nor using the thermal diameter in every subchannel, an acceptable agreement with experimental burnout flux was found. This can be attributed to the following facts:

1) when the shell is unheated, only the burnout rod contributes to the heated perimeter of the various subchannels of the 8-subchannels schematization; the resulting thermal diameters are too large to be included in the range of validity of the W-3 burnout correlation (see Appendix 3 for a numerical discussion of this point);

2) The rectilinear strips L of the shell must be accounted as wetted perimeter in friction pressure drop calculation, but not as part of the equivalent diameter in burnout calculation (in fact including them, that is using the hydraulic diameter in W-3 correlation, the obtained burnout flux are too high (see Appendix 3).

With the 8-subchannels schematization both when the shell was heated and when it was unheated, an acceptable agreement was found using in every subchannel along with the local enthalpy and mass velocity (obtained with THINC code) the hydraulic diameter of the infinite matrix to which the test section belongs (see fig. 1b). This quantity, equal to

$$4 \frac{\left(P^2 - \frac{\pi}{4} D^2_{rod} \right)}{\pi D_{rod}} , \qquad (4.3)$$

coincides with the thermal and hydraulic diameter of the subchannels 3, 4 of the 10-subchannels schematization and with the thermal diameter of subchannels 1, 2, 3, 4 of the 8-subchannels schematization when the shell is heated.

This agreement, found in all the burnout tests analyzed in the present work, can lead to the following conclusion.

The W-3 burnout correlation has been obtained by fitting a large number of experimental burnout points: all these burnout tests were performed using closed channel geometries that is a circular pipe, a rectangular cross section pipe, a bundle of equally heated rods enclosed in a can.

Open channel burnout tests (that is burnout tests in a bundle of rods not equally heated and with subchannels having different wetted perimeters and different flow areas) were not covered by the W-3 correlation. The W-3 correlation is a function of the following parameters: average pressure P; local quality X; mass velocity G; equivalent diameter De; inlet subcooling $H_{SAT} - H_{in}$.

Now in a closed channel the mass velocity G is constant along the channel length and equal to the inlet value; the equivalent diameter to be in burnout correlation of a rectangular channel, of a circular channel, and of an infinite rod bundle is equal to the hydraulic diameter because all the heated walls are also wetted walls. Therefore the application of the W-3 burnout correlation to a complex geometry like the present one (a fuel bundle of finite number of rods not equally heated with subchannels having a wetted perimeter different from the heated) is questionable. The obtained results seems to give a positive answer to the question.

In present analysis the following procedure seems to work satisfactorily :

a) subdivide the total flow cross sectional area in a suitable number of subchannels and then calculate the axial distribution of enthalpy, mass velocity and pressure. (It is worthwhile to remember that in an open channels configuration the mass velocities in the subchannels change from the inlet values, due to flow redistribution and also the enthalpy distribution is influenced by the cross flow and turbolent mixing);

b) use the local qualities and mass velocities in the W-3 correlation along with the hydraulic diameter of the infinite matrix, previously defined (see formula (4-3) above).

A parameter that must be introduced with care is the "suitable number of subchannels". In fact many different subdivisions of the total cross sectional area are possible. In performing these subdivisions the following two consideration must be taken into account:

1) the W-3 correlation (like other DNB correlations) is a function of the average value of qualities, and mass velocity. So it would be wrong to introduce in the W-3 correlation the local values of these quantities, for example the values obtained in subchannels 3, 6, 9 of the schematization sketched in figure 14b;

2) the conservation equations used in THINC and outlined in Appendix 1 cannot describe this local behaviour of enthalpy, mass velocity and pressure, neither in single phase nor in two phases flow regime. (More detailed equations must be used, that have begun to appear begun to appear in the literature; see for example Reference [11]).

So in a fuel rod bundle the number of subchannels has to be large enough in order to see the flow redistribution and the effect of cross flow and turbolent diffusion on enthalpy distribution, but not too large to force the thermal hydraulic conservation equations outlined in Appendix 1 to calculate local values that these equations cannot see and that cannot be used in present burnout correlation.

The problem may be quite different if local burnout equations would be available, that is equations that can predict burnout as a function of the local values of some governing thermal-hydraulic parameters calculated near the rod surface.

These considerations and conclusions are the result of the present two fuel rod analysis. However, before considering the above procedure reliable enough to be applied to an open lattice core design, it must be tested against different fuel rod numbers and configurations. This will be partially done in a following work, in which the experimental results of heating and burnout tests in 3x3 fuel rod configurations (that SORIN is presently performing) will be theoretically analyzed.

A P P E N D I X 1

DESCRIPTION OF THE OPEN CHANNEL CALCULATION METHOD

A calculation method developed by Westinghouse - APD (Reference 2) in order to evaluate the thermal-hydraulic conditions in un open channels core has been used. The total flow volume is divided in control volumes: each control volume may be adjacent to four lateral control volumes and two vertical control volumes.

In figure 14a two laterally adjacent control volumes (i and j) are sketched. Letting W_{ij} be the cross flow from channel i to channel j , the mass balance equation may be written

$$A_j V_{j1} \rho_{j1} + W_{ij} = A_j V_{j2} \rho_{j2} \qquad (*) \qquad (A1\text{-}1)$$

Similarly the heat balance equation is

$$A_j V_j \rho_{j1} H_{j1} + Q_j + (TC)_j + W_{ij} H_{ij} = A_j V_j \rho_{j2} H_j \; ; \qquad (A1\text{-}2)$$

the momentum balance equation is

$$A_j P_1 + A_j \rho_{j1} V_{j1}^2/g_c + W_{ij} V_{ij}/g_c = \qquad (A1\text{-}3)$$

$$A_j P_2 + A_j \rho_{j2} V_{j2}^2/g_c + K_j A_j \bar{\rho}_j \bar{V}_j^2/(2g_c) + A_j \bar{\rho}_j \Delta z \, g/g_c$$

Since the static pressure at any given elevation is considered to be the same in all subchannels, the channel subscript on the pressure has been removed.

The energy interchange resulting from turbolent diffusion between the two adjacent channels may be written

$$TC = W' \cdot \Delta z \cdot \Delta H \qquad (A1\text{-}4)$$

(*) - For the meaning of symbols used, see Nomenclature.

where :

W' is the lateral flow exchange rate per unit channel length.

Δz is the channel length.

ΔH is the difference in the fluid enthalpies of the two channels.

The thermal eddy diffusivity ϵ is defined by the relation

$$\epsilon = W'/\rho \qquad \text{(A1-5)}$$

where ρ is the fluid density. The thermal eddy diffusity can be correlated in terms of the dimensionless thermal diffusion coefficient γ. The relationship is

$$\gamma = \epsilon / V_{axial} \cdot a \qquad \text{(A1-6)}$$

where V_{axial} is the fluid axial velocity at channel boundary;

a is the lateral flow area per unit length.

Introducing in (A1-4) the thermal diffusion coefficient, we obtain the expression

$$TC = \gamma \Delta z \, G \, a \, \Delta H \qquad \text{(A1-7)}$$

where the fluid mass velocity G has been used in place of ρV_{axial}.

Since the lateral flow exchange rate W' can be expressed as $(\rho . a . V_{trans.})$, one may observe that the thermal diffusion coefficient is equal to the ratio between the turbolent transverse velocity and the axial velocity

$$\gamma = V_{trans.} / V_{axial} \qquad \text{(A1-8)}$$

Both single-phase and two-phase flow regimes have been considered. For two-phase flow the Martinelli-Nelson separated flow model has been used (see Reference [3]).

In equation (A1-3) the parameter K is equal to $f . \Delta z/De$. For the evaluation of the friction factor f, standard correlation have been used (see, for example, Reference [4]): non boiling, local boiling and bulk boiling conditions have been considered. In non boiling and local boiling flow regimes, the friction factor f has been expressed as $f_{iso}(f/f_{iso})$ and different expressions has been used for the correction factor (f/f_{iso}).

In bulk boiling, f is equal to $f_{iso,sat} \cdot \phi^2_{LO}(X,G,P)$, ϕ^2_{LO} being Martinelli Nelson two phase friction factor corrected by Sher (see Reference [5]).

If local obstructions were present, the factor K would also take care of the related contraction and expansion resistence factors.

For the evaluation of thermal crisis, the following W-3 Westinghouse - APD correlation (see Reference [10]) has been introduced in THINC digital program

$$q''_{DNB} = f\,(P;\ X;\ G;\ De;\ H_{SAT} - H_{in}) =$$

$$= \left[(a + bP) + (c + dP)\ \exp\,(e + fP)\ .\ X\right]\ .$$

$$\left[(g + hX + iX|X|)\ G/10^{6} + 1\right]\ .\ (m + nX)$$

$$\left[o + p\ \exp\,(q.De)\right]\left[r + s\ (H_{SAT} - H_{in})\right]\ x\ 10^{6}$$

where

$a = 2.022$; $b = -0.4302 \times 10^{-3}$; $c = 0.1722$

$d = -0.984 \times 10^{-4}$; $e = 18.177$; $f = -0.4129 \times 10^{-2}$

$g = 0.1484$; $h = -1.596$; $i = 0.1729$

$l = 1.037$; $m = 1.157$; $n = -0.869$

$o = 0.2664$; $p = 0.8357$; $q = -3.151$

$r = 0.8258$; $s = 0.794 \times 10^{-3}$.

A P P E N D I X 2

DEFINITION OF THEORETICAL BURNOUT FLUX

Let us suppose to have determined experimentally that, in a determined test section (for example, the section considered in this report)with an inlet enthalpy H_{in}^{*}, on inlet mass velocity G_{in}^{*}, an average pressure P^{*}, burnout starts when the effective rod surface flux is φ^{*} (for simplicity, let us suppose that the heat flux is axially uniform): φ^{*} is called experimental burnout flux.

What is the theoretical burnout flux predicted by a certain correlation C? Every burnout flux correlation is generally a function of certain parameters, that depend on inlet enthalpy, inlet mass velocity, average pressure and effective rod flux (*):

$$\varphi_{B.O.} = f\,(H_{in}\,;\ G_{in}\,;\ P\,;\ \varphi) \qquad \text{(A2-1)}$$

The theoretical burnout flux $(\varphi_{B.O.})_{th}$ can be defined as <u>that</u> value of the effective rod flux that satisfies the equation

$$\varphi = f\,(H_{in}^{*}\,;\ G_{in}^{*}\,;\ P^{*};\ \varphi) \qquad \text{(A2-2)}$$

that is that value of the effective heat flux that, when inserted in equation (A2-1), generates a burnout flux equal to itself.

Remembering the definition of the departure nucleate boiling ratio R_{DNB} (as the ratio of the burnout flux to the effective heat flux)

$$R_{DNB} = \frac{\varphi_{B.O.}}{\varphi}\ , \qquad \text{(A2.3)}$$

it can also be said that the theoretical burnout flux is that value of the effective rod flux in correspondence to which R_{DNB} is equal to one.

In order to find the theoretical burnout flux, one must solve equation (A2.2), necessarily in an iterative way.

(*) - A burnout correlation generally depends also on geometry (channel length and equivalent diameter); this dependence has no interest for the present discussion.

One may ask if the theoretical burnout flux is very different from the burnout flux obtained by using in (A2.2) the experimental burnout flux; this last value can be called the experimental-theoretical burnout flux $\varphi_{T,S}$

$$\varphi_{T,S} = f\left(H^*_{in}\ ;\ G^*_{in};\ P^*;\ \varphi^*\right) . \qquad \text{(A2-4)}$$

This fact has been analyzed in detail in a burnout flux experimental test, RUN 64 (21-2-67) (for its thermal hydraulic characteristic see Table III of Appendix 4): this run has been parametrically analyzed by varying the effective rod surface from 300. Btu/sec-ft^2 to 331.7 Btu/sec-ft^2, this figure being the value of the experimental burnout flux. The results of this analysis are summarized in Table VII of Appendix 4 and the conclusion sketched in figure [15a.] It can be seen that the theoretical burnout flux $(\varphi_{B.O.})_{th}$ is nearly equal to the experimental-theoretical, burnout flux $\varphi_{T,S}$; the percentual error $\left[(\varphi_{T,S} / \varphi_{B.O_{th}}) - 1\right]$ is equal to 7.3‰ . It has to be pointed out that the W-3 burnout correlation is a slowly varying function of the effective rod surface flux.

The same parametrical analysis of other burnout tests confirmed the fact that the experimental-theoretical burnout flux $\varphi_{T,S}$ is very close to the theoretical burnout flux $(\varphi_{B.O.})_{th}$. Table VIII of Appendix 4 and figure [15b] report the results of RUN 90 (7-12-66) analysis whose thermal hydraulic operating conditions are reported in Table III of Appendix 4. In this case $\varphi_{T,S}$ = 313.7 Btu/sec-ft^2 and $(\varphi_{B.O.})_{th}$ = 316.5 Btu/sec-ft^2 .

Therefore in order to avoid underly iterations, in the analysis of the present burnout tests the experimental-theoretical burnout flux has been computed $\varphi_{T,S}$ instead of the theoretical burnout flux $(\varphi_{B.O.})_{th}$; the former value can be compared with the experimental burnout flux φ^* .

APPENDIX 3

SOME REMARKS ON THE FLOW AND ENTHALPY REDISTRIBUTION IN THE SECTION SUBCHANNELS AND THEIR INFLUENCE ON DNB RATIO

The flow redistribution between the various subchannels both in the 8-subchannels and in the 10-subchannels schematization is mainly due to a geometrical reason, that is to the differences in the subchannels hydraulic diameter.

The differences in heating and thermal hydraulic regimes between the various subchannels have a secondary effect on the flow redistribution. So, for every burnout test, the subchannel outlet mass velocities G_{out} (and more generally the plottings of axial mass velocity versus axial position) vary around <u>two</u> values (or profiles) in the 8-subchannels schematization: in fact in this schematization there are two different hydraulic diameter,

$\left[De_h^{(8)} \right]^{(I)}$ relative to subchannels 1, 2, 3, 6, 7, 8

$\left[De_h^{(8)} \right]^{(II)}$ relative to subchannels 4,5.

In the same way, in the 10-subchannels schematization the subchannel outlet mass velocities vary around <u>three</u> different values, corresponding to the three different hydraulic diameters

$\left[De_h^{(10)} \right]^{(I)}$ relative to subchannels 1, 2, 9, 10

$\left[De_h^{(10)} \right]^{(II)}$ relative to subchannels 3, 4, 7, 8

$\left[De_h^{(10)} \right]^{(III)}$ relative to subchannels 5, 6.

In both schematizations the small differences between the axial mass velocity of two subchannels with equal hydraulic diameter are due to differences in thermal-hydraulic regimes and coolant density: namely the friction pressure drops of two subchannel length increments having equal inlet velocity and temperature are different if the two increments are in different regimes (non boiling, local boiling and bulk boiling) or if the two subchannels have different heating (in this case also the elevation and acceleration pressure drops are different).

So for example in the RUN 28 (19-7-67) with heat flux only on the burnout rod (see Table III - Appendix 4) the subchannel outlet mass velocity vary around the following values:

300 ; 350 lbm/sec-ft^2 (in the 8-subchannels schematization)

250 ; 300 ; 350 lbm/sec-ft^2 (in the 10-subchannels schematization)

as it can be been from Table III Results.

Subchannels 4 and 7 in the 10-sybchannels schematization have equal hydraulic diameters, but different outlet mass velocities: 357.4 and 349.1 lbm/sec-ft^2. In fact subchannel 4 is in local boiling condition and subchannel 7 in non boiling condition.

The mass velocity distribution among the various subchannels depends on the schematization used. However average values on an area covering several subchannels are nearly the sames, as physically it must be.

So, for example, always in RUN-28, denoting with A the left quarter of the test section flow area (see figure 2) and with B the right quarter of the same, the average values of mass velocity (in lbm/sec-ft^2) in the two schematizations have the following values:

schematization	8 subchannels	10 subchannels
region A	309.9	305.2
region B	298.6	304.2

Local values, however, show relatively large difference in the two schematizations: so un the quoted example the mass velocity in subchannel 1 and 3 of 10-S.C.S.(*)has the value 257.0 and 353.5 lbm/sec-ft^2 respectively, while in subchannel 1 of 8-S.C.S. the mass velocity is 309.6, a value that is nearly the arithmetic mean of the two above values, as it must physically be.

(*) - S.C.S. stands shortly for Sub Channel Schematization.

The outlet enthalpy distributions derived from the two schematizations show differences similar to those indicated by the outlet mass velocity. The reason of these differences is the different importance that has the turbolent heat diffusion in the two schematization. The 10-S.C.S. is much more sensitive than the 8-S.C.S. to a variation of the thermal diffusion coefficient χ : this fact, already observed in Section 2, has been better stressed in figures [16a] and [16b,] that show the axial variation of enthalpy rise in subchannels 3 and 8 of 10-S.C.S. The case considered is the heating RUN 1 bis (9-11-66), already analyzed in Section 2. It can be observed this fact: considering a closed channel with a flow area equal to half test section flow area, a constant mass velocity equal to inlet mass velocity and the power delivered by the burnout rod, the straight line axial variation of enthalpy rise shown by the dotted line in figure [16b] has been obtained; the open channel theoretical axial variation of enthalpy rise more close with the above straight line has been obtained with a value of the thermal diffusion coefficient equal to 1.46×10^{-2}. The closed channel outlet enthalpy is not too different by the experimental outlet enthalpy.

This simplified closed channel approach gives zero enthalpy rise on the other half of the test section (that enclosing the cold adjacent rod), and this is not correct.

Average values of outlet enthalpy on an area covering several subchannels are nearly the sames in the two schematizations, as for outlet mass velocity; this is shown in the table below always for RUN 28

schematization	8 subchannels	10 subchannels
region A	550.9	548.2
region B	462.8	466.5

With this enthalpy and flow redistribution, the following departure nucleate boiling ratios R_{DNB} have been obtained

- R_{DNB} with infinite matrix hydraulic diameter, 8-S.C.S., subch. 1 ; 0.9723

- R_{DNB} in 10-S.C.S., subch. 3 (in this subchannel the thermal diameter is equal to the hydraulic diameter). 0.9930

Remark. - The two results are comparable; 10-S.C.S. gives an higher enthalpy and an higher mass velocity (94.5 Btu/lbm and 353.5 lbm/sec-ft^2 against 93.3 Btu/lbm and 309.6 lbm/sec-ft^2). The higher enthalpy gives a lower burn out flux and the higher mass velocity an higher burnout flux according to W-3 correlation; so the two effects are contrary, and the net result is an higher burnout flux furnished by the 10-S.C.S.

- R_{DNB} with total hydraulic diameter in subch. 1 of 8-S.C.S. (the rectilinear strips are included in the wetted perimeter); 1.2270

- R_{DNB} with thermal equivalent diameter in subch. 1 of 8-S.C.S. (remember that in this run there is heat flux only on the burnout rod). 0.6656

Remark. - The thermal equivalent diameter (0.9708 in) in such. 1 of 8-S.C.S. when the shell is unheated is outside the range of validity of W-3 burnout correlation (0.2 ÷ 0.7 in).

In fact we have verified that in a closed circular tube with values of hydraulic diameter and length close to present subch. 1 value, the W-3 correlation predicts a burnout flux lower by nearly 40%.

It can be observed that, taking into account this underprediction of the W-3 correlation, the above value 0.66 of the R_{DNB} in subch. 1 of 8-S.C.S. using the thermal diameter in a shell unheated burnout test approaches the correct value 1. However we prefer to analyze all the burnout test (both with shell heated and unheated) using the approach described in Section 4: that is infinite matrix equivalent diameter along with local quality and mass velocity in W-3 burnout correlation.

This approach seems to be more correct than that of using W-3 correlation in a range of equivalent diameter where this correlation is not valid, and next correcting the obtained DNBR by taking into account the underprediction of the W-3 correlation in a closed tube burnout test with nearly equal value of equivalent diameter and length. Moreover must be added that not always such a closed tube burnout test is available in literature.

The R_{DNB} values on the other side of the burnout rod (the side close to adjacent rod) are as follows:

- R_{DNB} with hydraulic diameter in subchannel 4 of 8-S.C.S.; 1.036

- R_{DNB} in subchannel 4 of 10-S.C.S. (in this subch. the thermal diameter is equal to the hydraulic diameter); 1.027

- R_{DNB} with thermal equivalent diameter of subchannel 4 in 8-S.C.S. (no flux on the shell). 0.7086

The above trend of results and relative remarks are not peculiar of the particular burnout and heating tests here analyzed, but in general apply to all the studied cases.

A P P E N D I X 4

TABLES OF HEATING AND BURNOUT TEST ANALYSIS RESULTS

In this section the numerical results of the calculations described in the text are presented.

For every burnout test (designated with the number and the date of the run), the experimental conditions are first listed and next the more interesting results are reported. In the following tables, the following symbols have been used:

χ = thermal diffusion coefficient

$\Delta H_{H.B.}$ = thermal balance enthalpy rise (total power given to the test section / total mass flow rate) Btu/lbm

ΔH = enthalpy rise in every subchannel (Btu/lbm)

X = outlet quality in every subchannel (%)

G_{out} = outlet mass velocity in every subchannel ($lbm/sec-ft^2$)

R_{DNB} = departure nucleate boiling ratio in every subchannel (burnout flux / effective heat flux)

ϕ_{DNB} = experimental burnout flux ($Btu/sec-ft^2$)

$\phi_{calc.}$ = calculated burnout flux ($Btu/sec-ft^2$)

$T_{out\ theor.}$ = average outlet temperature in every subchannel, theoretically calculated (°F)

$T_{out\ eff.}$ = outlet temperature experimentally measured (remember that the corresponding thermocouples are placed in the points T_1, T_2, T_4, T_5 of figure 1)

H_{out} = calculated outlet enthalpy (Btu/lbm).

This is the list of the tables below reported :

Table I - Analysis of heating RUN 1 bis (9-11-66).

Table II - Analysis of heating RUN 2 (10-11-66).

Table III - Experimental conditions and detailed results of burnout tests of group A (burnout test with heat flux only on the burnout rod).
The following runs have been analyzed:
- RUN 28 (19-7-67)
- RUN 18 (21-2-67)
- RUN 56 (9-12-66)
- RUN 45 (7-12-66)
- RUN 45 (26-7-67)
- RUN 90 (7-12-67)
- RUN 28 (9-12-67)
- RUN 58 (26-7-67)
- RUN 74 (7-12-66)
- RUN 64 (21-2-67)
- RUN 49 (9-12-66)
- RUN 50 (21-2-67)
- RUN 6 (21-2-67)

Table IV - Experimental conditions and detailed results of burnout tests of group B (burnout tests with different heating on the burnout rod and on the adjacent rod).
The following runs have been analyzed:
- RUN 22 (21-7-67)
- RUN 16 (24-7-67)
- RUN 89 (21-7-67)
- RUN 58 (21-7-67)
- RUN 48 (21-7-67)
- RUN 81 (21-7-67)
- RUN 40 (21-7-67)

Table V - Experimental conditions and detailed results of burnout test of group C (burnout tests with different heating on the burnout rod and on the shell).
The following runs have been analyzed:
- RUN 40 (13-7-67)
- RUN 16 (13-7-67)
- RUN 53 (3-7-67)
- RUN 47 (13-7-67)
- RUN 35 (3-7-67)
- RUN 6 (3-7-67)

Table VI - Experimental conditions and detailed results of burnout tests of group D (burnout tests with different heating on the burnout rod, on the adjacent rod and on the shell).
The following runs have been analyzed:
- RUN 10 (19-1-67)
- RUN 37 (19-1-67)
- RUN 91 (17-1-67)
- RUN 50 (14-7-67)
- RUN 22 (18-1-67)
- RUN 24 (19-1-67)
- RUN 40 (17-1-67)
- RUN 117 (17-1-67)
- RUN 47 (18-1-67)
- RUN 38 (18-1-67)

Table VII - Results of flux parametrical analysis of RUN 64 (21-2-67); $\chi = 1.46 \times 10^{-2}$; subchannel 3 in the 10 subchannels schematization.

Table VIII - Results of flux parametrical analysis of RUN 90 (7-12-66); $\chi = 1.46 \times 10^{-2}$; subchannel 3 in the 10 subchannels schematization.

T A B L E I - ANALYSIS OF HEATING RUN 1 bis (9-11-66)

Pressure	= 1764 psi	Total power	= 29,85 Btu/sec
Inlet mass velocity	= 341,39 lbm/sec.ft^2	Burnout rod power	= 0 Btu/sec
Inlet enthalpy	= 381,33 Btu/lbm	Adjacent rod power	= 29,85 Btu/sec
$\Delta H_{H.B.}$	= 20,5 Btu/lb	Shell power	= 0 Btu/sec

Schematization with 8 subchannels

$\chi = 7.5 \times 10^{-3}$;

	1	2	3	4	5	6	7	8
ΔH ($\frac{Btu}{lb}$)	0,1	0,8	0,8	8,6	30,4	40,2	40,2	41,2
G_{out} ($\frac{lbm}{s.ft^2}$)	319,9	319,8	319,8	372,7	385,5	337,8	337,8	337,7
$T_{out\ theor.}$ (°F)	404,4			412,3	432,6			442,5
$T_{out\ eff.}$ (°F)	408,5			414,8	438,2			443,3

$\chi = 2.66 \times 10^{-2}$;

	1	2	3	4	5	6	7	8
ΔH ($\frac{Btu}{lb}$)	1,7	4,1	4,1	13,7	26,1	36,8	36,8	39,4
G_{out} ($\frac{lbm}{s.ft^2}$)	319,7	319,6	319,6	372,4	385,7	338,0	338,0	337,0
$T_{out\ theor.}$ (°F)	405,8			417,1	428,7		440,8	
$T_{out\ eff.}$ (°F)	408,5			414,8	438,2		443,3	

Continuation of TABLE I - ANALYSIS OF HEATING RUN 1 bis (9-11-66)

Schematization with 8 subchannels

$\chi = 0.$;

	1	2	3	4	5	6	7	8
ΔH ($\frac{Btu}{lb}$)	0	0	0	0	38,2	41,3	41,3	41,3
G_{out} ($\frac{lbm}{s.ft^2}$)	319,9	319,9	319,9	373,5	384,7	337,7	337,7	337,7
$T_{out\ theor.}$ (°F)	404,4			404,4	439,5			442,7
$T_{out\ eff.}$ (°F)	408,5			414,8	438,2			443,3

$\chi = 1.46 \times 10^{-2}$;

	1	2	3	4	5	6	7	8
ΔH ($\frac{Btu}{lb}$)	0,5	2,1	2,1	11,5	27,9	38,8	38,8	40,7
G_{out} ($\frac{lbm}{s.ft^2}$)	319,8	319,7	319,7	372,5	385,6	337,9	337,9	337,7
$T_{out\ theor.}$ (°F)	404,8		415	430,2			441,9	
$T_{out\ eff.}$ (°F)	408,5		414,8	438,2			443,3	

$\chi = 3.26 \times 10^{-2}$;

	1	2	3	4	5	6	7	8
ΔH ($\frac{Btu}{lb}$)	2,4	4,9	4,9	14,3	25,6	35,9	35,9	38,6
G_{out} ($\frac{lbm}{s.ft^2}$)	319,6	319,5	319,5	372,3	385,7	338,1	338,1	337,9
$T_{out\ theor.}$ (°F)	406,6			417,7	428,2			440,1
$T_{out\ eff.}$ (°F)	408,5			414,8	438,2			443,3

Continuation of TABLE I - ANALYSIS OF HEATING RUN 1 bis (9-11-66)

Schematization with 10 subchannels

$\gamma = 7.5 \times 10^{-3}$

	1	2	3	4	5	6	7	8	9	10
ΔH $(\frac{Btu}{lb})$	0,6	0,6	1,3	7,8	15,9	15,9	38,9	46,5	32,8	32,8
$G_{out}(\frac{lbm}{s.ft^2})$	276,6	276,6	376,9	377,2	323,6	323,6	389,3	387,2	276,4	276,4
$T_{out\ theor.}$ (°F)			405,5	411,6			440,6	447,2		
$T_{out\ eff.}$ (°F)			408,5	414,8			438,2	443,3		

$\gamma = 2.66 \times 10^{-2}$

	1	2	3	4	5	6	7	8	9	10
ΔH $(\frac{Btu}{lb})$	5,3	5,3	6,5	14,2	19,1	19,1	28,3	36,5	33,6	33,6
$G_{out}(\frac{lbm}{s.ft^2})$	276,3	276,3	376,3	376,7	323,5	323,5	389,6	387,8	276,9	276,9
$T_{out\ theor.}$ (°F)			410,5	407,4			430,6	438,2		
$T_{out\ eff.}$ (°F)			408,5	414,8			438,2	443,3		

Continuation of TABLE I - ANALYSIS OF HEATING RUN 1 bis (9-11-66)

Schematization with 10 subchannels

$\chi = 0.$

	1	2	3	4	5	6	7	8	9	10
ΔH $(\frac{Btu}{lb})$	0	0	0	0	0	0	72,8	73	0	0
G_{out} $(\frac{lbm}{s.ft^2})$	277,3	277,3	377,6	378,5	324,8	324,8	385,8	384,6	277,3	277,3
$T_{out\ theor.}$ (°F)			404,4	404,4			470,9	471,0		
$T_{out\ eff.}$ (°F)			408,5	414,8			438,2	443,3		

$\chi = 1.46 \times 10^{-2}$

	1	2	3	4	5	6	7	8	9	10
ΔH $(\frac{Btu}{lb})$	2,3	2,3	3,4	11,5	18,0	18,0	32,2	41,2	34,9	34,9
G_{out} $(\frac{lbm}{s.ft^2})$	276,4	276,4	376,6	376,9	323,5	323,5	389,5	387,5	276,7	276,7
$T_{out\ theor.}$ (°F)			407,5	415,1			434,3	442,6		
$T_{out\ eff.}$ (°F)			408,5	414,8			438,2	443,3		

$\chi = 3.26 \times 10^{-2}$

	1	2	3	4	5	6	7	8	9	10
ΔH $(\frac{Btu}{lb})$	6,7	6,7	7,8	14,9	19,4	19,4	27,2	34,9	32,7	32,7
G_{out} $(\frac{lbm}{s.ft^2})$	276,3	276,3	376,2	376,7	323,5	323,5	389,6	387,9	277,0	277,0
$T_{out\ theor.}$ (°F)			411,6	418,4			429,6	436,7		
$T_{out\ eff.}$ (°F)			408,5	414,8			438,2	443,3		

T A B L E II - ANALYSIS OF HEATING RUN 2 (10-11-66)

Pressure	= 1607 psi	Total power	= 28,89 Btu/sec
Inlet mass velocity	= 625,67 lbm/sec.ft^2	Burnout rod power	= 28,89 Btu/sec
Inlet enthalpy	= 364,7 Btu/lbm	Adjacent rod power	= 0 Btu/sec
$\Delta H_{H.B.}$	= 10,84 Btu/lbm	Shell power	= 0 Btu/sec

Schematization with 8 subchannels

$\gamma = 7.5 \times 10^{-3}$;

	1	2	3	4	5	6	7	8
ΔH ($\frac{Btu}{lb}$)	21,9	21,4	21,4	16,1	4,5	0,4	0,4	0,0
G_{out} ($\frac{lbm}{s.ft^2}$)	611,1	611,2	611,2	698,2	686,7	595,5	595,5	595,6
$T_{out\ theor.}$ (°F)	409,4			404,0	393,1		389,0	
$T_{out\ eff.}$ (°F)	411,2			408,2	393,8		392,0	

$\gamma = 2.66 \times 10^{-2}$

	1	2	3	4	5	6	7	8
ΔH ($\frac{Btu}{lb}$)	20,9	19,5	19,5	13,8	7,2	2,1	2,1	0,9
G_{out} ($\frac{lbm}{s.ft^2}$)	611,3	611,6	611,6	698,8	686,1	595,1	595,1	595,4
$T_{out\ theor.}$ (°F)	408,6			401,8	395,7		389,7	
$T_{out\ eff.}$ (°F)	411,2			408,2	393,8		392	

Continuation of TABLE II - ANALYSIS OF HEATING RUN 2 (10-11-66)

Schematization with 8 subchannels

$\gamma = 0.$;

	1	2	3	4	5	6	7	8
ΔH ($\frac{Btu}{lb}$)	21,9	21,9	21,9	20,4	0,0	0,0	0,0	0,0
G_{out} ($\frac{lbm}{s.ft^2}$)	611,0	611,0	611,0	697,0	687,9	595,7	595,7	595,7
$T_{out\ theor.}$ (°F)	409,4			408,1	389,0		389,0	
$T_{out\ eff.}$ (°F)	411,2			408,2	393,8		392,0	

$\gamma = 1.46 \times 10^{-2}$

	1	2	3	4	5	6	7	8
ΔH ($\frac{Btu}{lb}$)	21,6	20,66	20,66	14,8	6,0	1,1	1,1	0,3
G_{out} ($\frac{lbm}{s.ft^2}$)	611,1	611,4	611,4	698,5	686,4	595,4	595,4	595,6
$T_{out\ theor.}$ (°F)	409,1			402,9	394,6			389,2
$T_{out\ eff.}$ (°F)	411,2			408,2	393,8			392,0

$\gamma = 3.26 \times 10^{-2}$

	1	2	3	4	5	6	7	8
ΔH ($\frac{Btu}{lb}$)	20,5	19,11	19,11	13,6	7,5	2,6	2,6	1,2
G_{out} ($\frac{lbm}{s.ft^2}$)	611,4	611,7	611,7	698,8	686,0	595,0	595,0	595,3
$T_{out\ theor.}$ (°F)	408,2			401,6	396,0			390,3
$T_{out\ eff.}$ (°F)	411,2			408,2	393,8			392,0

Continuation of TABLE II - ANALYSIS OF HEATING RUN 2 (10-11-66)

Schematization with 10 subchannels

$\chi = 7.5 \times 10^{-3}$

	1	2	3	4	5	6	7	8	9	10
ΔH $(\frac{Btu}{lb})$	17,3	17,3	24,7	20,7	8,4	8,4	4,1	0,7	0,3	0,3
$G_{out}(\frac{lbm}{s.ft^2})$	513,8	513,8	697,8	700,8	597,7	597,7	690,9	690,1	516,3	516,3
$T_{out\ theor.}$ (°F)		412	408,3			392,8	389,5			
$T_{out\ eff.}$ (°F)		411,2	408,2			393,8	392			

$\chi = 2.66 \times 10^{-2}$

	1	2	3	4	5	6	7	8	9	10
ΔH $(\frac{Btu}{lb})$	17,8	17,8	19,3	15,0	10,1	10,1	7,5	3,4	2,8	2,8
$G_{out}(\frac{lbm}{s.ft^2})$	514,0	514,0	699,1	702,1	597,4	597,4	690,0	689,3	515,8	515,8
$T_{out\ theor.}$ (°F)			407,0	403,0			395,9	392,2		
$T_{out\ eff.}$ (°F)			411,2	408,2			393,8	392		

Continuation of TABLE II - ANALYSIS OF HEATING RUN 2 (10-11-66)

Schematization with 10 subchannels

$\gamma = 0.$

	1	2	3	4	5	6	7	8	9	10
ΔH ($\frac{Btu}{lb}$)	0	0	39,1	39	0	0	0	0	0	0
G_{out} ($\frac{lbm}{s.ft^2}$)	516,6	516,6	694,0	695,8	599,6	599,6	692,2	690,5	516,6	516,6
$T_{out\ theor.}$ (°F)			425,3	425,1			388,9	388,9		
$T_{out\ eff.}$ (°F)			411,2	408,2			393,8	392		

$\gamma = 1.46 \times 10^{-2}$

	1	2	3	4	5	6	7	8	9	10
ΔH ($\frac{Btu}{lb}$)	18,5	18,5	21,8	17,1	9,5	9,5	6,1	1,8	1,2	1,2
G_{out} ($\frac{lbm}{s.ft^2}$)	513,8	513,8	698,5	701,6	597,5	597,5	690,3	689,8	516,1	516,1
$T_{out\ theor.}$ (°F)			409,4	404,9			394,7	390,7		
$T_{out\ eff.}$ (°F)			411,2	408,2			393,8	392		

$\gamma = 3.26 \times 10^{-2}$

	1	2	3	4	5	6	7	8	9	10
ΔH ($\frac{Btu}{lb}$)	17,3	17,3	18,5	14,4	10,2	10,2	7,9	4,1	3,5	3,5
G_{out} ($\frac{lbm}{s.ft^2}$)	514,1	514,1	699,3	702,2	597,3	597,3	689,9	689,2	515,7	515,7
$T_{out\ theor.}$ (°F)			406,3	402,6			396,6	392,8		
$T_{out\ eff.}$ (°F)			411,2	408,2			393,8	392		

REFERENCES

[1] - A. Campanile (and others) - Forced convection burnout and hydrodynamic instability experiments for water at high pressure - Part IV: Burnout experiments in a double channel test section with transversely varying heat generation; SORIN Report T/519 (1967) (to be published as EUR Report).

[2] - W. Zernich (and others) - "THINC" A Thermal Hydrodynamic Interaction Code for a Semi-Open or Closed Channel Core, WCAP-3704; Westinghouse Electric Corporation, Atomic Power Department, Pittsburgh, Pennsylvania, February 1962.

[3] - J.E. Meyer - Conservation Laws in One-Dimensional Hydrodynamics, WAPD-BT-20, pp. 61-72 (September 1960).

[4] - Mendler, O.J., et al.- Natural Circulation Tests with Water at 800 to 2000 psia under Non-Boiling, Local Boiling, and Bulk Boiling Conditions, ASME Paper 60-HT-36, 1960.

[5] - Lottes, P.A.- Nuclear Reactor Heat Transfer, ANL-6469, December 1961, Figures 10-3, 10-4.

[6] - M. Debernardi, A. Valtancoli - Determinazione sperimentale del coefficiente di diffusità turbolenta in un fascio di barre con e senza griglie distanziatrici - Rapporto FIAT-GN-50.

[7] - A. Garro, C.D'Urso - Analisi teorica del fattore di mescolamento di massa in un fascio di barre a reticolo quadrato - Rapporto FIAT-GN-43.

[8] - Dean, R.A.- Coolant Mixing in Open Lattice Reactor Cores, WCAP-3735, August 1963.

[9] - F. Biancone (and others) - Forced convenction burnout and hydrodynamic instability experiments for water at high pressure - Part I: presentation of data for round tubes with uniform and non uniform power distribution - Report EUR 2498.e (August 1965).

[10] - L.S. Tong - Prediction of departure from nucleate boiling for an axially non-uniform heat flux distribution, J. Nucl. Energy 21 (1967).

[11] - F. Van der Walle - Theoretical determination of bubble flow characteristics in a vertical boiler - Rescona - Report 66-311 - October 1966.

T A B L E III

EXPERIMENTAL CONDITIONS AND DETAILED RESULTS OF BURNOUT TESTS OF GROUP A (BURNOUT TESTS WITH HEAT FLUX ONLY ON THE BURNOUT ROD)

The following runs have been analyzed:

- RUN 28 (19-7-67)
- RUN 58 (26-7-67)
- RUN 18 (21-2-67)
- RUN 74 (7-12-66)
- RUN 56 (9-12-66)
- RUN 64 (21-2-67)
- RUN 45 (7-12-66)
- RUN 49 (9-12-66)
- RUN 45 (26-7-67)
- RUN 50 (21-2-67)
- RUN 90 (7-12-67)
- RUN 6 (21-2-67)
- RUN 28 (9-12-67)

RUN 28 (19-7-67)

Pressure	= 1877 psi	Total power	= 62,9 Btu/sec
Inlet mass velocity	= 315,82 lbm/sec.ft^2	Burnout rod power	= 62,9 Btu/sec
Inlet enthalpy	= 459,8 Btu/lbm	Adjacent rod power	= 0 Btu/sec
γ	= 1,4624 x 10^{-2}	Shell power	= 0 Btu/sec

$\Delta H_{H.B.}$ = 46.8 Btu/lbm

Schematization with 10 subchannels

	1	2	3	4	5	6	7	8	9	10
ΔH $(\frac{Btu}{lb})$	80	80	94,5	73,8	41,2	41,2	26,3	7,9	5,2	5,2
X (%)			- 21,1							
G_{out} $(\frac{lbm}{s.ft^2})$	257	257	353,5	357.4	300,4	300,4	349,1	350,0	258,4	258,4
R_{DNB}			0,993	1,027						
ϕ_{DNB} $(\frac{Btu}{s.ft^2})$			308,9	308,9						
$\phi_{calc.}$ $(\frac{Btu}{s.ft^2})$			306,7	317,2						

Schematization with 8 subchannels

	1	2	3	4	5	6	7	8
ΔH $(\frac{Btu}{lb})$	93,3	89	89	63,8	26,3	4,9	4,9	1,2
X (%)	- 21,4							
G_{out} $(\frac{lbm}{s.ft^2})$	309,6	310,3	310,3	354,7	345,5	298,5	298,5	298,8
R_{DNB}	0,971	0,978	0,978	1,036				
ϕ_{DNB} $(\frac{Btu}{s.ft^2})$	308,9	308,9	308,9	308,9				
$\phi_{calc.}$ $(\frac{Btu}{s.ft^2})$	299,9	302,1	302,1	320,0				

RUN 58 (26-7-67)

Pressure	= 1877 psi	Total power	= 44,93 Btu/sec
Inlet mass velocity	= 102,614 $lbm/sec.ft^2$	Burnout rod power	= 44,93 Btu/sec
Inlet enthalpy	= 441,5 Btu/lbm	Adjacent rod power	= 0 Btu/sec
χ	= $1,4624 \times 10^{-2}$	Shell power	= 0 Btu/sec

$\Delta H_{H.B.}$ = 103. Btu/lbm

Schematization with 10 subchannels

	1	2	3	4	5	6	7	8	9	10
ΔH $(\frac{Btu}{lb})$	161,1	161,1	186,9	150,4	89,7	89,7	58,5	18,7	13	13
X (%)			- 5,9							
G_{out} $(\frac{lbm}{s.ft^2})$	104	104	142,9	140,8	96,3	96,3	101,5	90,3	48,4	48,4
R_{DNB}			0,951	1,055						
ϕ_{DNB} $(\frac{Btu}{s.ft^2})$			221	221						
$\phi_{calc.}$ $(\frac{Btu}{s.ft^2})$			210,1	233,1						

Schematization with 8 subchannels

	1	2	3	4	5	6	7	8
ΔH $(\frac{Btu}{lb})$	186,2	176,9	176,9	130,3	58,8	12,0	12,0	3,1
X (%)	- 6,09							
G_{out} $(\frac{lbm}{s.ft^2})$	125,8	126,4	126,4	134,5	104	68,8	68,8	65,8
R_{DNB}	0,957	0,983	0,983	1,072				
ϕ_{DNB} $(\frac{Btu}{s.ft^2})$	221	221	221	221				
$\phi_{calc.}$ $(\frac{Btu}{s.ft^2})$	211,4	217,2	217,2	236,9				

RUN 18 (21-2-67)

Pressure	= 1877 psi	Total power	= 47,02 Btu/sec
Inlet mass velocity	= 104,802 lbm/sec·ft^2	Burnout rod power	= 47,02 Btu/sec
Inlet enthalpy	= 440,105 Btu/lbm	Adjacent rod power	= 0 Btu/sec
χ	= 1.4624 x 10^{-2}	Shell power	= 0 Btu/sec

$\Delta H_{H.B.}$ = 105.4 Btu/lbm

Schematization with 10 subchannels

	1	2	3	4	5	6	7	8	9	10
ΔH ($\frac{Btu}{lb}$)	165,3	165,3	191,9	154,3	91,8	91,8	59,9	19,1	13,2	13,2
X (%)			- 5,2							
G_{out} ($\frac{lbm}{s.ft^2}$)	105,83	105,83	144,63	143,17	98,49	98,49	104,1	93	50,65	50,65
R_{DNB}			0,902	1,006						
ϕ_{DNB} ($\frac{Btu}{s.ft^2}$)			231,06	231,06						
$\phi_{calc.}$ ($\frac{Btu}{s.ft^2}$)			208,41	232,44						
$T_{out\ theor.}$ (°F)			611	585,2			510,7	475,2		
$T_{out\ eff.}$ (°F)			566,9	562,8			536,3	473,9		

Schematization with 8 subchannels

	1	2	3	4	5	6	7	8
ΔH ($\frac{Btu}{lb}$)	191,16	181,6	181,6	133,7	60,12	12,26	12,26	3,19
X (%)	- 5,3							
G_{out} ($\frac{lbm}{s.ft^2}$)	127,17	128,02	128,02	137,11	106,66	71,43	71,43	68,55
R_{DNB}	0,909	0,935	0,935	1,030				
ϕ_{DNB} ($\frac{Btu}{s.ft^2}$)	231,06	231,06	231,06	231,06				
$\phi_{calc.}$ ($\frac{Btu}{s.ft^2}$)	210,03	216,04	216,04	237,99				
$T_{out\ theor.}$ (°F)	610,2			570	511			461,22
$T_{out\ eff.}$ (°F)	566,9			562,8	536,3			473,9

RUN 74 (7-12-66)

Pressure	= 1849 psi	Total power	= 40,85 Btu/sec
Inlet mass velocity	= 105,896 lbm/sec.ft^2	Burnout rod power	= 40,85 Btu/sec
Inlet enthalpy	= 505,93 Btu/lbm	Adjacent rod power	= 0 Btu/sec
χ	= 1,4624 x 10^{-2}	Shell power	= 0 Btu/sec

$\Delta H_{H.B.}$ = 90.7 Btu/lbm

Schematization with 10 subchannels

	1	2	3	4	5	6	7	8	9	10
ΔH ($\frac{Btu}{lb}$)				145,2	79,4	79,4	51,5	16,1	10,9	10,9
X (%)	1,0	1,0	7,1							
G_{out} ($\frac{lbm}{s.ft^2}$)	108,3	108,3	113,9	111,6	109,1	109,1	117,5	108,4	69,1	69,1
R_{DNB}			0,802	0,9						
ϕ_{DNB} ($\frac{Btu}{s.ft^2}$)			200,78	200,78						
$\phi_{calc.}$ ($\frac{Btu}{s.ft^2}$)			161	180,7						

Schematization with 8 subchannels

	1	2	3	4	5	6	7	8
ΔH ($\frac{Btu}{lb}$)	199,5	185,8	185,8	126,5	50,1	9,7	9,7	2,6
X (%)	10,4							
G_{out} ($\frac{lbm}{s.ft^2}$)	98,8	98,8	98,8	113,7	131,8	102,1	102,1	100,8
R_{DNB}	0,774	0,808	0,808	0,951				
ϕ_{DNB} ($\frac{Btu}{s.ft^2}$)	200,78	200,78	200,78	200,78				
$\phi_{calc.}$ ($\frac{Btu}{s.ft^2}$)	155,4	162,23	162,23	190,94				

RUN 64 (21-2-67)

Pressure	= 1892 psi	Total power	= 67,49 Btu/sec
Inlet mass velocity	= 313,947 lbm/sec.ft^2	Burnout rod power	= 67,49 Btu/sec
Inlet enthalpy	= 446,6 Btu/lbm	Adjacent rod power	= 0 Btu/sec
χ	= 1,4624 x 10^{-2}	Shell power	= 0 Btu/sec

$\Delta H_{H.B.}$ = 50.55 Btu/lbm

Schematization with 10 subchannels

	1	2	3	4	5	6	7	8	9	10
ΔH ($\frac{Btu}{lb}$)	86,4	86,4	102,12	79,7	44,5	44,5	28,4	8,5	5,7	5,7
X (%)			- 22,8							
G_{out} ($\frac{lbm}{s.ft^2}$)	255,4	255,4	351,5	355,6	298,6	298,6	347	348	256,6	256,6
R_{DNB}			0,941	0,974						
ϕ_{DNB} ($\frac{Btu}{s.ft^2}$)			331,7	331,7						
$\phi_{calc.}$ ($\frac{Btu}{s.ft^2}$)			312,1	323						
$T_{out\ theor.}$ (°F)			550,7	532,7			489,2	471,6		
$T_{out\ eff.}$ (°F)			546,2	543,2			500,3	472,1		

Schematization with 8 subchannels

	1	2	3	4	5	6	7	8
ΔH ($\frac{Btu}{lb}$)	100,7	96,15	96,15	68,98	28,4	5,31	5,31	1,36
X (%)	- 23,1							
G_{out} ($\frac{lbm}{s.ft^2}$)	307,9	308,5	308,5	352,8	343,5	296,6	296,6	296,9
R_{DNB}	0,919	0,925	0,925	0,982				
ϕ_{DNB} ($\frac{Btu}{s.ft^2}$)	331,7	331,7	331,7	331,7				
$\phi_{calc.}$ ($\frac{Btu}{s.ft^2}$)	304,8	306,8	306,8	325,7				
$T_{out\ theor.}$ (°F)	549,4			523,7	489,2			465,2
$T_{out\ eff.}$ (°F)	546,2			543,2	500,3			472,1

RUN 56 (9-12-66)

Pressure	= 1863 psi	Total power	= 32,23 Btu/sec
Inlet mass velocity	= 105,099 lbm/sec.ft^2	Burnout rod power	= 32,23 Btu/sec
Inlet enthalpy	= 583,11 Btu/lbm	Adjacent rod power	= 0 Btu/sec
χ	= 1,4624 x 10^{-2}	Shell power	= 0 Btu/sec

$\Delta H_{H.B.}$ = 72.1 Btu/lbm

Schematization with 10 subchannels

	1	2	3	4	5	6	7	8	9	10
ΔH ($\frac{Btu}{lb}$)	120,7	120,7	141,7	109,9	62,3	62,3	40,5	12,6	8,5	8,5
X (%)	9,48	9,48	13,7	7,27						
G_{out} ($\frac{lbm}{s.ft^2}$)	93,2	93,2	126,0	125,0	104,3	104,3	113,7	106,2	67,7	67,7
R_{DNB}			0,837	0,943						
ϕ_{DNB} ($\frac{Btu}{s.ft^2}$)			158,39	158,39						
$\phi_{calc.}$ ($\frac{Btu}{s.ft^2}$)			132,5	149,3						

Schematization with 8 subchannels

	1	2	3	4	5	6	7	8
ΔH ($\frac{Btu}{lb}$)	145,6	136,5	136,5	96,4	39,7	7,7	7,7	2,0
X (%)	14,6	12,7	12,7	4,4				
G_{out} ($\frac{lbm}{s.ft^2}$)	108,3	109,0	109,0	117,0	120,6	92,6	92,6	91,2
R_{DNB}	0,841	0,872	0,872	0,983				
ϕ_{DNB} ($\frac{Btu}{s.ft^2}$)	158,39	158,39	158,39	158,39				
$\phi_{calc.}$ ($\frac{Btu}{s.ft^2}$)	133,2	138,1	138,1	155,7				

RUN 45 (7-12-66)

Pressure	= 1849 psi	Total power	= 55,17 Btu/sec
Inlet mass velocity	= 300,06 lbm/sec.ft^2	Burnout rod power	= 55,17 Btu/sec
Inlet enthalpy	= 516,68 Btu/lbm	Adjacent rod power	= 0 Btu/sec
χ	= 1,4624 x 10^{-2}	Shell power	= 0 Btu/sec

$\Delta H_{H.B.}$ = 43.2 Btu/lbm

Schematization with 10 subchannels

	1	2	3	4	5	6	7	8	9	10
ΔH ($\frac{Btu}{lb}$)	76,0	76,0	91,5	70,8	38,2	38,2	24,5	7,3	4,9	4,9
X (%)			- 9,3							
G_{out} ($\frac{lbm}{s.ft^2}$)	255,7	255,7	297,3	302,1	298,1	298,1	344,4	345,4	259,0	259,0
R_{DNB}			0,878	0,956						
ϕ_{DNB} ($\frac{Btu}{s.ft^2}$)			271,1	271,1						
$\phi_{calc.}$ ($\frac{Btu}{s.ft^2}$)			238,0	259,1						
$T_{out\ theor.}$ (°F)			596,7	572,1			544,2	525,7		
$T_{out\ eff.}$ (°F)			595	580,2			544,7	530,7		

Schematization with 8 subchannels

	1	2	3	4	5	6	7	8
ΔH ($\frac{Btu}{lb}$)	93,7	88,7	88,7	60,0	24,0	4,5	4,5	1,2
X (%)	- 8,8							
G_{out} ($\frac{lbm}{s.ft^2}$)	250,6	251,8	251,8	323,1	363,3	319,7	319,7	320,1
R_{DNB}	0,859	0,875	0,875	1,008				
ϕ_{DNB} ($\frac{Btu}{s.ft^2}$)	271,1	271,1	271,1	271,1				
$\phi_{calc.}$ ($\frac{Btu}{s.ft^2}$)	232,8	237,2	237,2	273,2				
$T_{out\ theor.}$ (°F)	596,7			572,1	544,2			525,7
$T_{out\ eff.}$ (°F)	608			593,6	545,3			532,4

RUN 49 (9-12-66)

Pressure	= 1884 psi	Total power	= 42 Btu/sec
Inlet mass velocity	= 326,5 lbm/sec.ft^2	Burnout rod power	= 42 Btu/sec
Inlet enthalpy	= 589,2 Btu/lbm	Adjacent rod power	= 0 Btu/sec
γ	= 1,4624 x 10^{-2}	Shell power	= 0 Btu/sec

$\Delta H_{H.B.}$ = 30.2 Btu/lbm

Schematization with 10 subchannels

	1	2	3	4	5	6	7	8	9	10
ΔH ($\frac{Btu}{lb}$)	52,4	52,4	62,6	48,7	26,7	26,7	17,1	5,1	3,41	3,41
X (%)			- 1,3							
G_{out} ($\frac{lbm}{s.ft^2}$)	272,4	272,4	339,2	347,5	318,5	318,5	368,7	369,8	278,2	278,2
R_{DNB}			0,925	0,994						
ϕ_{DNB} ($\frac{Btu}{s.ft^2}$)			206,37	206,37						
$\phi_{calc.}$ ($\frac{Btu}{s.ft^2}$)			190,8	205,1						
$T_{out\ theor.}$ (°F)			624	615,3			593,9	585,3		
$T_{out\ eff.}$ (°F)			621,5	619,3			588,2	585,5		

Schematization with 8 subchannels

	1	2	3	4	5	6	7	8
ΔH ($\frac{Btu}{lb}$)	62,3	59,3	59,3	41,5	16,8	3,1	3,1	0,86
X (%)	- 1,3							
G_{out} ($\frac{lbm}{s.ft^2}$)	292,8	294,7	294,7	360,4	376,3	331,0	331,0	331,4
R_{DNB}	0,926	0,940	0,940	1,036				
ϕ_{DNB} ($\frac{Btu}{s.ft^2}$)	206,37	206,37	206,37	206,37				
$\phi_{calc.}$ ($\frac{Btu}{s.ft^2}$)	191,1	193,9	193,9	213,8				
$T_{out\ theor.}$ (°F)	623,7			610,1	593,5			582,1
$T_{out\ eff.}$ (°F)	621,5			619,3	588,2			585,5

RUN 45 (26-7-67)

Pressure	= 1877 psi	Total power	= 79,7 Btu/sec
Inlet mass velocity	= 467,174 lbm/sec.ft^2	Burnout rod power	= 79,7 Btu/sec
Inlet enthalpy	= 438,84 Btu/lbm	Adjacent rod power	= 0 Btu/sec
χ	= 1,4624 x 10^{-2}	Shell power	= 0 Btu/sec

$\Delta H_{H.B.}$ = 40.1 Btu/lbm

Schematization with 10 subchannels

	1	2	3	4	5	6	7	8	9	10
ΔH ($\frac{Btu}{lb}$)	68,6	68,6	81,2	63,4	35,3	35,3	22,6	6,7	4,5	4,5
X (%)			- 28,2							
G_{out} ($\frac{lbm}{s.ft^2}$)	380,3	380,3	518,6	524,6	445,5	445,5	516,4	518,4	387,8	387,8
R_{DNB}			0,997	1,029						
ϕ_{DNB} ($\frac{Btu}{s.ft^2}$)			391,48	391,48						
$\phi_{calc.}$ ($\frac{Btu}{s.ft^2}$)			390,3	402,8						

Schematization with 8 subchannels

	1	2	3	4	5	6	7	8
ΔH ($\frac{Btu}{lb}$)	80	76,3	76,3	54,8	22,5	4,2	4,2	1,1
X (%)	- 28,4							
G_{out} ($\frac{lbm}{s.ft^2}$)	455,6	456,5	456,5	521,3	511,0	445,2	445,2	445,8
R_{DNB}	0,96	0,965	0,965	1,037				
ϕ_{DNB} ($\frac{Btu}{s.ft^2}$)	391,48	391,48	391,48	391,48				
$\phi_{calc.}$ ($\frac{Btu}{s.ft^2}$)	375,8	377,7	377,7	405,9				

RUN 50 (21-2-67)

Pressure = 1870 psi
Inlet mass velocity = 446,6 lbm/sec.ft^2
Inlet enthalpy = 456,67 Btu/lbm
χ = 1,4624 x 10^{-2}

Total power = 78,68 Btu/sec
Burnout rod power = 78,68 Btu/sec
Adjacent rod power = 0 Btu/sec
Shell power = 0 Btu/sec

$\Delta H_{H.B.}$ = 41.4 Btu/lbm

Schematization with 10 subchannels

	1	2	3	4	5	6	7	8	9	10
ΔH ($\frac{Btu}{lb}$)	71	71	84	65,5	36,5	36,5	23,3	6,9	4,6	4,6
X (%)			-23,7							
G_{out} ($\frac{lbm}{s.ft^2}$)	363,1	363,1	494,6	501,0	425,9	425,9	493,6	495,8	371,0	371,0
R_{DNB}			0,938	0,974						
ϕ_{DNB} ($\frac{Btu}{s.ft^2}$)			386,6	386,6						
$\phi_{calc.}$ ($\frac{Btu}{s.ft^2}$)			362,6	376,5						
$T_{out\ theor.}$ (°F)			544,2	529,3			493,6	479,2		
$T_{out\ eff.}$ (°F)			539,6	535,1			500	478,4		

Schematization with 8 subchannels

	1	2	3	4	5	6	7	8
ΔH ($\frac{Btu}{lb}$)	82,7	79	79	56,7	23,2	4,3	4,3	1,1
X (%)	- 24,0							
G_{out} ($\frac{lbm}{s.ft^2}$)	434,6	435,5	435,5	498,1	488,6	426	426	426,5
R_{DNB}	0,907	0,914	0,914	0,984				
ϕ_{DNB} ($\frac{Btu}{s.ft^2}$)	386,6	386,6	386,6	386,6				
$\phi_{calc.}$ ($\frac{Btu}{s.ft^2}$)	350,6	353,3	353,3	380,4				
$T_{out\ theor.}$ (°F)	543,3			522	493,6			474
$T_{out\ eff.}$ (°F)	539,6			535,1	500			478,4

RUN 90 (7-12-67)

Pressure = 1877 psi
Inlet mass velocity = 434,6 lbm/sec·ft^2
Inlet enthalpy = 507,3 Btu/lbm
χ = 1,4624 x 10^{-2}

Total power = 67,5 Btu/sec
Burnout rod power = 67,5 Btu/sec
Adjacent rod power = 0 Btu/sec
Shell power = 0 Btu/sec

$\Delta H_{H.B.}$ = 36.5 Btu/lbm

Schematization with 10 subchannels

	1	2	3	4	5	6	7	8	9	10
ΔH ($\frac{Btu}{lb}$)	62,6	62,6	74	57,7	32,1	32,1	20,5	6,1	4,1	4,1
X (%)			- 15,6							
G_{out} ($\frac{lbm}{s.ft^2}$)	353,6	353,6	480,8	487,0	414,7	414,7	480,5	483	362,3	362,3
R_{DNB}			0,946	0,989						
ϕ_{DNB} ($\frac{Btu}{s.ft^2}$)			331,7	331,7						
$\phi_{calc.}$ ($\frac{Btu}{s.ft^2}$)			313,7	328,0						
$T_{out\ theor.}$ (°F)			575,7	563,4			533,9	522		
$T_{out\ eff.}$ (°F)			597,2	576,1			532,4	518,9		

Schematization with 8 subchannels

	1	2	3	4	5	6	7	8
ΔH ($\frac{Btu}{lb}$)	73	69,6	69,6	50,0	20,4	3,8	3,8	0,99
X (%)	- 15,8							
G_{out} ($\frac{lbm}{s.ft}$)	422,7	423,7	423,7	484,1	475,5	415,4	415,4	416,0
R_{DNB}	0,925	0,932	0,932	1,003				
ϕ_{DNB} ($\frac{Btu}{s.ft^2}$)	331,7	331,7	331,7	331,7				
$\phi_{calc.}$ ($\frac{Btu}{s.ft^2}$)	306,8	309,1	309,1	332,7				
$T_{out\ theor.}$ (°F)	575			557,3	533,9			517,5
$T_{out\ eff.}$ (°F)	597,2			576,1	532,4			518,9

RUN 6 (21-2-67)

Pressure = 1877 psi
Inlet mass velocity = 450,6 lbm/sec.ft^2
Inlet enthalpy = 587,7 Btu/lbm
X = 1,4624 x 10^{-2}

Total power = 48,16 Btu/sec
Burnout rod power = 48,16 Btu/sec
Adjacent rod power = 0 Btu/sec
Shell power = 0 Btu/sec

$\Delta H_{H.B.}$ = 25.1 Btu/lbm

Schematization with 10 subchannels

	1	2	3	4	5	6	7	8	9	10
ΔH ($\frac{Btu}{lb}$)	43,3	43,3	51,7	40,2	22,1	22,1	14,2	4,2	2,8	2,8
X (%)			- 3,6							
G_{out} ($\frac{lbm}{s.ft^2}$)	374,11	374,11	476,0	485,7	437,0	437,0	504,4	506,6	383,8	383,8
R_{DNB}			0,924	0,990						
ϕ_{DNB} ($\frac{Btu}{s.ft^2}$)			236,6	236,6						
$\phi_{calc.}$ ($\frac{Btu}{s.ft^2}$)			218,6	234,2						
$T_{out\ theor.}$ (°F)			616,0	608,5			590,8	583,5		
$T_{out\ eff.}$ (°F)			613,2	611,0			597,5	584,0		

Schematization with 8 subchannels

	1	2	3	4	5	6	7	8
ΔH ($\frac{Btu}{lb}$)	51,2	48,8	48,8	34,5	14,0	2,6	2,6	0,7
X (%)	- 3,7							
G_{out} ($\frac{lbm}{s.ft^2}$)	414,3	416,4	416,4	496,9	510,6	449,8	449,8	450,4
R_{DNB}	0,918	0,930	0,930	1,028				
ϕ_{DNB} ($\frac{Btu}{s.ft^2}$)	236,6	236,6	236,6	236,6				
$\phi_{calc.}$ ($\frac{Btu}{s.ft^2}$)	217,2	220,0	220,0	243,2				
$T_{out\ theor.}$ (°F)	615,7			604,9	590,5			581,0
$T_{out\ eff.}$ (°F)	613,2			611,0	597,5			584,0

RUN 28 (9-12-67)

Pressure	= 1877 psi	Total power	= 46,16 Btu/sec
Inlet mass velocity	= 466,38 lbm/sec/ft^2	Burnout power	= 46,16 Btu/sec
Inlet enthalpy	= 606,24 Btu/lbm	Adjacent rod power	= 0 Btu/sec
χ	= 1,4624 x 10^{-2}	Shell power	= 0 Btu/sec

$\Delta H_{H.B.}$ = 23.2 Btu/lbm

Schematization with 10 subchannels

	1	2	3	4	5	6	7	8	9	10
ΔH ($\frac{Btu}{lb}$)	40,37	40,37	48,3	37,5	20,5	20,5	13,2	3,9	2,6	2,6
X (%)			- 0,5							
G_{out} ($\frac{lbm}{s.ft^2}$)	389,6	389,6	483,3	492,6	456,0	456,0	525,0	527,3	400,9	400,9
R_{DNB}			0,869	0,932						
ϕ_{DNB} ($\frac{Btu}{s.ft^2}$)			226,8	226,8						
$\phi_{calc.}$ ($\frac{Btu}{s.ft^2}$)			197,0	211,3						
$T_{out\ theor.}$ (°F)			625,4	618,8			603	596,4		
$T_{out\ eff.}$ (°F)			629,6	624,2			598,4	596,8		

Schematization with 8 subchannels

	1	2	3	4	5	6	7	8
ΔH ($\frac{Btu}{lb}$)	48,1	45,8	45,8	32	12,9	2,4	2,4	0,66
X (%)	- 0,6							
G_{out} ($\frac{lbm}{s.ft^2}$)	418,9	420,9	420,9	509,6	536,8	474,2	474,2	475,0
R_{DNB}	0,867	0,879	0,879	0,970				
ϕ_{DNB} ($\frac{Btu}{s.ft^2}$)	226,8	226,8	226,8	226,8				
$\phi_{calc.}$ ($\frac{Btu}{s.ft^2}$)	196,6	199,3	199,3	220,0				
$T_{out\ theor.}$ (°F)	625,4			615,3	603,0			594,2
$T_{out\ eff.}$ (°F)	629,6			624,2	598,4			596,8

T A B L E IV

EXPERIMENTAL CONDITIONS AND DETAILED RESULTS OF BURNOUT TESTS OF GROUP B (BURNOUT TESTS WITH DIFFERENT HEATING ON THE BURNOUT ROD AND ON THE ADJACENT ROD)

The following runs have been analyzed:

- RUN 22 (21-7-67)
- RUN 48 (21-7-67)
- RUN 16 (24-7-67)
- RUN 81 (21-7-67)
- RUN 89 (21-7-67)
- RUN 40 (21-7-67)
- RUN 58 (21-7-67)

RUN '22 (21-7-67)

Pressure	= 1906 psi	Total power	= 69,58 Btu/sec
Inlet mass velocity	= 103,607 lbm/sec.ft^2	Burnout rod power	= 43,6 Btu/sec
Inlet enthalpy	= 451,624 Btu/lbm	Adjacent rod power	= 25,98 Btu/sec
χ	= 1,4624 x 10^{-2}	Shell power	= 0 Btu/sec

Schematization with 10 subchannels

	1	2	3	4	5	6	7	8	9	10
ΔH ($\frac{Btu}{lb}$)	171,6	171,6	202,1	185,5	139,3	139,3	149,2	139,1	116,6	116,6
X (%)			- 1,4							
G_{out} ($\frac{lbm}{s.ft^2}$)	89,3	89,3	126,7	126,8	91,4	91,4	118,5	116,1	68,1	68,1
R_{DNB}			0,887	0,933			1,717	1,757		
ϕ_{DNB} ($\frac{Btu}{s.ft^2}$)			214,8	214,8			127,8	127,8		
$\phi_{calc.}$ ($\frac{Btu}{s.ft^2}$)			190,5	200,4			219,4	224,5		

$\Delta H_{H.B.}$ = 158,21 Btu/lb

RUN 48 (21-7-67)

Pressure	= 1920 psi	Total power	= 63,04 Btu/sec
Inlet mass velocity	= 102,01 lbm/sec.ft^2	Burnout rod power	= 39,72 Btu/sec
Inlet enthalpy	= 495,78 Btu/lbm	Adjacent rod power	= 23,32 Btu/sec
χ	= 1,4624 x 10^{-2}	Shell power	= 0 Btu/sec

Schematization with 10 subchannels

	1	2	3	4	5	6	7	8	9	10
ΔH ($\frac{Btu}{lb}$)	159,3	159,3	189,7	172,2	128,4	128,4	136,6	126,2	105,5	105,5
X (%)		4,8	1,1							
G_{out} ($\frac{lbm}{s.ft^2}$)	93,7	93,7	111,1	115,8	95,7	95,7	115,7	114,6	73,5	73,5
R_{DNB}			0,839	0,893			1,690	1,738		
ϕ_{DNB} ($\frac{Btu}{s.ft^2}$)			195,2	195,2			114,5	114,5		
$\phi_{calc.}$ ($\frac{Btu}{s.ft^2}$)			163,7	174,3			193,6	199,1		

$\Delta H_{H.B.}$ = 145,28 Btu/lb

RUN 16 (24-7-67)

Pressure	= 1877 psi	Total power	= 87,5 Btu/sec
Inlet mass velocity	= 101,17 lbm/sec.ft^2	Burnout rod power	= 44,65 Btu/sec
Inlet enthalpy	= 437,6 Btu/lbm	Adjacent rod power	= 42,85 Btu/sec
χ	= 1,4624 x 10^{-2}	Shell power	= 0 Btu/sec

Schematization with 10 subchannels

	1	2	3	4	5	6	7	8	9	10
ΔH ($\frac{Btu}{lb}$)	188,3	188,3	221,5	217,4	179,4	179,4	213,7	216,5	182,9	182,9
X (%)			+ 0,35							
G_{out} ($\frac{lbm}{s.ft^2}$)	80,4	80,4	117,4	118,6	89,3	89,3	118,0	117,8	78,1	78,1
R_{DNB}			0,859	0,870			0,917	0,909		
ϕ_{DNB} ($\frac{Btu}{s.ft^2}$)			219,12	219,12			210,13	210,13		
$\phi_{calc.}$ ($\frac{Btu}{s.ft^2}$)			188,22	190,6			192,7	191,0		

$\Delta H_{H.B.}$ = 203 Btu/lb

RUN 81 (21-7-67)

Pressure	= 1892 psi	Total power	= 75,93 Btu/sec
Inlet mass velocity	= 107,6 $lbm/sec.ft^2$	Burnout rod power	= 38,67 Btu/sec
Inlet enthalpy	= 497,59 Btu/lbm	Adjacent rod power	= 37,26 Btu/sec
χ	= $1,4624 \times 10^{-2}$	Shell power	= 0 Btu/sec

Schematization with 10 subchannels

	1	2	3	4	5	6	7	8	9	10
ΔH $(\frac{Btu}{lb})$	166,2	166,2	191,0	179,2	146,9	146,9	176,5	177,8	158,1	158,1
X (%)	1,25	1,25	6,36	3,92						
G_{out} $(\frac{lbm}{s.ft^2})$	88,12	88,12	115,16	115,21	107,4	107,4	115,8	115,8	95,8	95,8
R_{DNB}			0,856	0,890			0,933	0,929		
ϕ_{DNB} $(\frac{Btu}{s.ft^2})$			190,07	190,07			183,03	183,03		
$\phi_{calc.}$ $(\frac{Btu}{s.ft^2})$			162,7	169,16			170,77	170,04		

$\Delta H_{H.B.}$ = 165,9 Btu/lb

RUN 89 (21-7-67)

Pressure	= 1934 psi	Total power	= 62,75 Btu/sec
Inlet mass velocity	= 108,13 lbm/sec.ft^2	Burnout rod power	= 32,13 Btu/sec
Inlet enthalpy	= 556,54 Btu/lbm	Adjacent rod power	= 30,62 Btu/sec
χ	= 1,4624 x 10^{-2}	Shell power	= 0 Btu/sec

Schematization with 10 subchannels

	1	2	3	4	5	6	7	8	9	10
ΔH ($\frac{Btu}{lb}$)	126,0	126,0	152,6	148,2	119,6	119,6	144,9	146,5	121,1	121,1
X (%)	3,5	3,5	9,15	8,22	2,17	2,17	7,51	7,87	2,48	2,48
G_{out} ($\frac{lbm}{s.ft^2}$)	90,12	90,12	117,2	117,9	106,2	106,2	116,91	116,92	93,2	93,2
R_{DNB}			0,903	0,919			0,976	0,970		
ϕ_{DNB} ($\frac{Btu}{s.ft^2}$)			157,92	157,92			150,5	150,5		
$\phi_{calc.}$ ($\frac{Btu}{s.ft^2}$)			142,6	145,1			146,8	145,9		

$\Delta H_{H.B.}$ = 136,47 Btu/lb

RUN 40 (21-7-67)

Pressure	= 1906 psi	Total power	= 113,19 Btu/sec
Inlet mass velocity	= 449,047 lbm/sec.ft^2	Burnout rod power	= 70,91 Btu/sec
Inlet enthalpy	= 482,5 Btu/lbm	Adjacent rod power	= 42,28 Btu/sec
χ	= 1,4624 x 10^{-2}	Shell power	= 0 Btu/sec

Schematization with 10 subchannels

	1	2	3	4	5	6	7	8	9	10
ΔH ($\frac{Btu}{lb}$)	66,1	66,1	79,0	71,3	52,1	52,1	55,8	50,7	41,8	41,8
X (%)			- 20,6							
G_{out} ($\frac{lbm}{s.ft^2}$)	365,7	365,7	497,0	500,6	425,3	425,3	504,3	504,3	369,5	369,5
R_{DNB}			0,979	0,999			1,733	1,749		
ϕ_{DNB} ($\frac{Btu}{s.ft^2}$)			348,46	348,46			207,68	207,68		
$\phi_{calc.}$ ($\frac{Btu}{s.ft^2}$)			341,14	348,11			359,9	363,23		

$\Delta H_{H.B.}$ = 59,25 Btu/lb

RUN 58 (21-7-67)

Pressure	= 1934 psi	Total power	= 105,41 Btu/sec
Inlet mass velocity	= 449,3 lbm/sec.ft^2	Burnout rod power	= 65,69 Btu/sec
Inlet enthalpy	= 508,2 Btu/lbm	Adjacent rod power	= 39,72 Btu/sec
χ	= 1,4624 x 10^{-2}	Shell power	= 0 Btu/sec

Schematization with 10 subchannels

	1	2	3	4	5	6	7	8	9	10
ΔH ($\frac{Btu}{lb}$)	61,2	61,2	73,2	66,2	48,5	48,5	52,1	47,5	39,1	39,1
X (%)			- 17,3							
G_{out} ($\frac{lbm}{s.ft^2}$)	366,2	366,2	497,3	500,7	425,6	425,6	504,1	504,3	370,3	370,3
R_{DNB}			0,991	1,011			1,733	1,751		
ϕ_{DNB} ($\frac{Btu}{s.ft^2}$)			322,84	322,84			195	195		
$\phi_{calc.}$ ($\frac{Btu}{s.ft^2}$)			319,9	326,3			337,93	341,43		

$\Delta H_{H.B.}$ = 55,13 Btu/lb

T A B L E V

EXPERIMENTAL CONDITIONS AND DETAILED RESULTS OF BURNOUT TESTS OF GROUP C (BURNOUT TESTS WITH DIFFERENT HEATING ON THE BURNOUT ROD AND ON THE SHELL)

The following runs have been analyzed:

- RUN 40 (13-7-67)
- RUN 47 (13-7-67)
- RUN 16 (13-7-67)
- RUN 35 (3-7-67)
- RUN 53 (3-7-67)
- RUN 6 (3-7-67)

RUN 40 (13-7-67)

Pressure	= 1877 psi	Total power	= 104,28 Btu/sec
Inlet mass velocity	= 281,73 lbm/sec.ft^2	Burnout rod power	= 36 Btu/sec
Inlet enthalpy	= 593,0 Btu/lbm	Adjacent rod power	= 0 Btu/sec
χ	= 1,4624 x 10^{-2}	Shell power	= 68,28 Btu/sec

Schematization with 10 subchannels

	1	2	3	4	5	6	7	8	9	10
ΔH ($\frac{Btu}{lb}$)	130,6	130,6	122,3	100,0	88,3	88,3	66,5	58,4	70,9	70,9
X (%)	13,5	13,5	11,8	7,2	4,8	4,8				
G_{out} ($\frac{lbm}{s.ft^2}$)	191,9	191,9	257,7	282,0	262,3	262,3	366,2	371,8	246,7	246,7
R_{DNB}			0,758	0,856						
ϕ_{DNB} ($\frac{Btu}{s.ft^2}$)			177,0	177,0						
$\phi_{calc.}$ ($\frac{Btu}{s.ft^2}$)			134,1	151,5						

$\Delta H_{H.B.}$ = 88,51 Btu/lb

RUN 47 (13-7-67)

Pressure	= 1892 psi	Total power	= 153,2 Btu/sec
Inlet mass velocity	= 273,85 lbm/sec.ft^2	Burnout rod power	= 52,42 Btu/sec
Inlet enthalpy	= 456,0 Btu/lbm	Adjacent rod power	= 0 Btu/sec
χ	= 1,4624 x 10^{-2}	Shell power	= 100,78 Btu/sec

Schematization with 10 subchannels

	1	2	3	4	5	6	7	8	9	10
ΔH ($\frac{Btu}{lb}$)	181,3	181,3	172,4	147,0	132,4	132,4	101,2	88,0	107,8	107,8
X (%)			- 6,3							
G_{out} ($\frac{lbm}{s.ft^2}$)	221,3	221,3	294,3	302,1	270,0	270,0	296,1	297,0	239,7	239,7
R_{DNB}			0,90	1,004						
ϕ_{DNB} ($\frac{Btu}{s.ft^2}$)			257,61	257,61						
$\phi_{calc.}$ ($\frac{Btu}{s.ft^2}$)			231,8	258,6						

$\Delta H_{H.B.}$ = 132,2 Btu/lb

RUN 16 (13-7-67)

Pressure	= 1906 psi	Total power	= 127,69 Btu/sec
Inlet mass velocity	= 285,04 lbm/sec.ft^2	Burnout rod power	= 44,65 Btu/sec
Inlet enthalpy	= 518,16 Btu/lbm	Adjacent rod power	= 0 Btu/sec
χ	= 1,4624 x 10^{-2}	Shell power	= 83,04 Btu/sec

Schematization with 10 subchannels

	1	2	3	4	5	6	7	8	9	10
ΔH ($\frac{Btu}{lb}$)	150,0	150,0	141,7	120,2	108,0	108,0	82,7	71,7	87,3	87,3
X (%)	1,3	1,3	- 0,2							
G_{out} ($\frac{lbm}{s.ft^2}$)	207,6	207,6	303,5	314,2	280,4	280,4	318,4	319,5	256,2	256,2
R_{DNB}			0,881	0,979						
ϕ_{DNB} ($\frac{Btu}{s.ft^2}$)			219,41	219,41						
$\phi_{calc.}$ ($\frac{Btu}{s.ft^2}$)			193,3	214,8						

$\Delta H_{H.B.}$ = 107,83 Btu/lb

RUN 35 (3-7-67)

Pressure	= 1913 psi	Total power	= 80,58 Btu/sec
Inlet mass velocity	= 306,09 lbm/sec.ft^2	Burnout rod power	= 38,2 Btu/sec
Inlet enthalpy	= 593,2 Btu/lbm	Adjacent rod power	= 0 Btu/sec
χ	= 1,4624 x 10^{-2}	Shell power	= 42,38 Btu/sec

Schematization with 10 subchannels

	1	2	3	4	5	6	7	8	9	10
ΔH ($\frac{Btu}{lb}$)	93,1	93,1	93,2	75,3	60,4	60,4	44,8	34,8	41,3	41,3
X (%)	5,1	5,1	5,1	1,4						
G_{out} ($\frac{lbm}{s.ft^2}$)	211,2	211,2	292,7	325,5	301,1	301,1	373,3	373,8	269,8	269,8
R_{DNB}			0,840	0,933						
ϕ_{DNB} ($\frac{Btu}{s.ft^2}$)			187,7	187,7						
$\phi_{calc.}$ ($\frac{Btu}{s.ft^2}$)			157,6	175,1						

$\Delta H_{H.B.}$ = 61,87 Btu/lb

RUN 53 (3-7-67)

Pressure	= 1849 psi	Total power	= 113,6 Btu/sec
Inlet mass velocity	= 283,1 lbm/sec.ft^2	Burnout rod power	= 54,4 Btu/sec
Inlet enthalpy	= 467,2 Btu/lbm	Adjacent rod power	= 0 Btu/sec
χ	= 1,4624 x 10^{-2}	Shell power	= 59,2 Btu/sec

Schematization with 10 subchannels

	1	2	3	4	5	6	7	8	9	10
ΔH ($\frac{Btu}{lb}$)	141,9	141,9	142,4	115,9	91,8	91,8	67,9	52,5	62,7	62,7
X (%)			- 9,0							
G_{out} ($\frac{lbm}{s.ft^2}$)	207,5	207,5	291,5	298,0	279,8	279,8	334,6	334,8	238,9	238,9
R_{DNB}			0,918	1,022						
ϕ_{DNB} ($\frac{Btu}{s.ft^2}$)			267,4	267,4						
$\phi_{calc.}$ ($\frac{Btu}{s.ft^2}$)			245,4	273,2						

$\Delta H_{H.B.}$ = 94,38 Btu/lb

RUN 6 (3-7-67)

Pressure	= 1877 psi.	Total power	= 106,46 Btu/sec
Inlet mass velocity	= 294,84 lbm/sec.ft^2	Burnout rod power	= 49,86 Btu/sec
Inlet enthalpy	= 508,2 Btu/lbm	Adjacent rod power	= 0 Btu/sec
χ	= 1,4624 x 10^{-2}	Shell power	= 56,6 Btu/sec

Schematization with 10 subchannels

	1	2	3	4	5	6	7	8	9	10
ΔH ($\frac{Btu}{lb}$)	122,3	122,3	123,0	102,3	83,0	83,0	61,8	48,2	57,5	57,5
X (%)			- 5,3							
G_{out} ($\frac{lbm}{s.ft^2}$)	236,6	236,6	314,8	323,6	290,7	290,7	321,0	322,1	258,9	258,9
R_{DNB}			0,907	0,998						
ϕ_{DNB} ($\frac{Btu}{s.ft^2}$)			245,04	245,04						
$\phi_{calc.}$ ($\frac{Btu}{s.ft^2}$)			222,2	244,5						

$\Delta H_{H.B.}$ = 84,89 Btu/lb

T A B L E VI

EXPERIMENTAL CONDITIONS AND DETAILED RESULTS OF BURNOUT TESTS OF GROUP D (BURNOUT TESTS WITH DIFFERENT HEATING ON THE BURNOUT ROD, ON THE ADJACENT ROD AND ON THE SHELL)

The following runs have been analyzed:

- RUN 10 (19-1-67)
- RUN 24 (19-1-67)
- RUN 37 (19-1-67)
- RUN 40 (17-1-67)
- RUN 91 (17-1-67)
- RUN 117 (17-1-67)
- RUN 50 (14-7-67)
- RUN 47 (18-1-67)
- RUN 22 (18-1-67)
- RUN 38 (18-1-67)

RUN 10 (19-1-67)

Pressure	= 1899 psi	Total power	= 126,84 Btu/sec
Inlet mass velocity	= 301,61 lbm/sec.ft^2	Burnout rod power	= 52,6 Btu/sec
Inlet enthalpy	= 473,3 Btu/lbm	Adjacent rod power	= 22,8 Btu/sec
χ	= 1,4624 x 10^{-2}	Shell power	= 51,4 Btu/sec

Schematization with 10 subchannels

	1	2	3	4	5	6	7	8	9	10
ΔH ($\frac{Btu}{lb}$)	126,0	126,0	129,7	115,4	99,5	99,5	91,0	84,4	86,9	86,9
X (%)			- 11,6							
G_{out} ($\frac{lbm}{s.ft^2}$)	252,5	252,5	325,6	329,8	292,1	292,1	331,8	331,8	257,1	257,1
R_{DNB}			1,012	1,076			2,597	2,625		
ϕ_{DNB} ($\frac{Btu}{s.ft^2}$)			258,5	258,5			112,2	112,2		
$\phi_{calc.}$ ($\frac{Btu}{s.ft^2}$)			261,6	278,1			291,3	294,5		

$\Delta H_{H.B.}$ = 98,8 Btu/lb

RUN 24 (19-1-67)

Pressure	= 1913 psi	Total power	= 114,8 Btu/sec
Inlet mass velocity	= 306,29 $lbm/sec.ft^2$	Burnout rod power	= 47,58 Btu/sec
Inlet enthalpy	= 511,8 Btu/lbm	Adjacent rod power	= 20,76 Btu/sec
χ	= 1,4624 x 10^{-2}	Shell power	= 46,46 Btu/sec

Schematization with 10 subchannels

	1	2	3	4	5	6	7	8	9	10
ΔH $(\frac{Btu}{lb})$	107,1	107,1	110,3	98,2	84,2	84,2	76,8	71,1	73,1	73,1
X (%)			- 8,2							
G_{out} $(\frac{lbm}{s.ft^2})$	250,1	250,1	328,1	333,6	297,7	297,7	339,0	339,3	264,4	264,4
R_{DNB}			1,004	1,063			2,670	2,70		
ϕ_{DNB} $(\frac{Btu}{s.ft^2})$			233,862	233,862			102,02	102,02		
$\phi_{calc.}$ $(\frac{Btu}{s.ft^2})$			234,79	248,59			272,39	275,45		

$\Delta H_{H.B.}$ = 88,1 Btu/lb

RUN 37 (19-1-67)

Pressure	= 1934 psi	Total power	= 107,22 Btu/sec
Inlet mass velocity	= 317,4 $lbm/sec.ft^2$	Burnout rod power	= 44,46 Btu/sec
Inlet enthalpy	= 552,69 Btu/lbm	Adjacent rod power	= 19,43 Btu/sec
χ	= $1,4624 \times 10^{-2}$	Shell power	= 43,33 Btu/sec

Schematization with 10 subchannels

	1	2	3	4	5	6	7	8	9	10
ΔH $(\frac{Btu}{lb})$	97,3	97,3	99,99	88,5	75,8	75,8	69,0	63,8	65,7	65,7
X (%)			- 2,3							
G_{out} $(\frac{lbm}{s.ft^2})$	250,7	250,7	339,2	346,3	307,5	307,5	356,2	357,9	274,0	274,0
R_{DNB}			0,911	0,967			2,443	2,505		
ϕ_{DNB} $(\frac{Btu}{s.ft^2})$			218,48	218,48			95,5	95,5		
$\phi_{theor.}$ $(\frac{Btu}{s.ft^2})$			199,0	211,2			233,3	239,2		

$\Delta H_{H.B.}$ = 79,39 Btu/lb

RUN 40 (17-1-67)

Pressure	= 1842 psi	Total power	= 141,25 Btu/sec
Inlet mass velocity	= 311,95 lbm/sec.ft^2	Burnout rod power	= 48,91 Btu/sec
Inlet enthalpy	= 494,7 Btu/lbm	Adjacent rod power	= 28,42 Btu/sec
χ	= 1,4624 x 10^{-2}	Shell power	= 63,92 Btu/sec

Schematization with 10 subchannels

	1	2	3	4	5	6	7	8	9	10
ΔH ($\frac{Btu}{lb}$)	125,7	125,7	124,7	112,4	102,1	102,1	95,5	93,3	98,0	98,0
X (%)			- 7,0							
G_{out} ($\frac{lbm}{s.ft^2}$)	237,96	237,96	339,0	343,8	302,5	302,5	360,8	360,0	248,7	248,7
R_{DNB}			0,99	1,048			1,962	1,979		
ϕ_{DNB} ($\frac{Btu}{s.ft^2}$)			240,38	240,38			139,75	139,75		
$\phi_{calc.}$ ($\frac{Btu}{s.ft^2}$)			237,97	251,91			274,19	276,56		

$\Delta H_{H.B.}$ = 106,43 Btu/lb

RUN 91 (17-1-67)

Pressure	= 1913 psi	Total power	= 115,94 Btu/sec
Inlet mass velocity	= 316,79 $lbm/sec.ft^2$	Burnout rod power	= 40,29 Btu/sec
Inlet enthalpy	= 571,5 Btu/lbm	Adjacent rod power	= 23,32 Btu/sec
χ	= $1,4624 \times 10^{-2}$	Shell power	= 52,33 Btu/sec

Schematization with 10 subchannels

	1	2	3	4	5	6	7	8	9	10
ΔH $(\frac{Btu}{lb})$	100,7	100,7	100,4	90,6	82,8	82,8	77,6	75,4	78,5	78,5
X (%)	2,2	2,2	2,1	0,1						
G_{out} $(\frac{lbm}{s.ft^2})$	233,8	233,8	323,3	354,7	311,8	311,8	363,8	363,8	270,9	270,9
R_{DNB}			0,885	0,943			1,749	1,769		
ϕ_{DNB} $(\frac{Btu}{s.ft^2})$			197,98	197,98			114,59	114,59		
$\phi_{calc.}$ $(\frac{Btu}{s.ft^2})$			175,2	186,7			200,4	202,7		

$\Delta H_{H.B.}$ = 86,02 Btu/lb

RUN 117 (17-1-67)

Pressure	= 1906 psi	Total power	= 92,05 Btu/sec
Inlet mass velocity	= 315,01 lbm/sec.ft^2	Burnout rod power	= 32,42 Btu/sec
Inlet enthalpy	= 617,7 Btu/lbm	Adjacent rod power	= 18,39 Btu/sec
χ	= 1,4624 x 10^{-2}	Shell power	= 41,24 Btu/sec

Schematization with 10 subchannels

	1	2	3	4	5	6	7	8	9	10
ΔH ($\frac{Btu}{lb}$)	81,3	81,3	81,4	73,0	65,8	65,8	61,3	59,4	62,0	62,0
X (%)	7,9	7,9	7,9	6,2	4,7	4,7	3,7	3,4	3,9	3,9
G_{out} ($\frac{lbm}{s.ft^2}$)	253,0	253,0	330,5	342,1	305,0	305,0	356,7	359,2	268,2	268,2
R_{DNB}			0,904	0,952			1,801	1,822		
ϕ_{DNB} ($\frac{Btu}{s.ft^2}$)			159,31	159,31			90,37	90,37		
$\phi_{calc.}$ ($\frac{Btu}{s.ft^2}$)			144,0	151,6			162,7	164,6		

$\Delta H_{H.B.}$ = 68,68

RUN 50 (14-7-67)

Pressure	= 1892 psi	Total power	= 187,79 Btu/sec
Inlet mass velocity	= 274,63 lbm/sec.ft^2	Burnout rod power	= 48,34 Btu/sec
Inlet enthalpy	= 474,2 Btu/lbm	Adjacent rod power	= 43,03 Btu/sec
χ	= 1,4624 x 10^{-2}	Shell power	= 96,42 Btu/sec

Schematization with 10 subchannels

	1	2	3	4	5	6	7	8	9	10
ΔH ($\frac{Btu}{lb}$)	178,3	178,3	171,5	162,3	160,7	160,7	157,4	162,0	169,6	169,6
χ (%)			- 2,7							
G_{out} ($\frac{lbm}{s.ft^2}$)	224,4	224,4	298,8	303,2	267,2	267,2	304,3	302,4	229,2	229,2
R_{DNB}			0,898	0,938			1,078	1,055		
ϕ_{DNB} ($\frac{Btu}{s.ft^2}$)			237,58	237,58			211,45	211,45		
$\phi_{calc.}$ ($\frac{Btu}{s.ft^2}$)			213,3	222,8			227,9	223,0		

$\Delta H_{H.B.}$ = 160,38 Btu/lb

RUN 47 (18-1-67)

Pressure	= 1877 psi	Total power	= 158,3 Btu/sec
Inlet mass velocity	= 316,39 lbm/sec.ft^2	Burnout rod power	= 41,61 Btu/sec
Inlet enthalpy	= 548,7 Btu/lbm	Adjacent rod power	= 35,91 Btu/sec
χ	= 1,4624 x 10^{-2}	Shell power	= 80,78 Btu/sec

Schematization with 10 subchannels

	1	2	3	4	5	6	7	8	9	10
ΔH ($\frac{Btu}{lb}$)	128,7	128,7	123,3	115,7	114,2	114,2	111,3	114,4	120,5	120,5
X (%)	4,1	4,1	3,0	1,4	1,1	1,1	0,5	1,1	2,4	2,4
G_{out} ($\frac{lbm}{s.ft^2}$)	248,2	248,2	330,6	350,8	311,5	311,5	364,9	353,3	260,1	260,1
R_{DNB}			0,868	0,91			1,085	1,062		
ϕ_{DNB} ($\frac{Btu}{s.ft^2}$)			204,5	204,5			176,5	176,5		
$\phi_{calc.}$ ($\frac{Btu}{s.ft^2}$)			177,5	186,0			191,5	187,4		

$\Delta H_{H.B.}$ = 117,61 Btu/lb

RUN 22 (18-1-67)

Pressure	= 1920 psi	Total power	= 150,35 Btu/sec
Inlet mass velocity	= 326,88 lbm/sec.ft^2	Burnout rod power	= 39,53 Btu/sec
Inlet enthalpy	= 563,06 Btu/lbm	Adjacent rod power	= 34,31 Btu/sec
χ	= 1,4624 x 10^{-2}	Shell power	= 76,51 Btu/sec

Schematization with 10 subchannels

	1	2	3	4	5	6	7	8	9	10
ΔH ($\frac{Btu}{lb}$)	118,1	118,1	113,2	106,4	104,8	104,8	102,1	105,0	110,6	110,6
X (%)	3,9	3,9	2,9	1,4	1,1	1,1	0,5	1,1	2,3	2,3
G_{out} ($\frac{lbm}{s.ft^2}$)	257,0	257,0	344,2	362,2	320,8	320,8	376,0	365,2	268,4	268,4
R_{DNB}			0,894	0,935			1,110	1,087		
ϕ_{DNB} ($\frac{Btu}{s.ft^2}$)			194,25	194,25			168,63	168,63		
$\phi_{calc.}$ ($\frac{Btu}{s.ft^2}$)			173,66	181,6			187,1	183,3		

$\Delta H_{H.B.}$ = 108,11 Btu/lb

RUN 38 (18-1-67)

Pressure	= 1977 psi	Total power	= 124,1 Btu/sec
Inlet mass velocity	= 313,04 lbm/sec.ft^2	Burnout rod power	= 32,61 Btu/sec
Inlet enthalpy	= 615,5 Btu/lbm	Adjacent rod power	= 28,34 Btu/sec
χ	= 1,4624 x 10^{-2}	Shell power	= 63,15 Btu/sec

Schematization with 10 subchannels

	1	2	3	4	5	6	7	8	9	10
ΔH ($\frac{Btu}{lb}$)	101,7	101,7	97,9	91,7	90,1	90,1	87,9	90,7	95,2	95,2
X (%)	10,3	10,3	9,5	8,1	7,8	7,8	7,3	7,9	8,9	8,9
G_{out} ($\frac{lbm}{s.ft^2}$)	258,6	258,6	334,5	343,4	305,1	305,1	347,7	343,6	265,9	265,9
R_{DNB}			0,831	0,867			1,023	1,004		
ϕ_{DNB} ($\frac{Btu}{s.ft^2}$)			160,2	160,2			139,3	139,3		
$\phi_{calc.}$ ($\frac{Btu}{s.ft^2}$)			133,1	138,9			142,5	139,8		

$\Delta H_{H.B.}$ = 93,18 Btu/lb

TABLE VII

RESULTS OF FLUX PARAMETRICAL ANALYSIS OF RUN 64 (21-2-67); $\gamma = 1.46 \times 10^{-2}$; SUBCHANNEL 3 IN THE 10 SUBCHANNELS SCHEMATIZATION

Input	Output			
φ (Btu/s.ft^2)	G_{out} (lbm/s.ft^2)	H_{out} (Btu/lbm)	R_{DNB}	B.O. (Btu/s.ft^2)
300.	352.1	538.8	1.055	316.5
305.	352.0	540.4	1.036	315.9
310.	351.9	541.9	1.017	315.2
315.	351.8	543.5	0.998	314.3
320.	351.7	545.0	0.980	313.6
325.	351.6	546.6	0.963	312.9
331.7	351.5	548.7	0.941	312.1

$\varphi \equiv$ effective rod surface flux.

$\varphi_{B.O.} \equiv$ W-3 calculated burnout flux.

TABLE VIII

RESULTS OF FLUX PARAMETRICAL ANALYSIS OF RUN 90 (7-12-66); $\gamma = 1.46 \times 10^{-2}$; SUBCHANNEL 3 IN THE 10 SUBCHANNELS SCHEMATIZATION

Input	Output			
φ (Btu/s.ft^2)	G_{out} (lbm/s.ft^2)	H_{out} (Btu/lbm)	R_{DNB}	B.O. (Btu/s.ft^2)
300.	482.1	574.2	1.066	319.8
305.	481.9	575.3	1.045	318.7
310.	481.7	576.4	1.026	318.0
315.	481.5	577.5	1.006	316.9
320.	481.3	578.7	0.988	316.1
325.	481.1	579.8	0.970	315.2
331.7	480.8	581.3	0.946	313.7

NOMENCLATURE

H_{SAT}	=	saturation enthalpy (Btu/lbm)
H_{in}	=	inlet enthalpy (Btu/lbm)
ΔH_{SUB}	=	subcooling enthalpy difference (Btu/lbm)
p	=	rod pitch (ft)
D_{rod}	=	rod diameter (ft)
A	=	flow area (ft^2)
V	=	fluid velocity (ft/sec)
ρ	=	fluid density (lbm/ft^3)
W	=	cross flow rate between adjacent channels (lbm/sec)
H	=	coolant enthalpy (Btu/lbm)
Q	=	heat input to channel from fuel rods (Btu/sec)
(TC)	=	thermal diffusion heat contribution term in energy balance (Btu/sec)
P	=	pressure (lb_f/ft^2)
g_c	=	conversion factor (= 32.174) ($lbm.ft/lb_f/sec^2$)
K	=	pressure loss coefficient
Δz	=	control volume axial length (ft)
g	=	gravitational acceleration
G	=	coolant mass velocity ($lbm/sec-ft^2$)
De	=	channel equivalent diameter (ft)
f	=	friction factor

f_{iso} = isothermal friction factor

$f_{iso,sat}$ = isothermal friction factor at saturation condition

X = quality

φ = heat flux (Btu/sec-ft^2)

$\varphi_{B.O.}$ = burnout flux

Subscripts

1 = bottom of axial increment

2 = top of axial increment

j = channel index

i = channel index

Superscripts

$\bar{}$ = average value over length increment

Note : - The symbols are listed in the order with which they appear in the text.

FIG 1a

A = burn out rod
B = adiacent rod
G = shell curved cylindrical surface
L = shell flat boundary

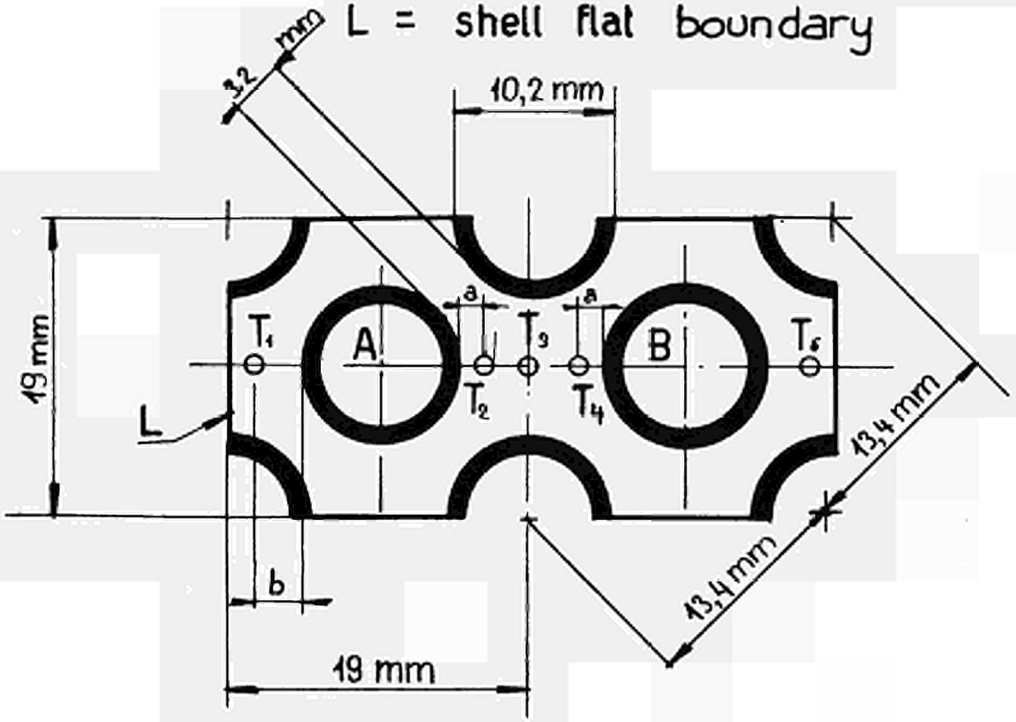

Test section lenght = 588,2mm; $T_1, \ldots, T_5 \equiv$ outlet termocouples
a = 1,5 mm
b = 2,9 mm

Double channel test section configuration and dimensions

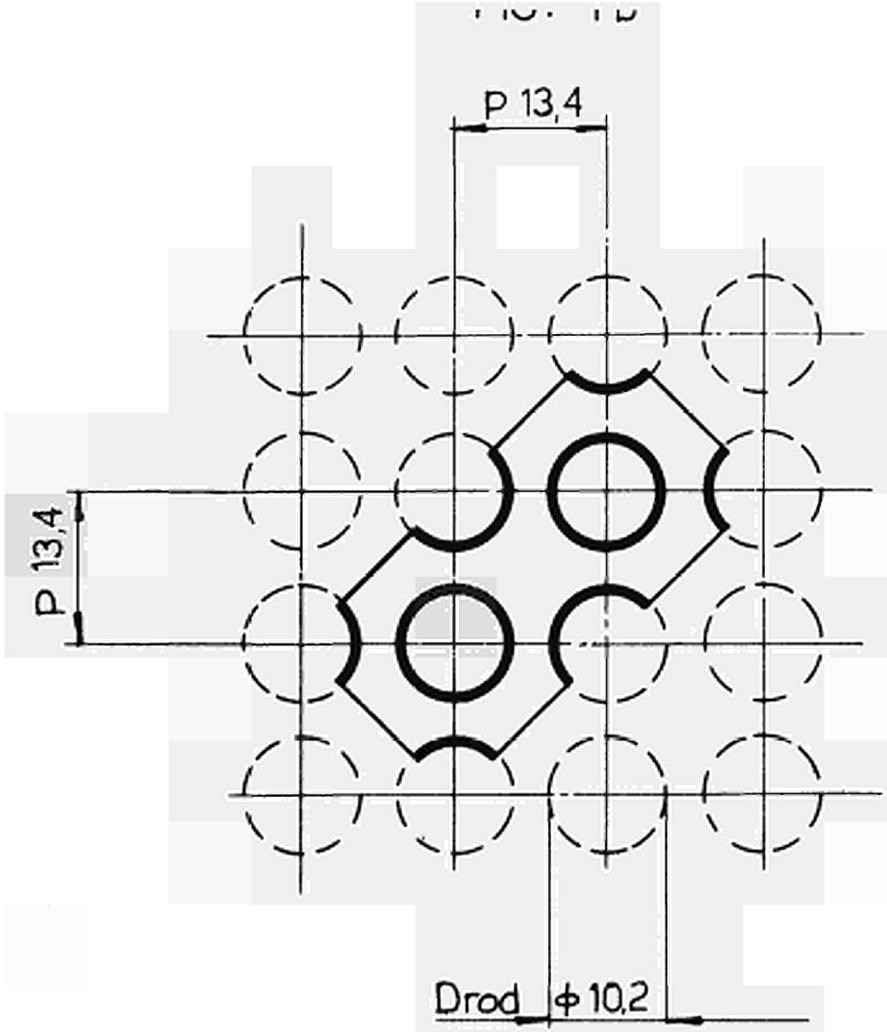

Drod = rod diameter

P = pitch

SCHEMATIZATION OF THE INFINITE FUEL ROD

MATRIX TO WHICH THE TEST SECTION BELONGS

FIG. 2

A = burn out rod

B = adiacent rod

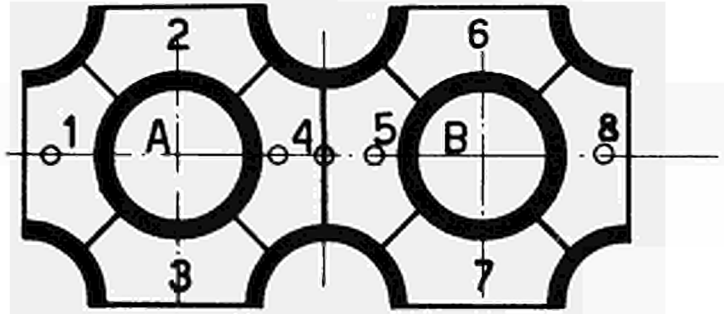

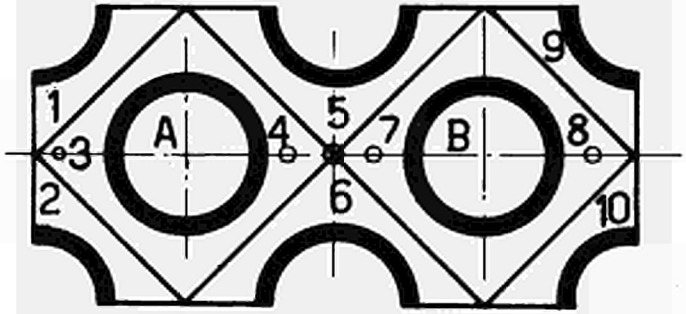

8 subchannels schematization

10 subchannels schematization

Possible subdivisions in subchannels of the test section

FIG. 3

Outlet enthalpy rise profiles and comparison with experimental results ; burnout test 1 BIS (9-11-66) ; 10 subchannels schematization

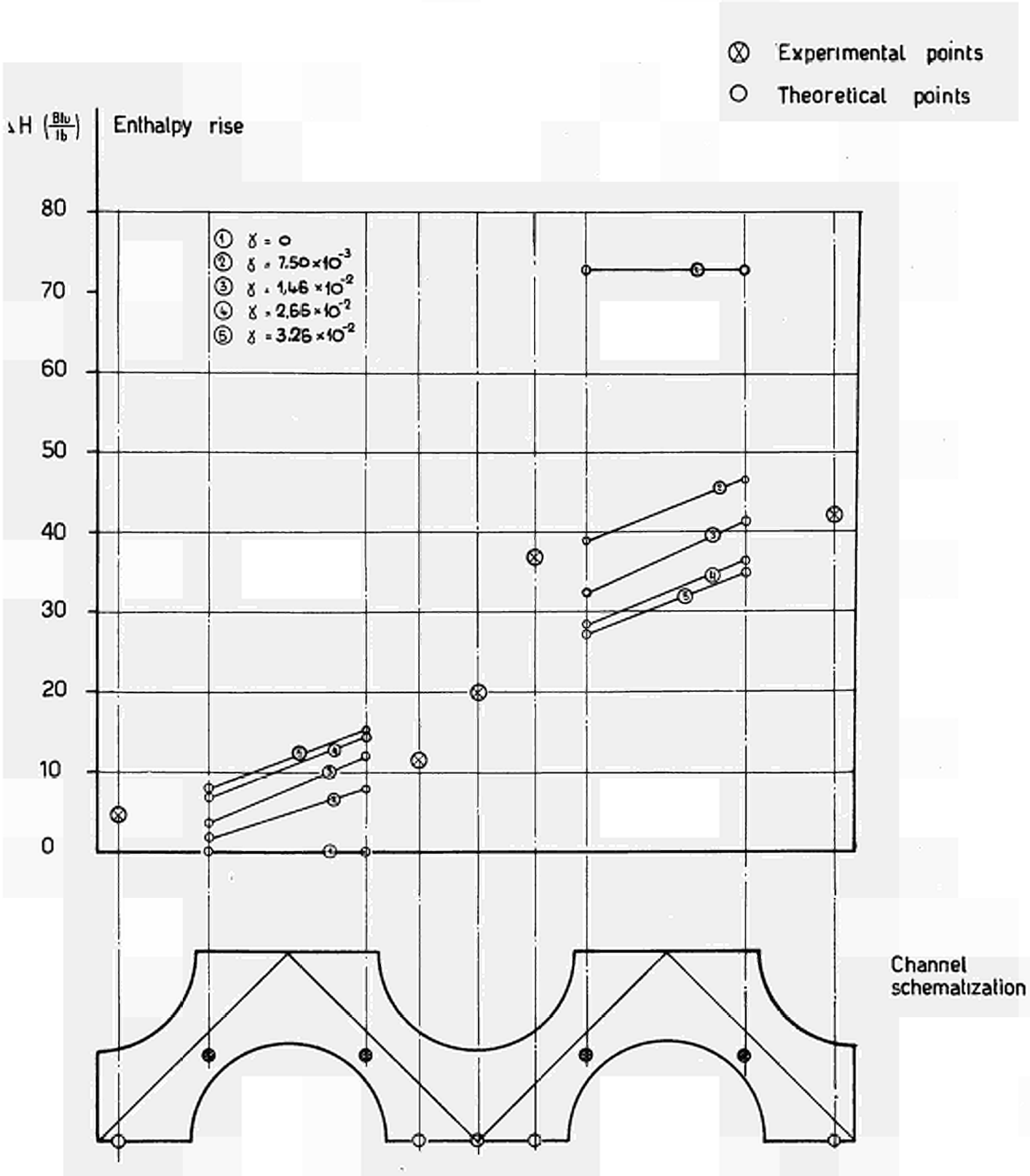

FIG. 4

Outlet enthalpy rise profiles and comparison with experimental results ; burnout test 1 BIS (9-11-66) ; 8 subchannels schematization

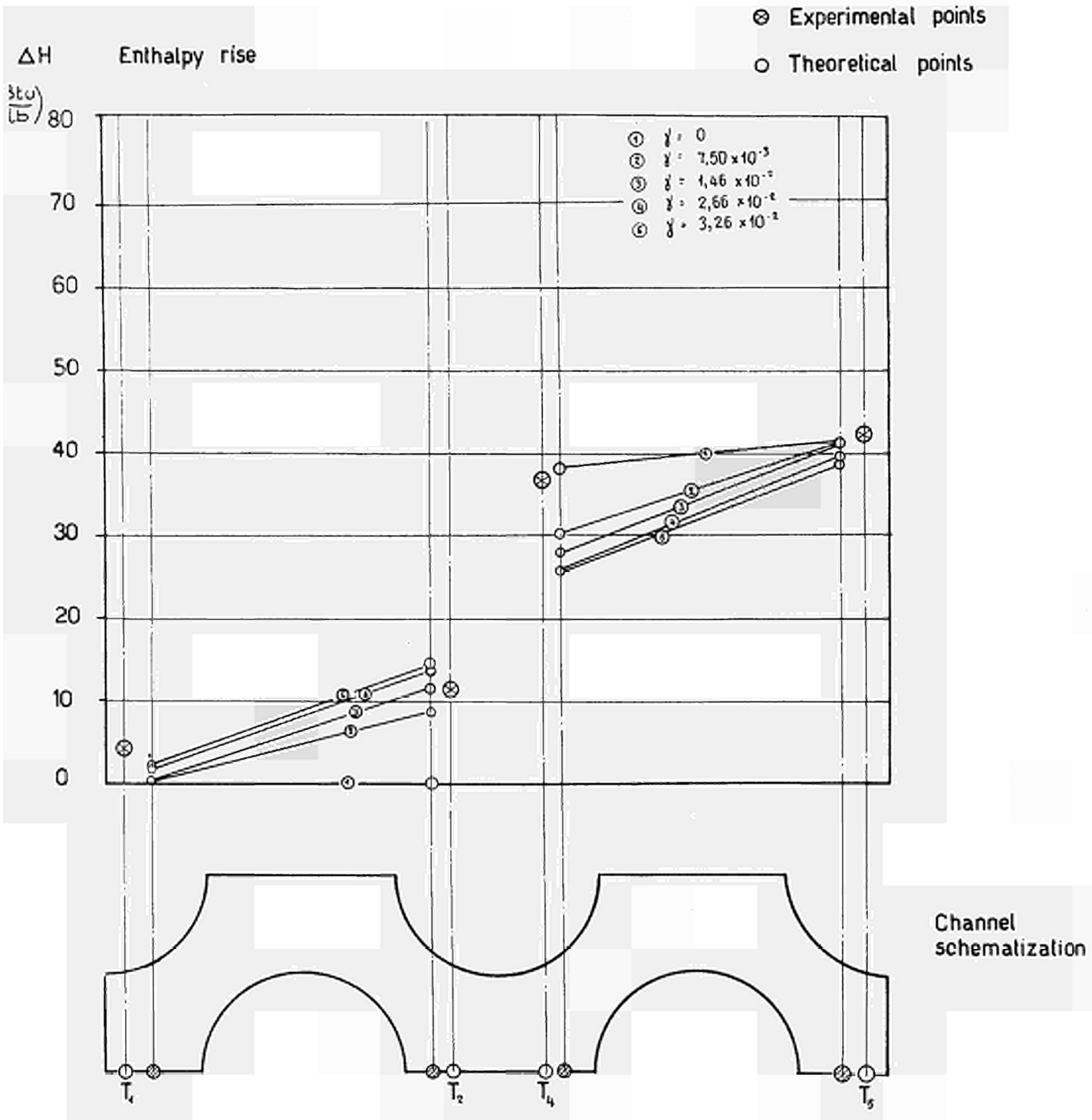

FIG. 5

Outlet enthalpy rise profiles and comparison with experimental results ; burnout test 2 (10-11-66); 10 subchannels schematization

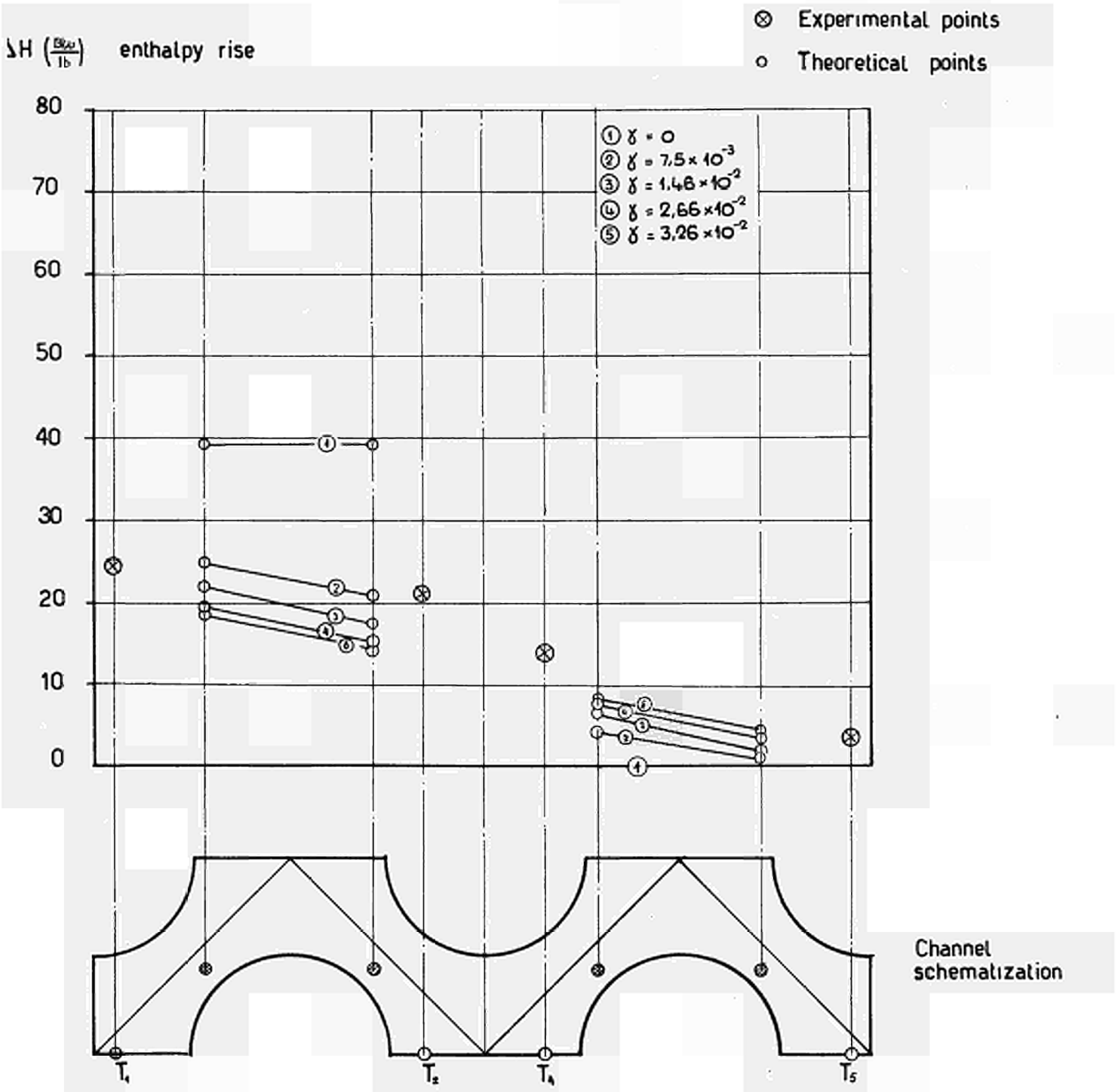

FIG. 6

Outlet enthalpy rise profiles and comparison with experimental results ; burnout test 2 (10-11-66) ; 8 subchannels schematization

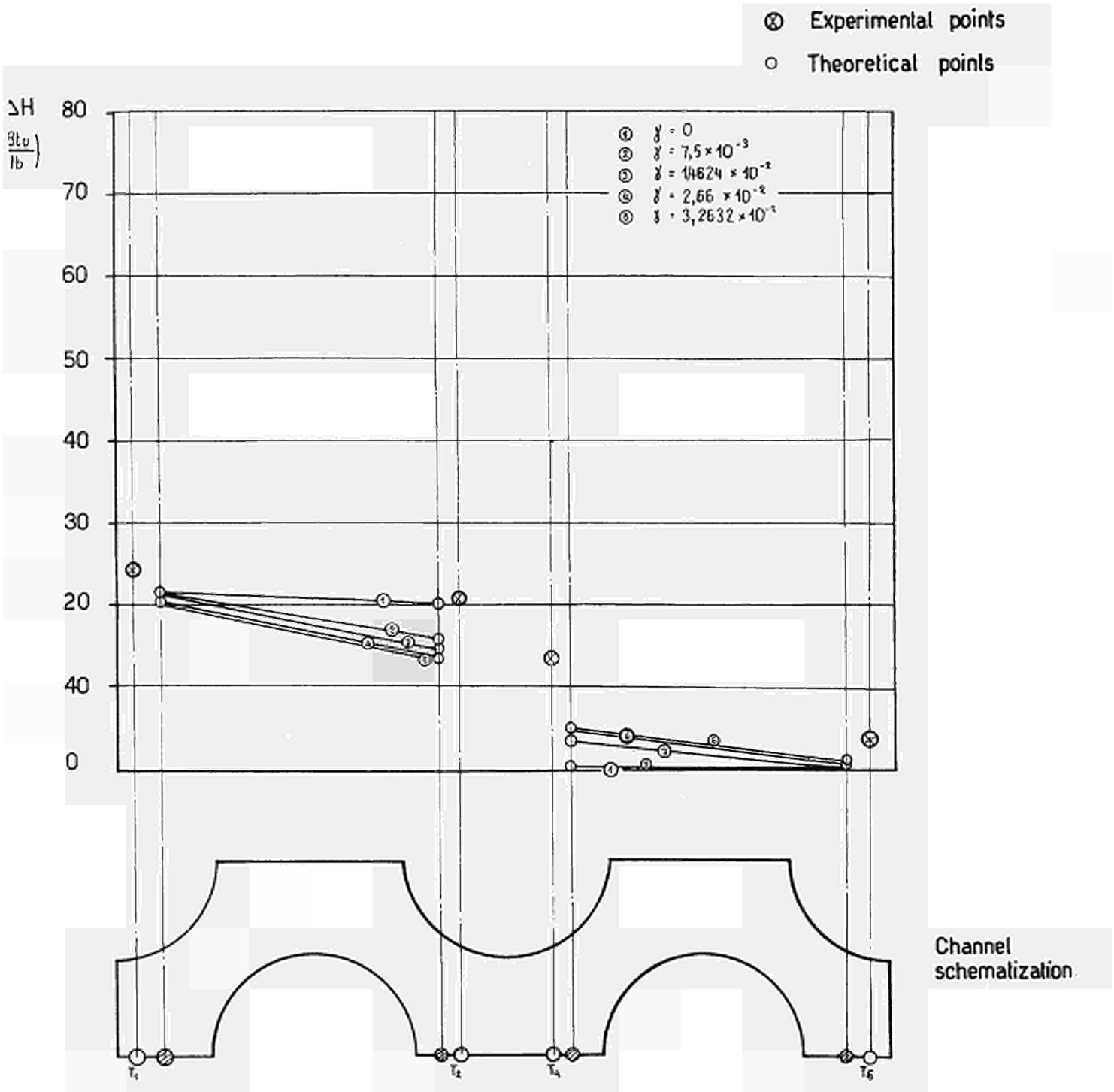

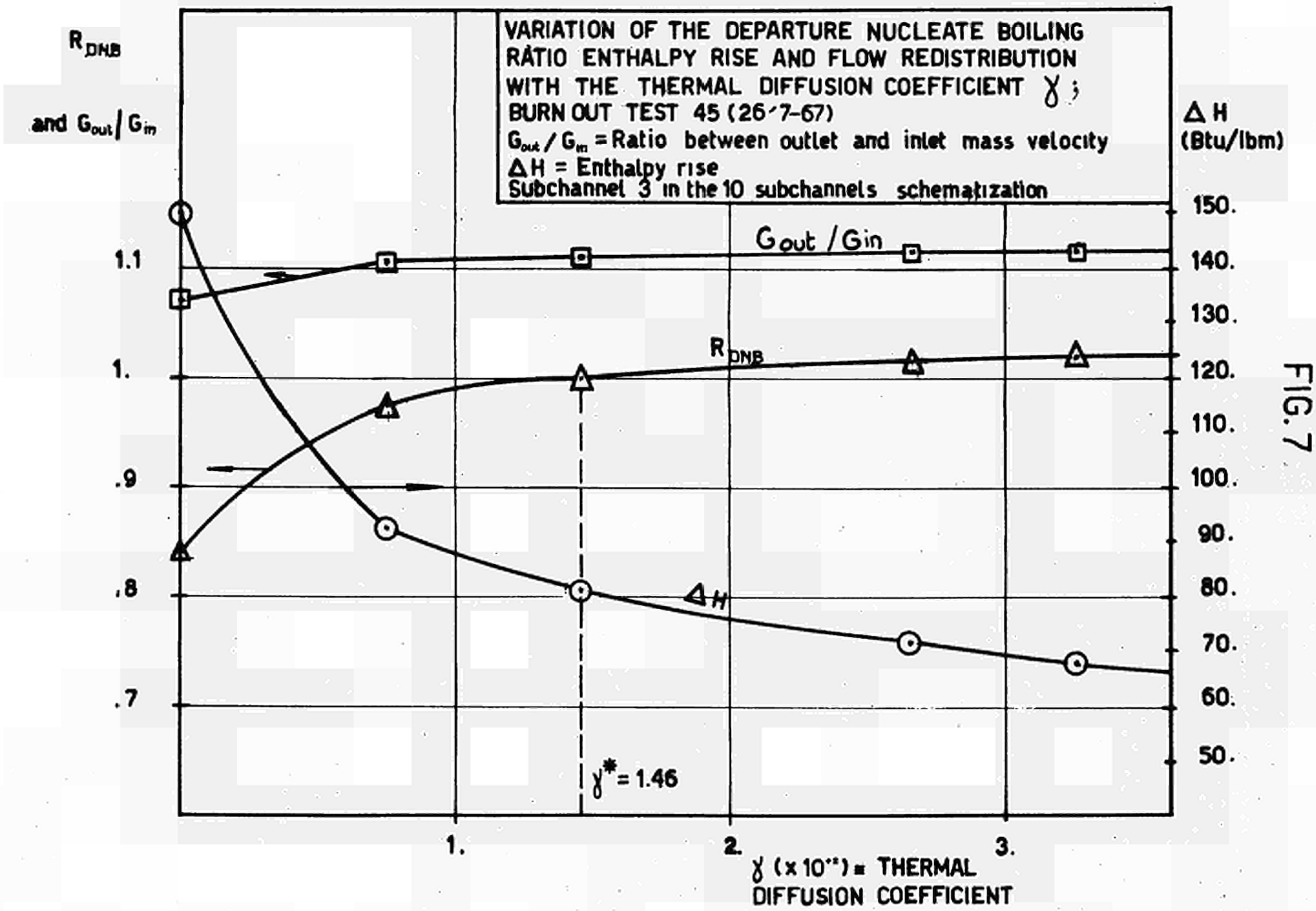
VARIATION OF THE DEPARTURE NUCLEATE BOILING RATIO ENTHALPY RISE AND FLOW REDISTRIBUTION WITH THE THERMAL DIFFUSION COEFFICIENT γ ;
BURN OUT TEST 45 (26-7-67)
G_{out}/G_{in} = Ratio between outlet and inlet mass velocity
ΔH = Enthalpy rise
Subchannel 3 in the 10 subchannels schematization
R_{DNB} and G_{out}/G_{in}
ΔH (Btu/lbm)
G_{out}/G_{in}
R_{DNB}
ΔH
$\gamma^* = 1.46$
1.1
1.
.9
.8
.7
150.
140.
130.
120.
110.
100.
90.
80.
70.
60.
50.
1.
2.
3.
γ (x 10⁻⁴) = THERMAL DIFFUSION COEFFICIENT

FIG. 7

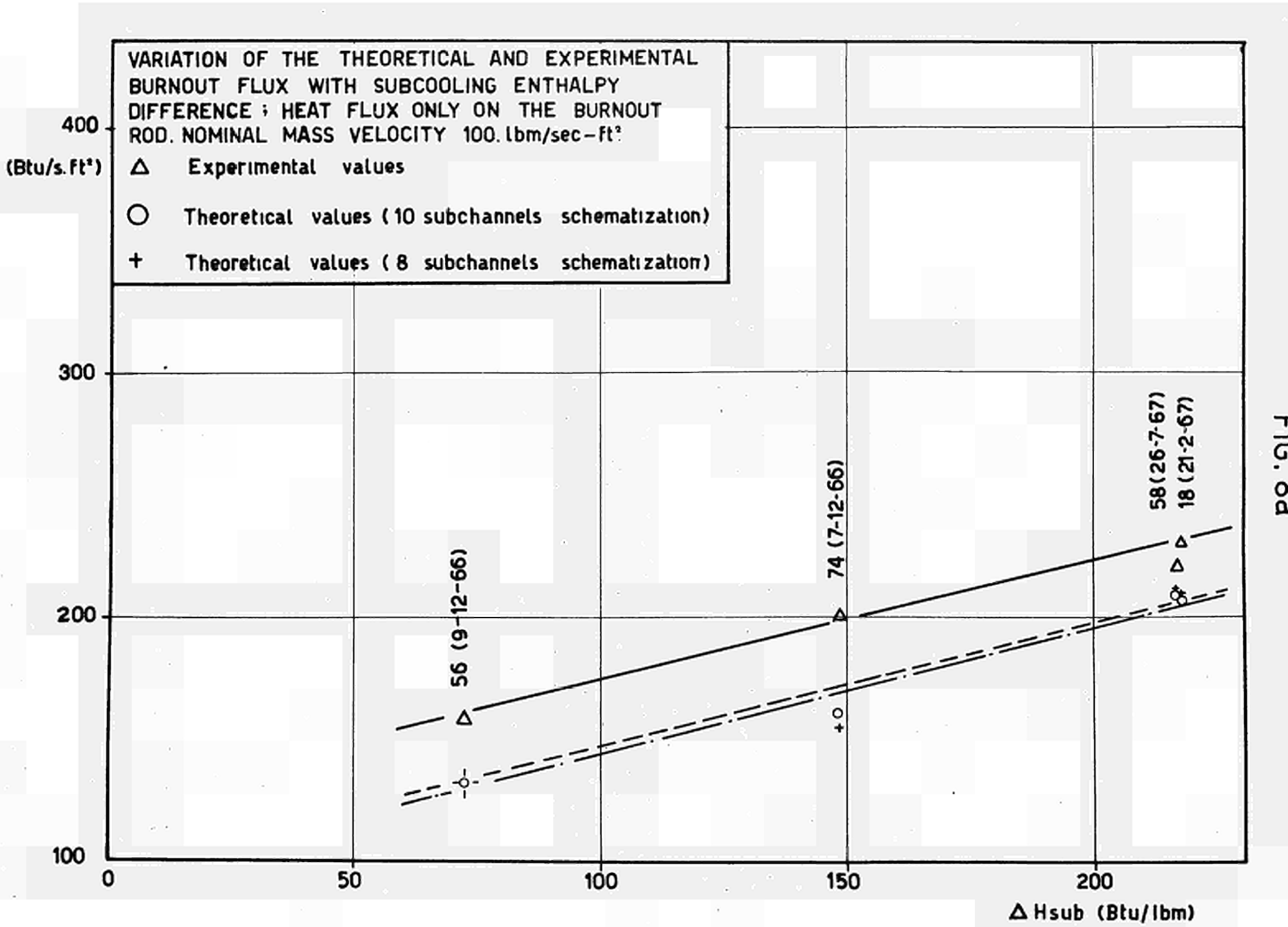
VARIATION OF THE THEORETICAL AND EXPERIMENTAL BURNOUT FLUX WITH SUBCOOLING ENTHALPY DIFFERENCE ; HEAT FLUX ONLY ON THE BURNOUT ROD. NOMINAL MASS VELOCITY 100. lbm/sec-ft²
Δ Experimental values
○ Theoretical values (10 subchannels schematization)
+ Theoretical values (8 subchannels schematization)
(Btu/s.ft²)
400
300
200
100
0
50
100
150
200
Δ Hsub (Btu/lbm)
56 (9-12-66)
74 (7-12-66)
58 (26-7-67)
18 (21-2-67)

FIG. 8a

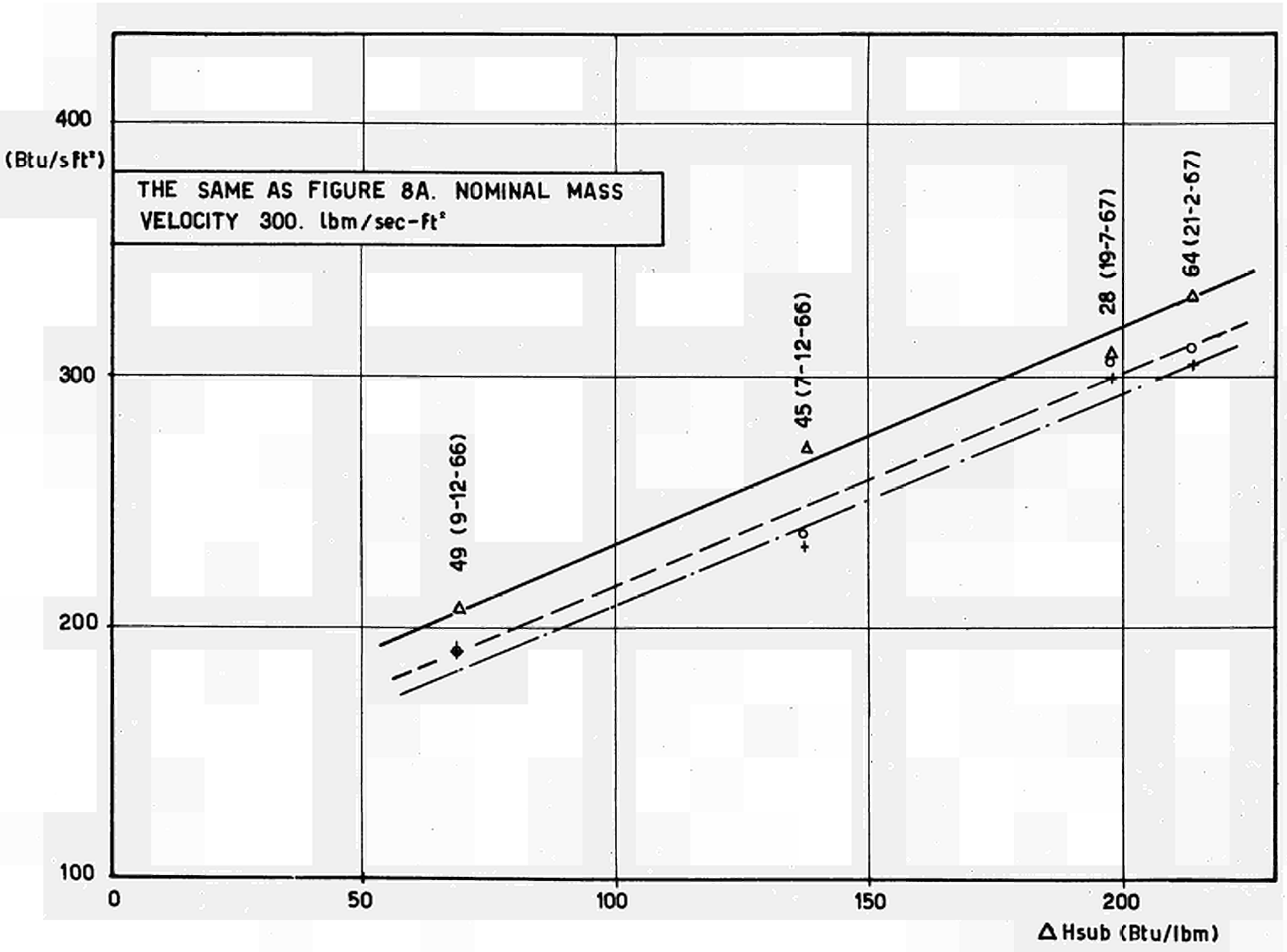
400
(Btu/s ft²)
300
200
100
0
50
100
150
200
Δ Hsub (Btu/lbm)
THE SAME AS FIGURE 8A. NOMINAL MASS VELOCITY 300. lbm/sec-ft²
49 (9-12-66)
45 (7-12-66)
28 (19-7-67)
64 (21-2-67)

FIG. 8b

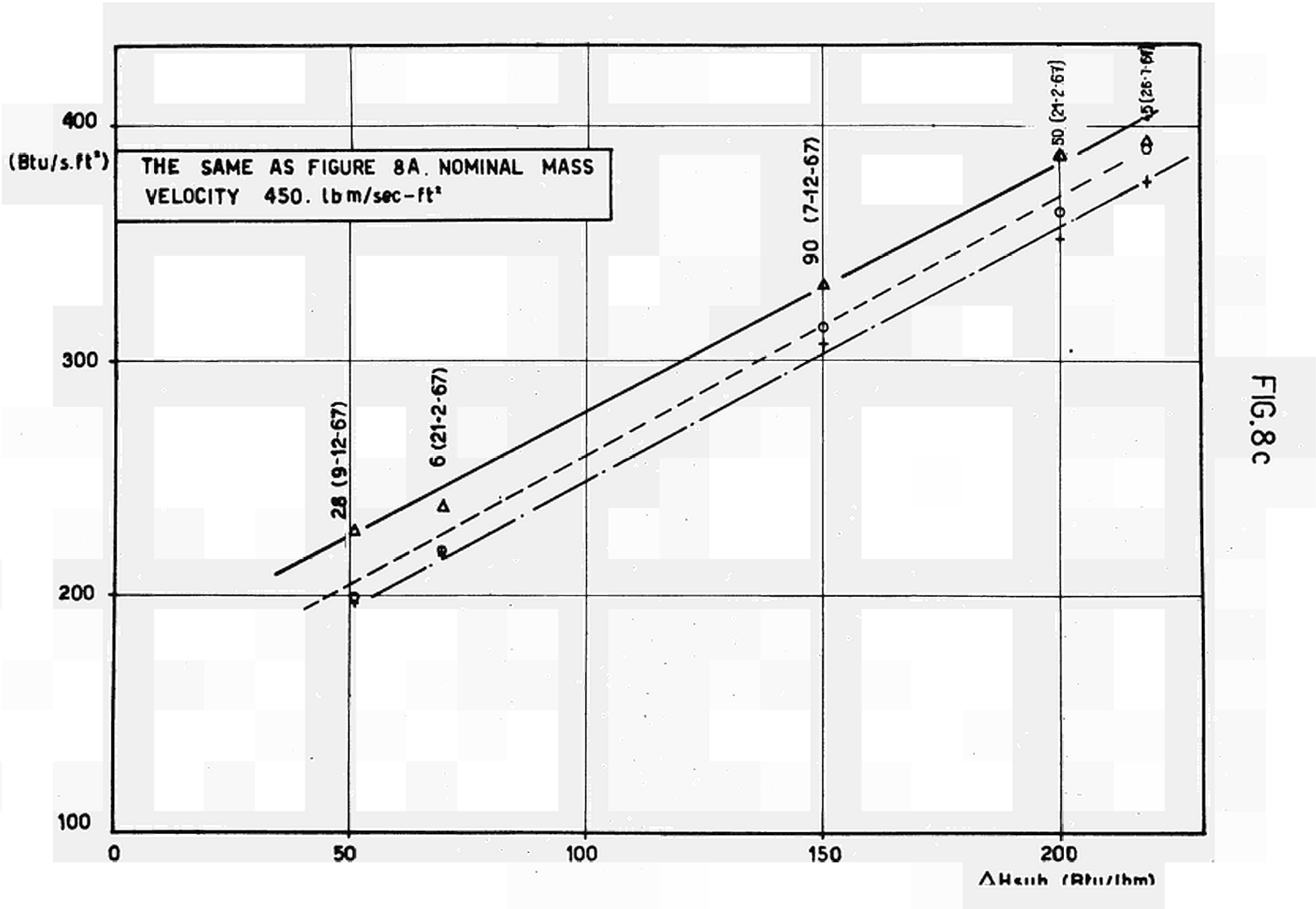
THE SAME AS FIGURE 8A. NOMINAL MASS VELOCITY 450. lbm/sec-ft²
(Btu/s.ft²)
400
300
200
100
0
50
100
150
200
ΔHeat (Btu/lbm)
28 (9-12-67)
6 (21-2-67)
90 (7-12-67)
50 (21-2-67)

FIG. 8c

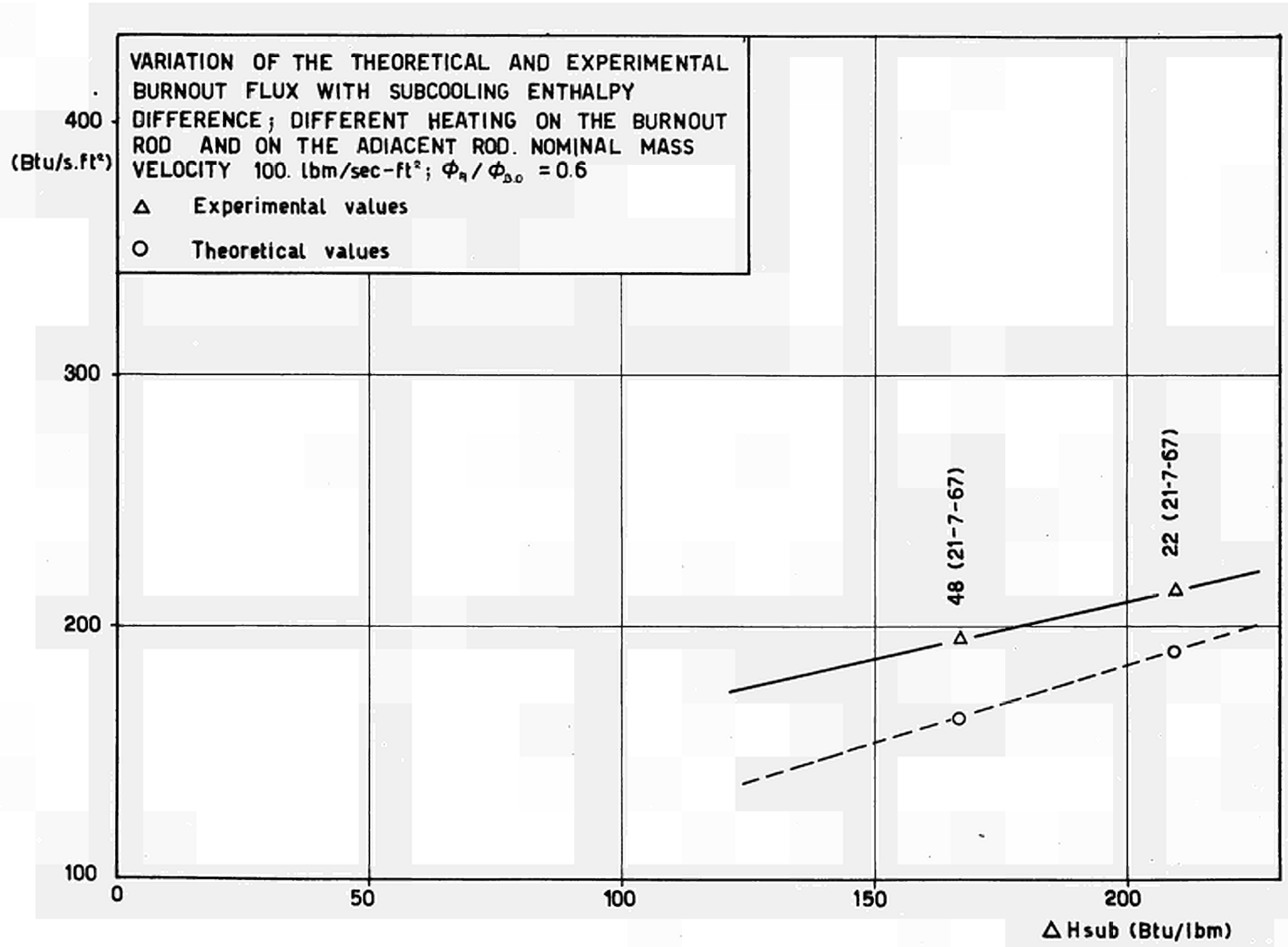
VARIATION OF THE THEORETICAL AND EXPERIMENTAL BURNOUT FLUX WITH SUBCOOLING ENTHALPY DIFFERENCE; DIFFERENT HEATING ON THE BURNOUT ROD AND ON THE ADIACENT ROD. NOMINAL MASS VELOCITY 100. lbm/sec-ft²; $\Phi_a / \Phi_{a.o} = 0.6$
△ Experimental values
○ Theoretical values
(Btu/s.ft²)
400
300
200
100
0
50
100
150
200
Δ Hsub (Btu/lbm)
48 (21-7-67)
22 (21-7-67)

FIG. 9a

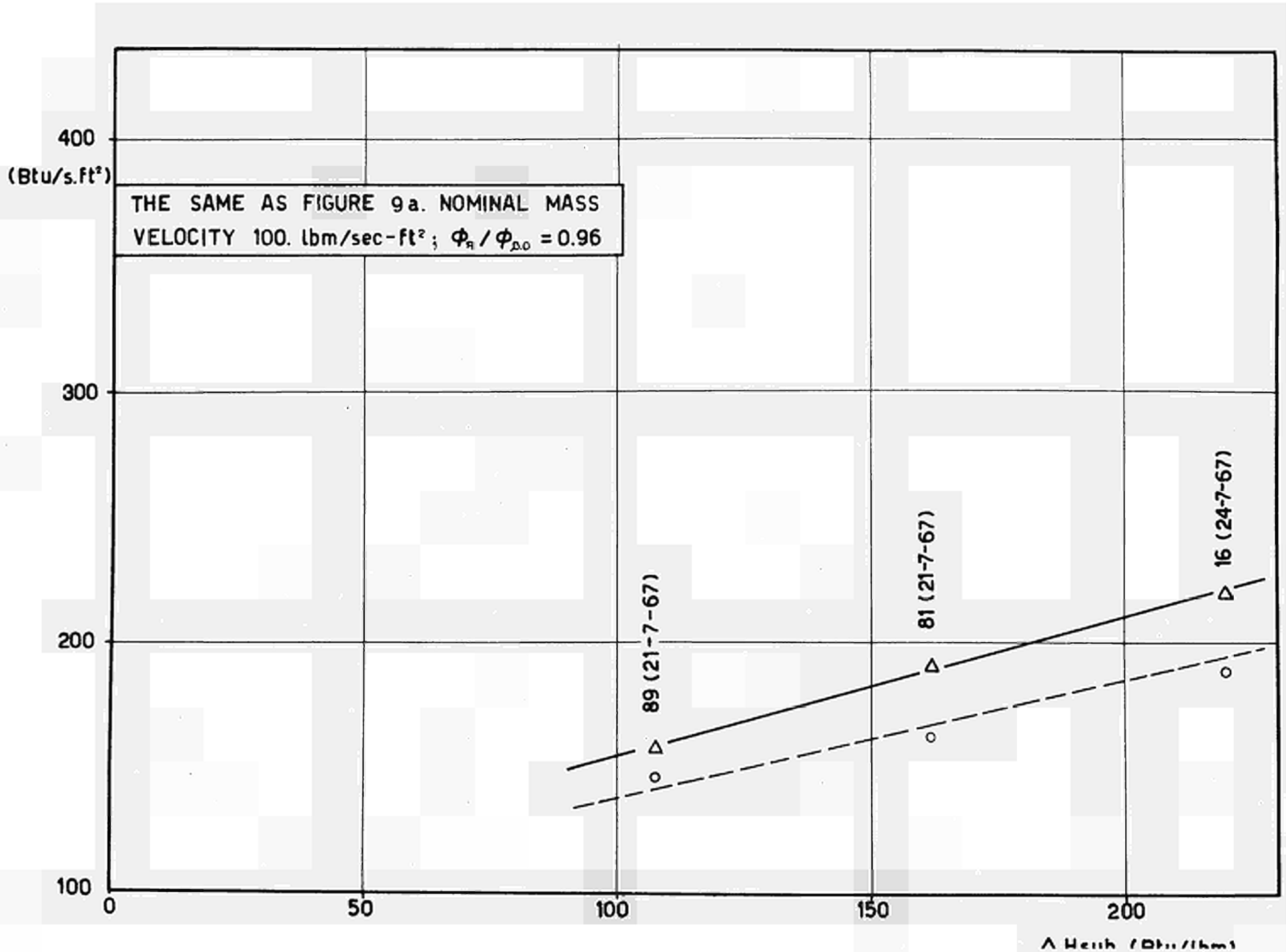
400
(Btu/s.ft²)
300
200
100
0
50
100
150
200
THE SAME AS FIGURE 9a. NOMINAL MASS VELOCITY 100. lbm/sec-ft² ; $\Phi_g / \Phi_{l,o} = 0.96$
89 (21-7-67)
81 (21-7-67)
16 (24-7-67)

FIG. 9b

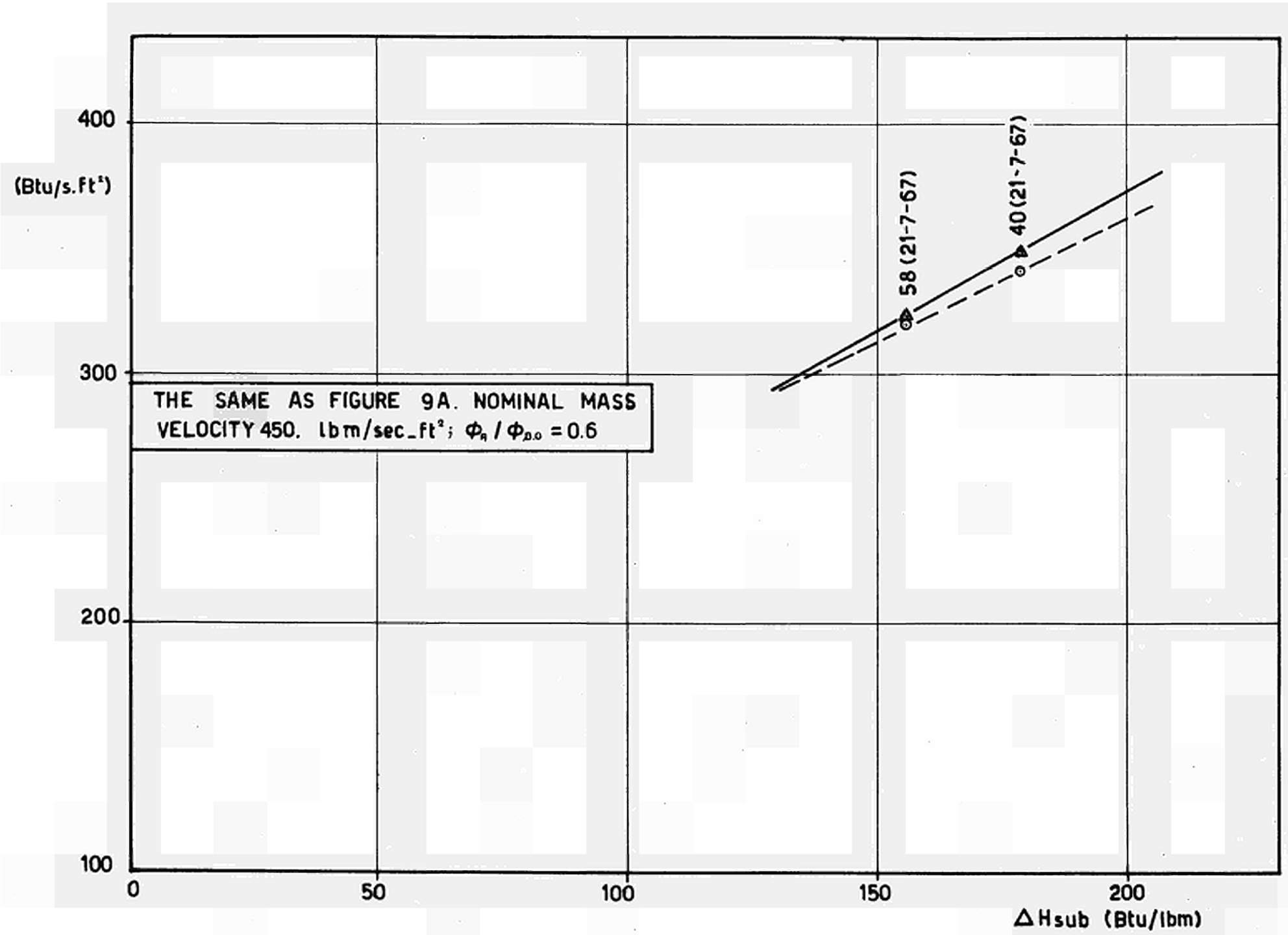
400
300
200
100
(Btu/s.Ft²)
0
50
100
150
200
ΔHsub (Btu/lbm)
58 (21-7-67)
40 (21-7-67)
THE SAME AS FIGURE 9A. NOMINAL MASS VELOCITY 450. lbm/sec_ft²; Φn / Φn.o = 0.6

FIG. 9c

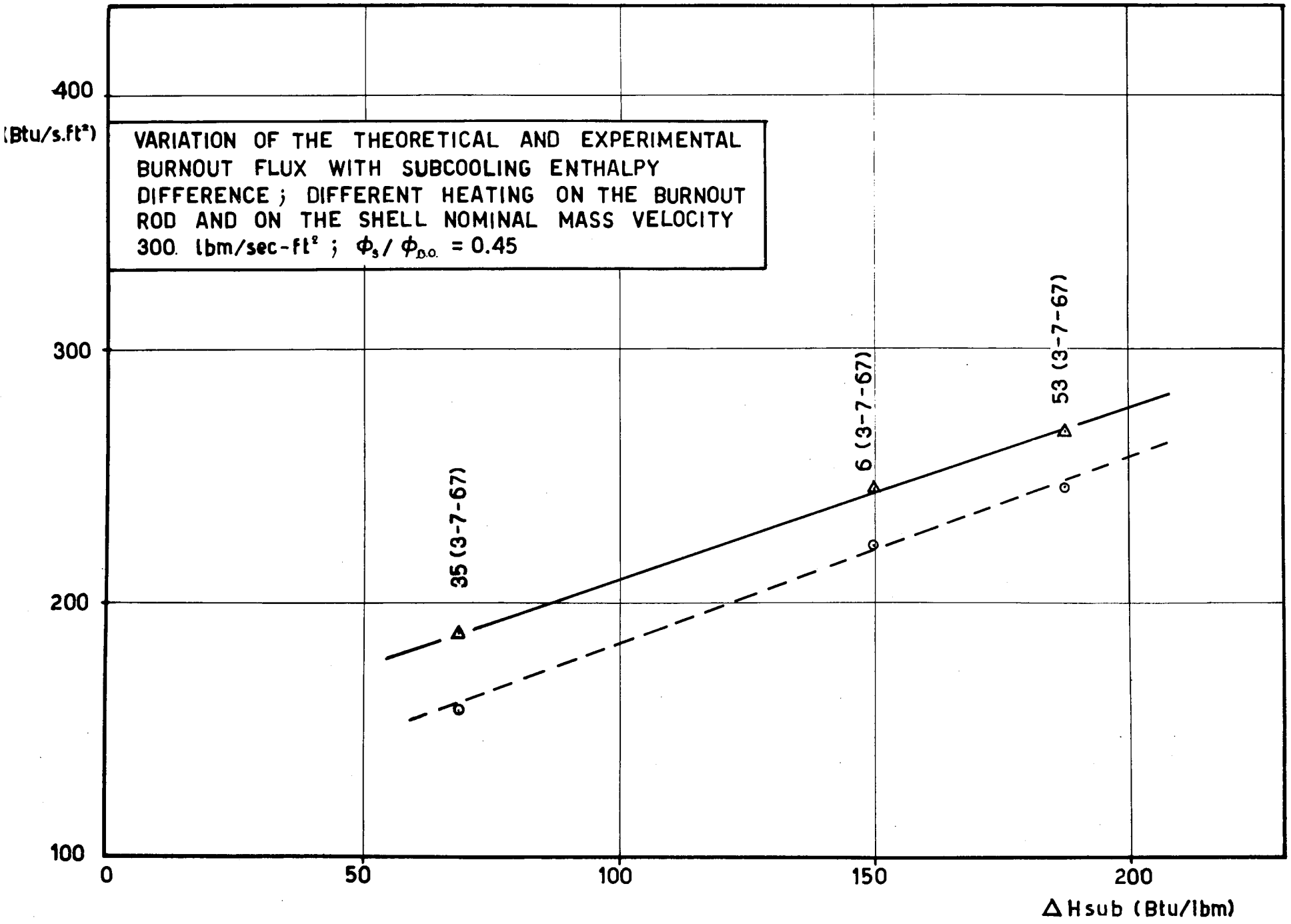
VARIATION OF THE THEORETICAL AND EXPERIMENTAL BURNOUT FLUX WITH SUBCOOLING ENTHALPY DIFFERENCE ; DIFFERENT HEATING ON THE BURNOUT ROD AND ON THE SHELL NOMINAL MASS VELOCITY 300. lbm/sec-ft² ; $\phi_s / \phi_{D.O.} = 0.45$
(Btu/s.ft²)
400
300
200
100
0
50
100
150
200
Δ Hsub (Btu/lbm)
35 (3-7-67)
6 (3-7-67)
53 (3-7-67)

FIG. 10a

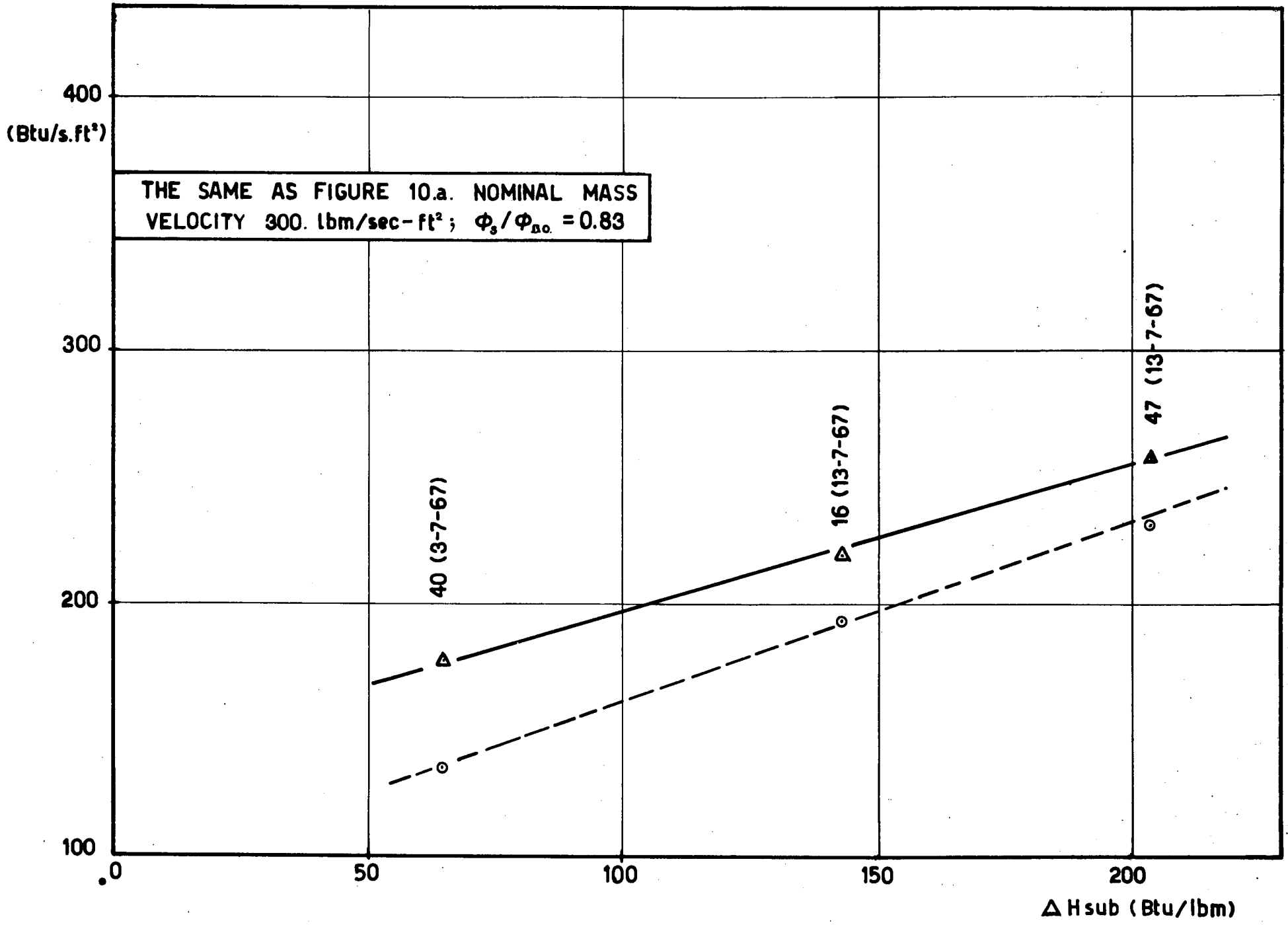
400
(Btu/s.ft²)
300
200
100
0
50
100
150
200
Δ H sub (Btu/lbm)
THE SAME AS FIGURE 10.a. NOMINAL MASS VELOCITY 300. lbm/sec-ft² ; $\Phi_s / \Phi_{no.} = 0.83$
40 (3-7-67)
16 (13-7-67)
47 (13-7-67)

FIG. 10b

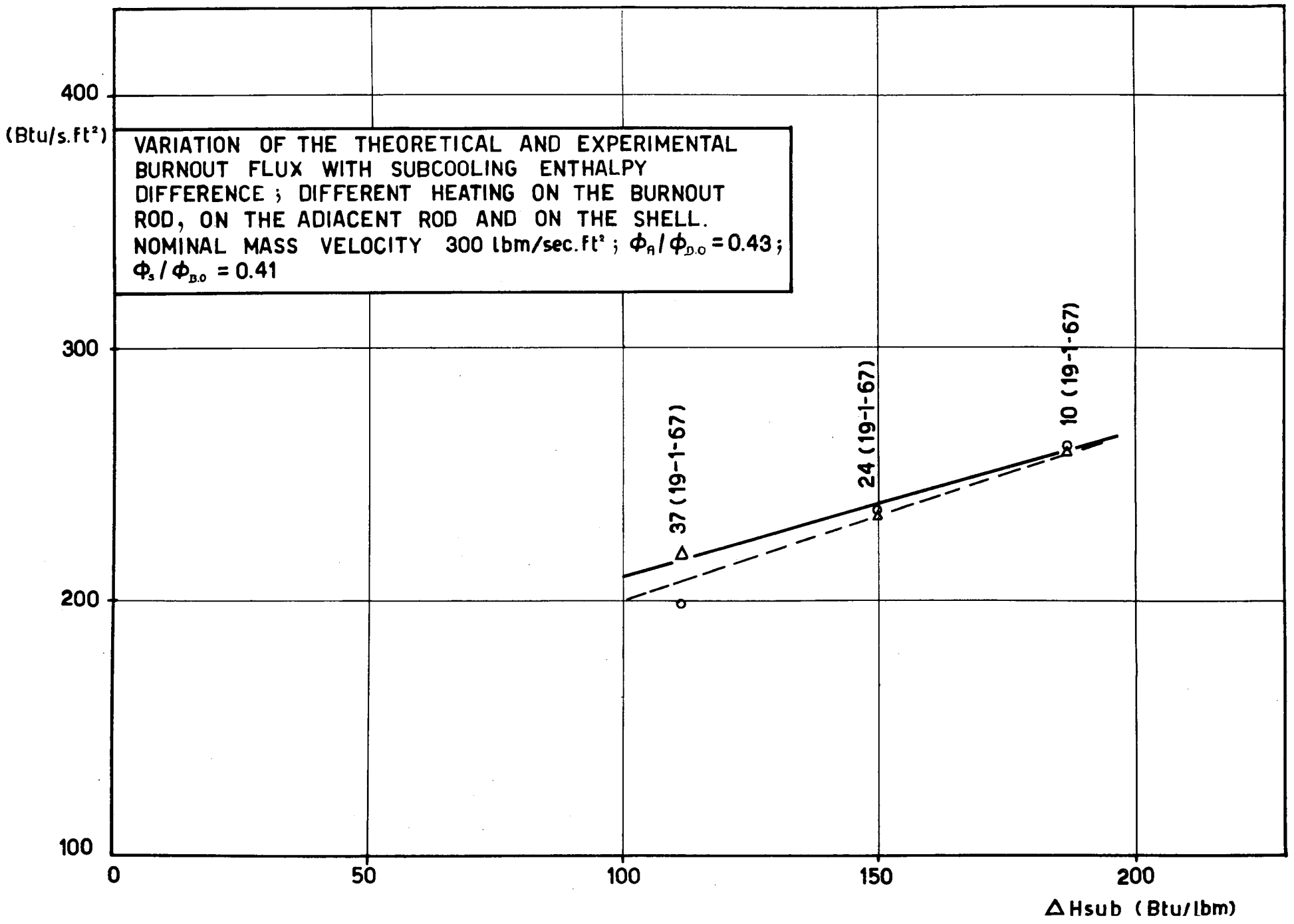
400
(Btu/s.ft²)
VARIATION OF THE THEORETICAL AND EXPERIMENTAL BURNOUT FLUX WITH SUBCOOLING ENTHALPY DIFFERENCE ; DIFFERENT HEATING ON THE BURNOUT ROD, ON THE ADIACENT ROD AND ON THE SHELL. NOMINAL MASS VELOCITY 300 lbm/sec.ft² ; $\Phi_A / \Phi_{D.O} = 0.43$; $\Phi_s / \Phi_{D.O} = 0.41$
300
200
100
0
50
100
150
200
37 (19-1-67)
24 (19-1-67)
10 (19-1-67)
ΔHsub (Btu/lbm)

FIG. 11a

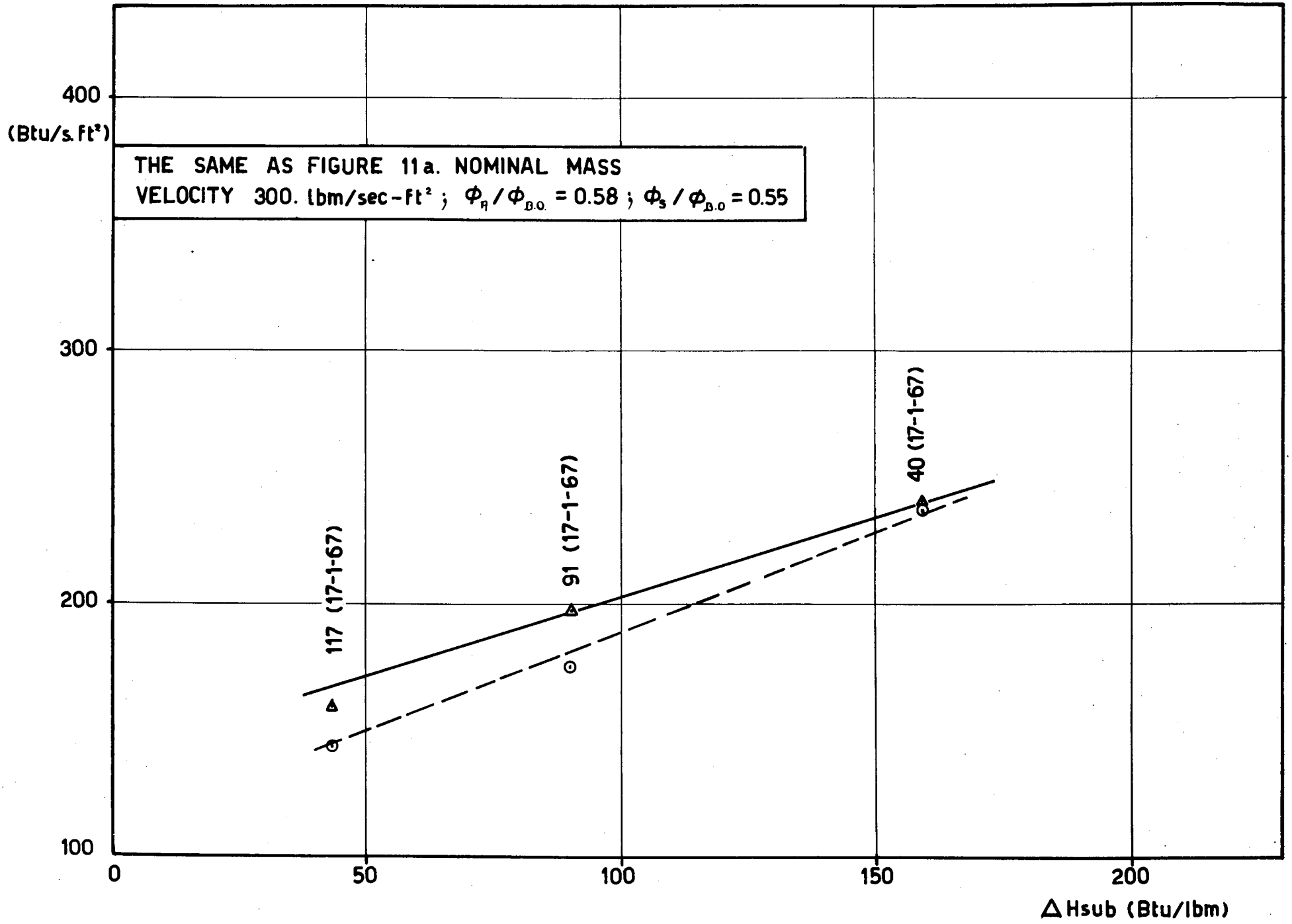
400
(Btu/s.ft²)
300
200
100
0
50
100
150
200
ΔHsub (Btu/lbm)
THE SAME AS FIGURE 11a. NOMINAL MASS VELOCITY 300. lbm/sec-ft² ; Φη / ΦB.O. = 0.58 ; Φs / ΦB.O = 0.55
117 (17-1-67)
91 (17-1-67)
40 (17-1-67)

FIG. 11b

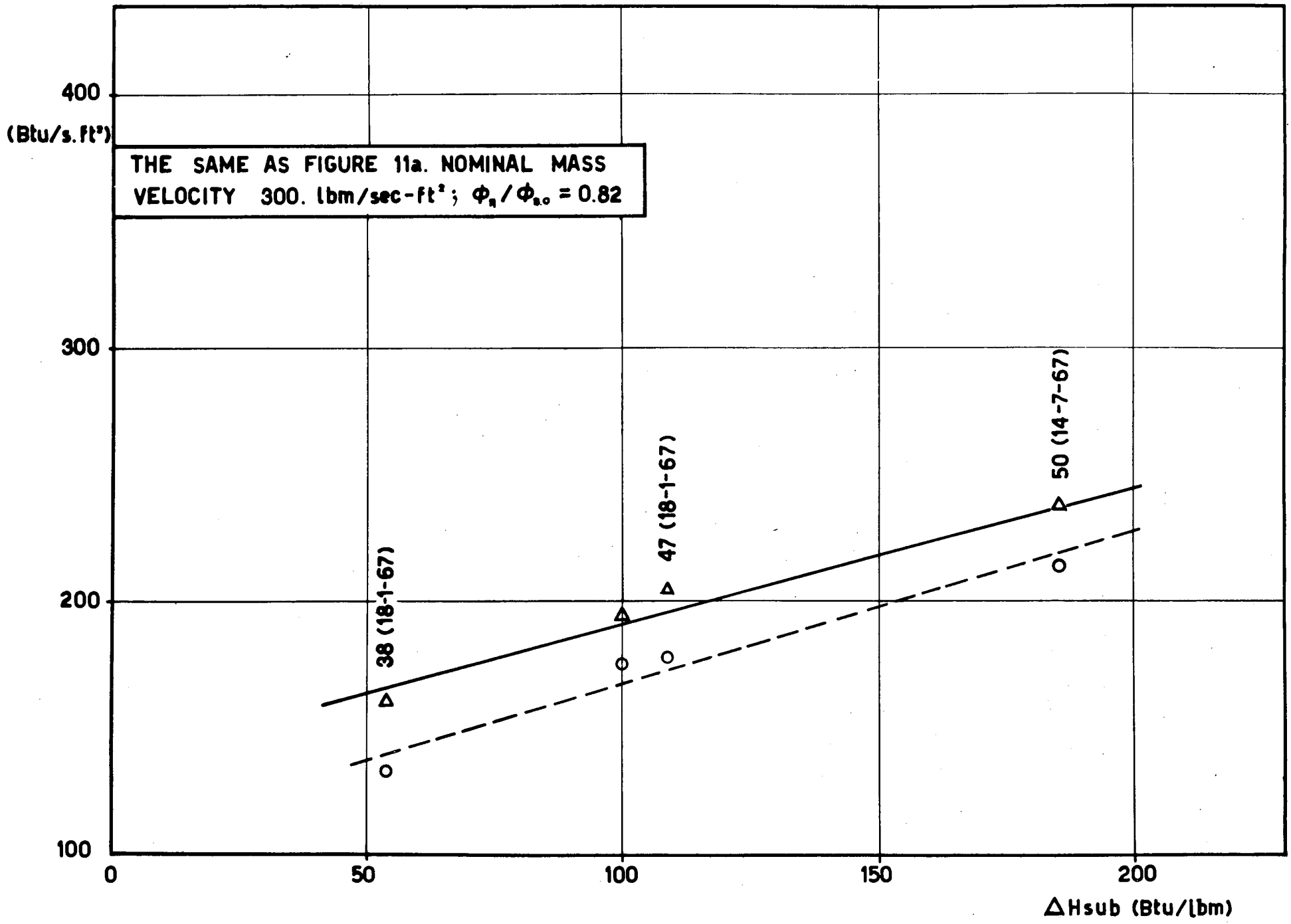
400
(Btu/s.ft²)
300
200
100
0
50
100
150
200
ΔHsub (Btu/lbm)
THE SAME AS FIGURE 11a. NOMINAL MASS VELOCITY 300. lbm/sec-ft²; Φn/Φn.o = 0.82
38 (18-1-67)
47 (18-1-67)
50 (14-7-67)

FIG. 11c

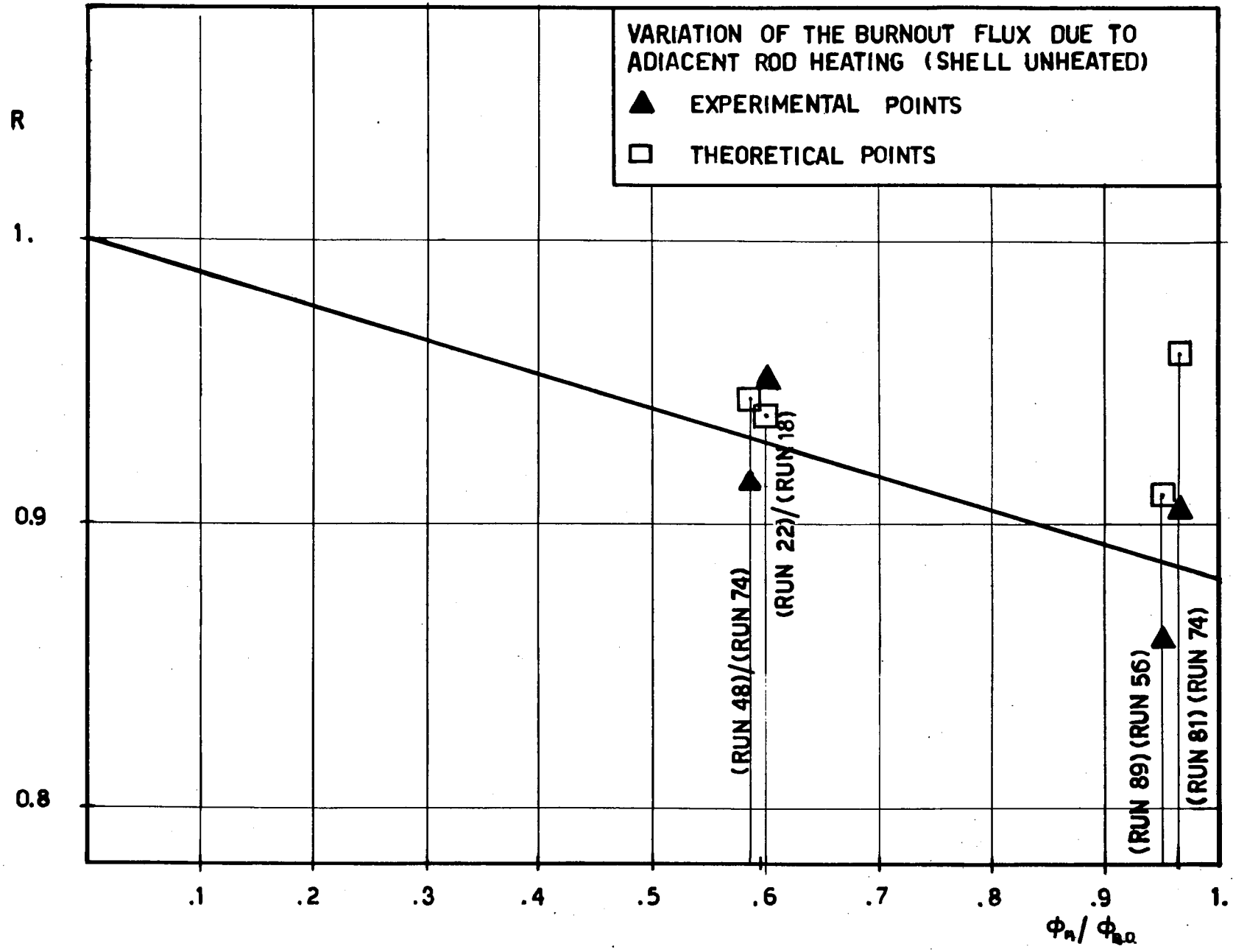
VARIATION OF THE BURNOUT FLUX DUE TO ADIACENT ROD HEATING (SHELL UNHEATED)
EXPERIMENTAL POINTS
THEORETICAL POINTS
R
1.
0.9
0.8
.1
.2
.3
.4
.5
.6
.7
.8
.9
1.
$\Phi_n / \Phi_{s.a}$
(RUN 48)/(RUN 74)
(RUN 22)/(RUN 18)
(RUN 89) (RUN 56)
(RUN 81) (RUN 74)

FIG. 12

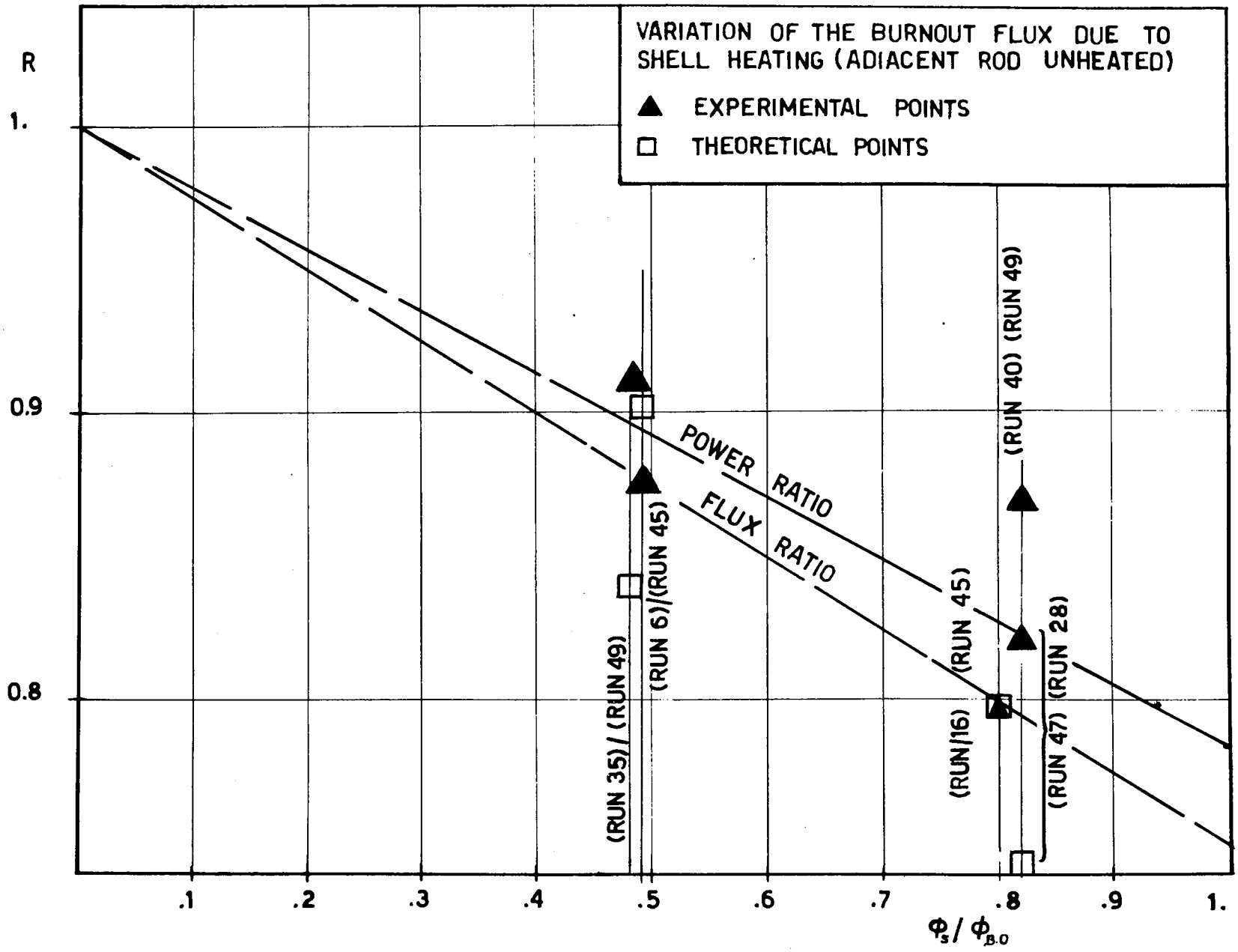
VARIATION OF THE BURNOUT FLUX DUE TO SHELL HEATING (ADIACENT ROD UNHEATED)
EXPERIMENTAL POINTS
THEORETICAL POINTS
R
1.
0.9
0.8
POWER RATIO
FLUX RATIO
(RUN 35)/(RUN 49)
(RUN 6)/(RUN 45)
(RUN/16)
(RUN 45)
(RUN 40) (RUN 49)
(RUN 47) (RUN 28)
.1
.2
.3
.4
.5
.6
.7
.8
.9
1.
$\Phi_s / \Phi_{B.O}$

FIG.13

FIG. 14 a

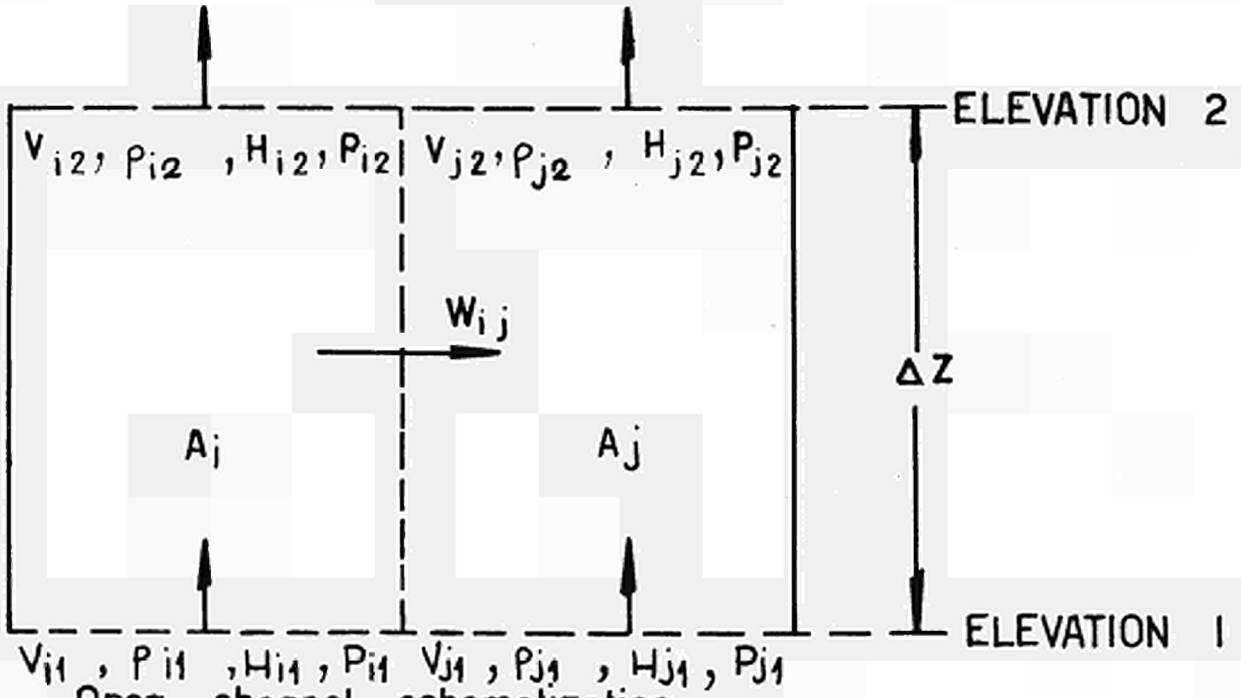

Open channel schematization

FIG. 14 b

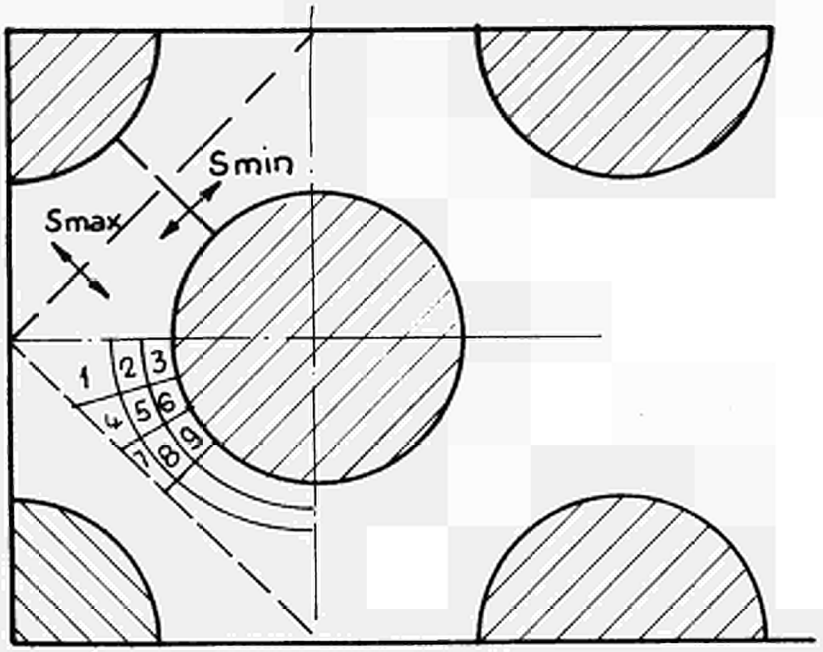

Detailed subchannels subdivision

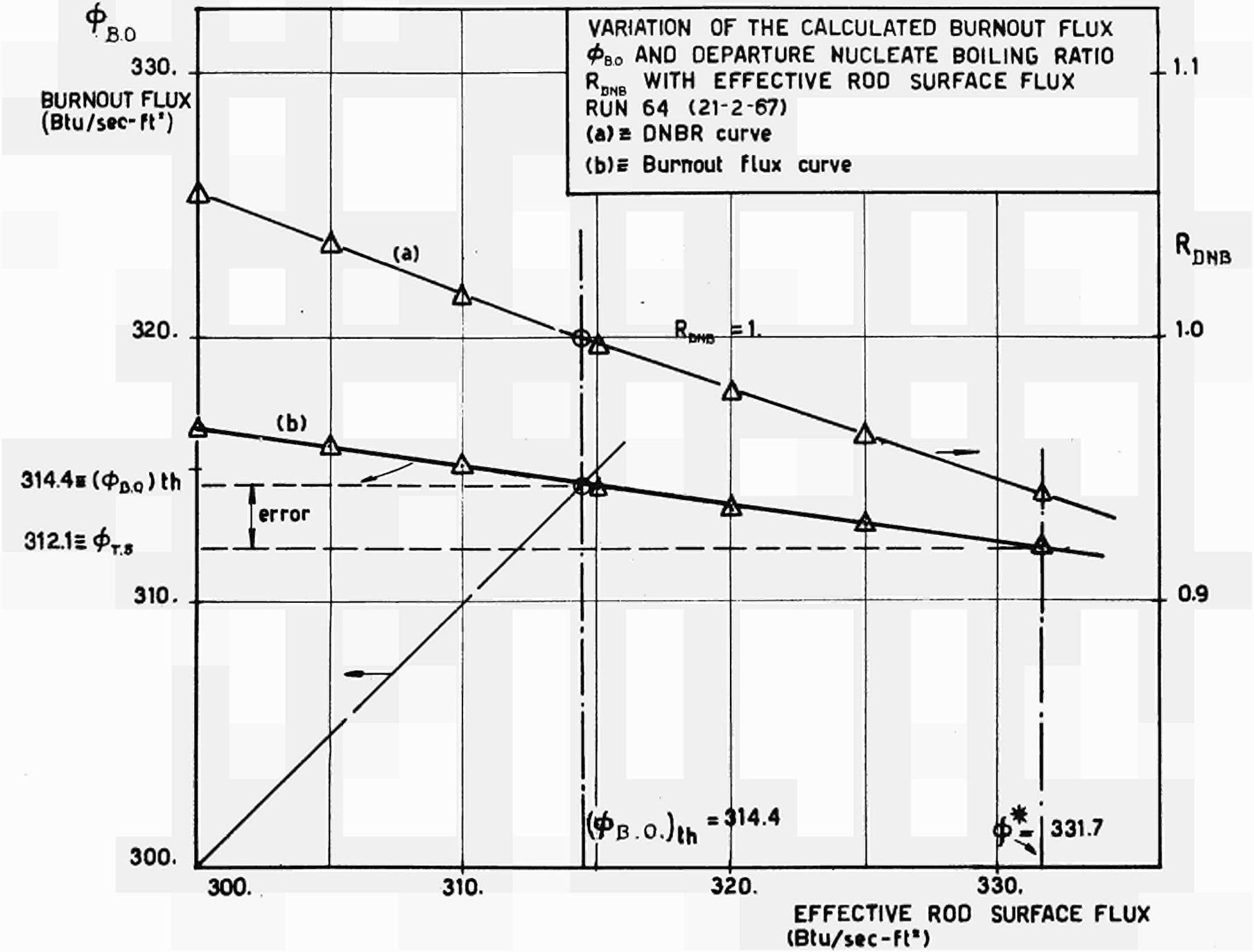
$\phi_{B.O}$
330.
BURNOUT FLUX
(Btu/sec-ft²)
320.
314.4≡ $(\phi_{B.O})$ th
312.1≡ $\phi_{T.S}$
error
310.
300.
VARIATION OF THE CALCULATED BURNOUT FLUX
$\phi_{B.O}$ AND DEPARTURE NUCLEATE BOILING RATIO
R_{DNB} WITH EFFECTIVE ROD SURFACE FLUX
RUN 64 (21-2-67)
(a) ≡ DNBR curve
(b) ≡ Burnout flux curve
(a)
(b)
R_{DNB} = 1.
$(\phi_{B.O.})_{th}$ = 314.4
ϕ^* = 331.7
1.1
R_{DNB}
1.0
0.9
300.
310.
320.
330.
EFFECTIVE ROD SURFACE FLUX
(Btu/sec-ft²)

FIG. 15a

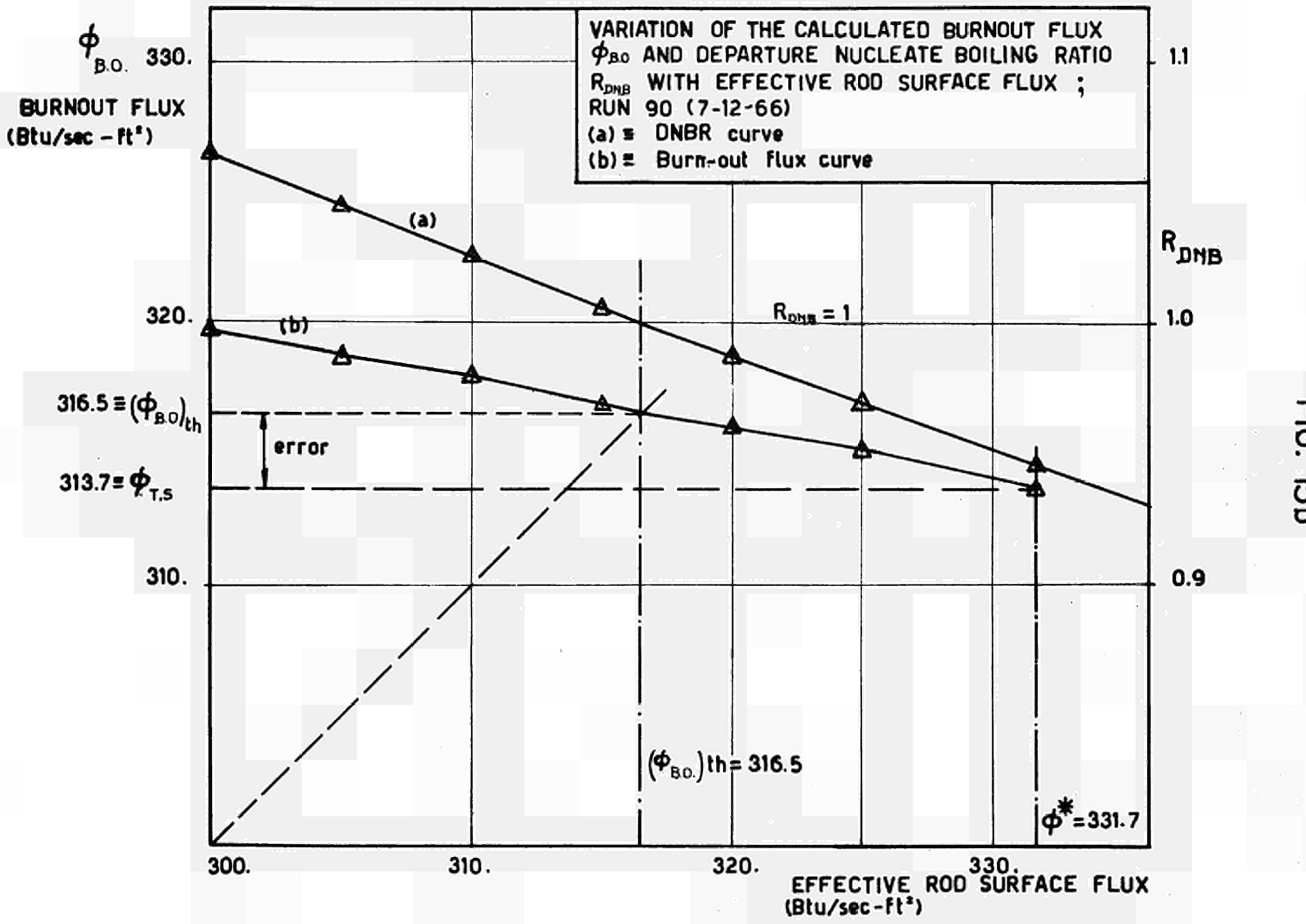
VARIATION OF THE CALCULATED BURNOUT FLUX
$\phi_{B.O}$ AND DEPARTURE NUCLEATE BOILING RATIO
R_{DNB} WITH EFFECTIVE ROD SURFACE FLUX ;
RUN 90 (7-12-66)
(a) ≡ DNBR curve
(b) ≡ Burn-out flux curve
$\phi_{B.O.}$
BURNOUT FLUX
(Btu/sec - ft²)
330.
320.
310.
316.5 ≡ $(\phi_{B.O})_{th}$
313.7 ≡ $\phi_{T.S}$
error
(a)
(b)
$R_{DNB} = 1$
1.1
1.0
0.9
R_{DNB}
$(\phi_{B.O.})th = 316.5$
$\phi^* = 331.7$
300.
310.
320.
330.
EFFECTIVE ROD SURFACE FLUX
(Btu/sec-ft²)

FIG. 15b

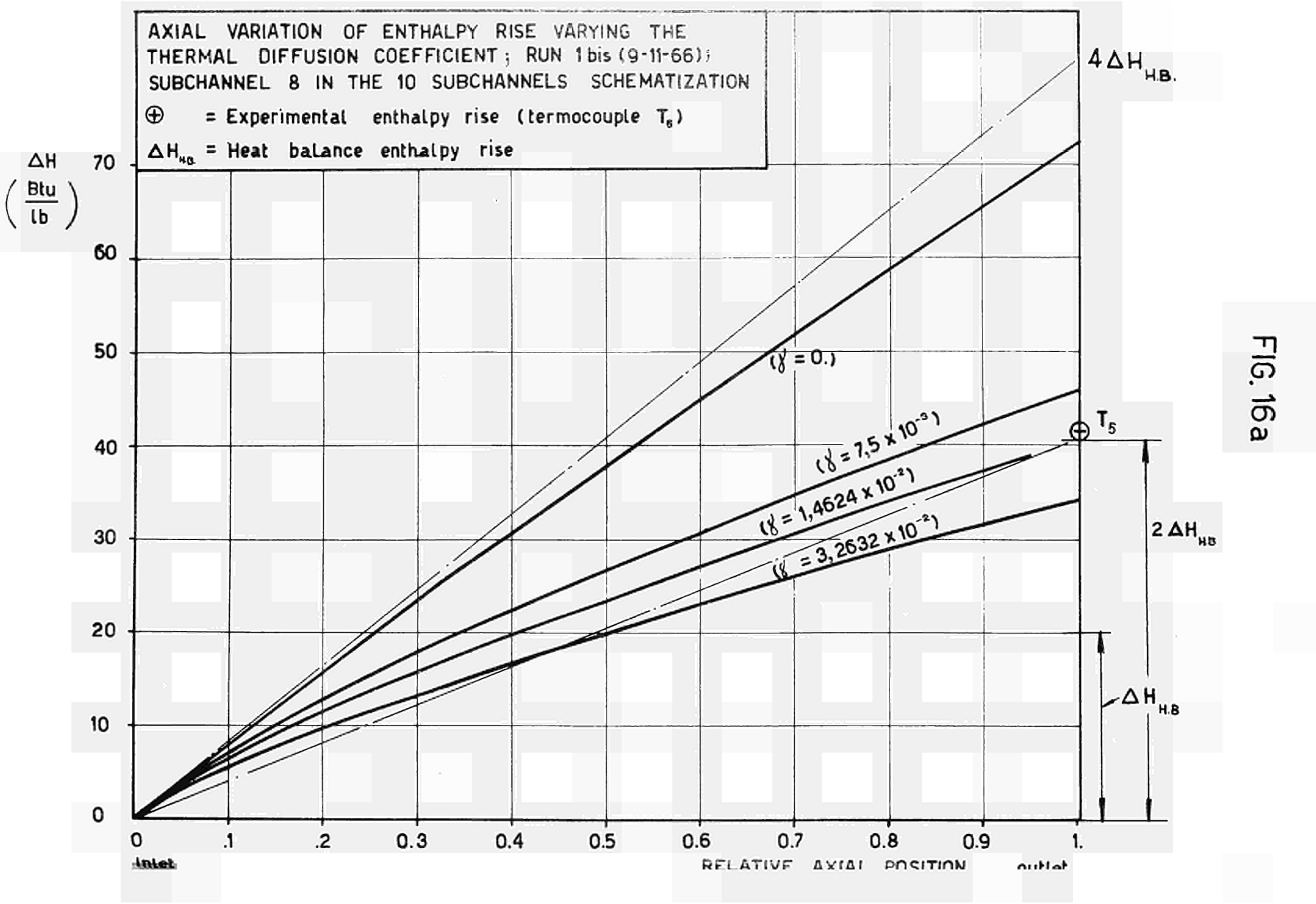
AXIAL VARIATION OF ENTHALPY RISE VARYING THE THERMAL DIFFUSION COEFFICIENT ; RUN 1 bis (9-11-66); SUBCHANNEL 8 IN THE 10 SUBCHANNELS SCHEMATIZATION
⊕ = Experimental enthalpy rise (termocouple T6)
ΔH H.B. = Heat balance enthalpy rise
ΔH (Btu/lb)
70
60
50
40
30
20
10
0
0
.1
.2
0.3
0.4
0.5
0.6
0.7
0.8
0.9
1.
inlet
RELATIVE AXIAL POSITION
outlet
4 ΔH H.B.
(γ = 0.)
(γ = 7,5 x 10⁻³)
(γ = 1,4624 x 10⁻²)
(γ = 3,2632 x 10⁻²)
⊕ T5
2 ΔH H.B.
ΔH H.B.

FIG. 16a

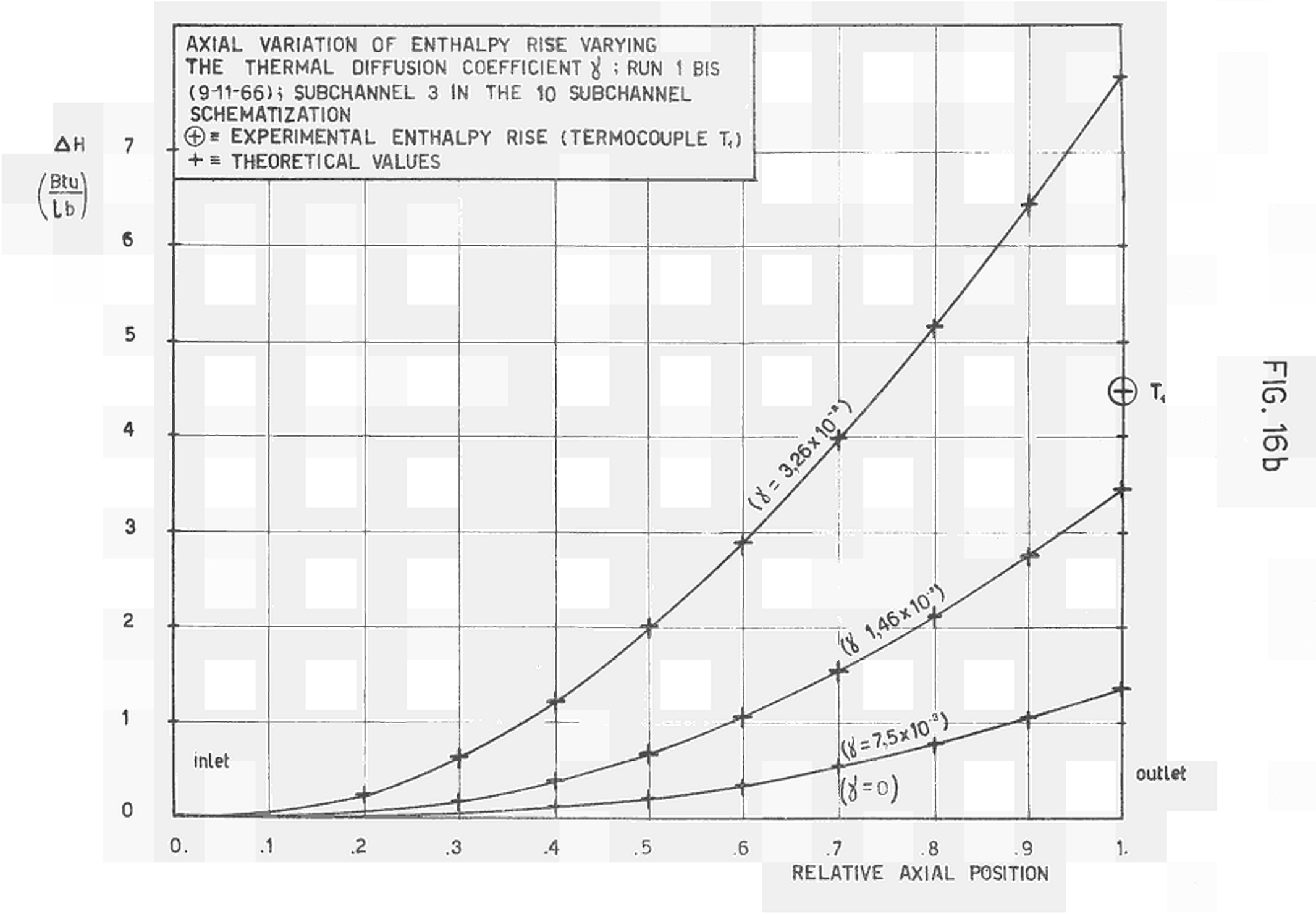
AXIAL VARIATION OF ENTHALPY RISE VARYING THE THERMAL DIFFUSION COEFFICIENT γ ; RUN 1 BIS (9-11-66); SUBCHANNEL 3 IN THE 10 SUBCHANNEL SCHEMATIZATION
⊕ ≡ EXPERIMENTAL ENTHALPY RISE (TERMOCOUPLE T4)
+ ≡ THEORETICAL VALUES
ΔH
(Btu/Lb)
7
6
5
4
3
2
1
0
inlet
outlet
(γ = 3,26x10⁻³)
(γ 1,46x10⁻³)
(γ = 7,5x10⁻⁴)
(γ = 0)
⊕ T4
0.
.1
.2
.3
.4
.5
.6
.7
.8
.9
1.
RELATIVE AXIAL POSITION

FIG. 16b

NOTICE TO THE READER

All Euratom reports are announced, as and when they are issued, in the monthly periodical **EURATOM INFORMATION**, edited by the Centre for Information and Documentation (CID). For subscription (1 year : US$ 15, £ 6.5) or free specimen copies please write to :

Handelsblatt GmbH
"Euratom Information"
Postfach 1102
D-4 Düsseldorf (Germany)

or

Office de vente des publications
des Communautés européennes
2, Place de Metz
Luxembourg

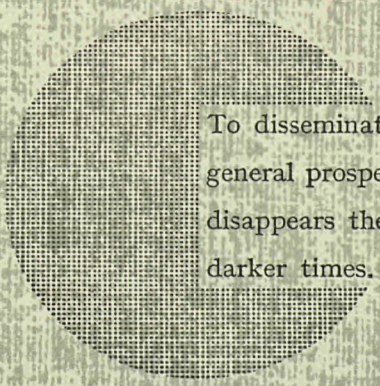

To disseminate knowledge is to disseminate prosperity — I mean general prosperity and not individual riches — and with prosperity disappears the greater part of the evil which is our heritage from darker times.

Alfred Nobel

SALES OFFICES

All Euratom reports are on sale at the offices listed below, at the prices given on the back of the front cover (when ordering, specify clearly the EUR number and the title of the report, which are shown on the front cover).

OFFICE CENTRAL DE VENTE DES PUBLICATIONS DES COMMUNAUTES EUROPEENNES
2, place de Metz, Luxembourg (Compte chèque postal N° 191-90)

BELGIQUE — BELGIË
MONITEUR BELGE
40-42, rue de Louvain - Bruxelles
BELGISCH STAATSBLAD
Leuvenseweg 40-42, - Brussel

DEUTSCHLAND
BUNDESANZEIGER
Postfach - Köln 1

FRANCE
SERVICE DE VENTE EN FRANCE
DES PUBLICATIONS DES
COMMUNAUTES EUROPEENNES
26, rue Desaix - Paris 15e

ITALIA
LIBRERIA DELLO STATO
Piazza G. Verdi, 10 - Roma

LUXEMBOURG
OFFICE CENTRAL DE VENTE
DES PUBLICATIONS DES
COMMUNAUTES EUROPEENNES
9, rue Goethe - Luxembourg

NEDERLAND
STAATSDRUKKERIJ
Christoffel Plantijnstraat - Den Haag

UNITED KINGDOM
H. M. STATIONERY OFFICE
P. O. Box 569 - London S.E.1

EURATOM — C.I.D.
51-53, rue Belliard
Bruxelles (Belgique)